Cyclic Behavior of Superelastic Nickel-Titanium and Nickel-Titanium-Chromium Shape Memory Alloys

A Thesis
Presented to
The Academic Faculty

by

Laura Isabel Barbero Bernal

In Partial Fulfillment
of the Requirements for the Degree
Master of Science in Civil Engineering

Georgia Institute of Technology

December, 2004

Cyclic Behavior of Superelastic Nickel-Titanium and Nickel-Titanium-Chromium Shape Memory Alloys

Approved by:

Dr. Reginald DesRoches, Advisor

Dr. Laurence Jacobs

Dr. Barry Goodno

November 22, 2004

Acknowledgements

I would like to thank my advisor, Dr. Reginald DesRoches, for his guidance, vision and support. I would also like to thank my Thesis Advisory Committee members, Dr. Laurence Jacobs and Dr. Barry Goodno for reading and reviewing my thesis with great care. A big thank you goes to Dr. Kenneth "Mac" Will for always being there to answer my questions and offer his guidance.

I want to thank my husband, Michael Buffa, for his encouragement, and for trying to get me to stop procrastinating so I could get my research and my schoolwork done on time. Without him, I would have never gotten out. I would also like to thank my parents for all the sacrifices they made to allow me the opportunity to study at Georgia Tech, and for their continuing support in everything I do.

I would also like to thank my officemates, Jason McCormick, Brad Penar, Jamie Padgett, and Monique Hite, thank you for putting up with my ramblings and for never telling me to shut up (except Brad that one time), even though you were probably all thinking about it. Enjoy the space I've vacated, and don't let them stick anyone else in our broom closet. Very special thanks to Jason McCormick, for helping me get my research done on time, for letting me ask him a billion questions, for organizing the office events and tailgates, and for not yelling at me anymore after the IM incident. He's the best assistant a girl could ever ask for.

TABLE OF CONTENTS

LIST OF TABLES

LIST OF FIGURES

LIST OF SYMBOLS OR ABBREVIATIONS

A_f	Austenite finish temperature
Al	Aluminum
A_s	Austenite start temperature
CuAlMn	Copper-Alumnium-Manganese Shape Memory Alloy
CuAlNi	Copper-Aluminum-Nickel Shape Memory Alloy
CuZnAl	Copper-Zinc-Aluminum Shape Memory Alloy
cm	Centimeter
E	Young's modulus or elastic modulus
E_D	Energy dissipated by viscous damping in one cycle
E_{So}	Strain energy
Fe	Iron
FeMnSiCrNi	Iron-Manganese-Silicon-Chromium-Nickel Shape Memory Alloy
FeNi	Iron-Nickel Shape Memory Alloy
FeNiAl	Iron-Nickel-Aluminum Shape Memory Alloy
FeNiCo	Iron-Nickel-Cobalt Shape Memory Alloy
FeNiTi	Iron-Nickel-Titanium Shape Memory Alloy
g	grams
GPa	Giga-Pascal
Hz	Hertz
in	Inch
ksi	Kips per square inch

M_d	Martensite deformation temperature
M_f	Martensite finish temperature
mm	millimeter
MPa	Mega-Pascal
M_s	Martensite start temperature
Ni	Nickel
Nb	Niobium
NiTi	Nickel-Titanium Shape Memory Alloy
NiTiCr	Nickel-Titanium-Chromium Shape Memory Alloy
NiTiCu	Nickel-Titanium-Copper Shape Memory Alloy
NiTiNb	Nickel-Titanium-Niobium Shape Memory Alloy
NiTiZr	Nickel-Titanium-Zirconium Shape Memory Alloy
Si	Silicon
SMA(s)	Shape Memory Alloy(s)
Ta	Tantalum
Ti	Titanium
TiNiCoV	Nickel-Titanium-Cobalt-Vanadium Shape Memory Alloy
TiNiFe	Nickel-Titanium-Iron Shape Memory Alloy
wt %	Percent by weight
Zr	Zirconium
ε_r	Residual strain
K	Slope of loading plateau for first 6% strain cycle between 2% and 6% strain
μ	Micro

Ω	Ohm
π	Pi (3.1416)
σ_L	Loading plateau stress
σ_{UL}	Unloading plateau stress
ζ_{eq}	Equivalent viscous damping

SUMMARY

Shape memory alloys (SMAs) are a class of alloys that display the unique ability to undergo nonlinear deformations and return to their original shape when heat is applied or the stress causing the deformation is removed. This unique "shape memory" characteristic is a result of a martensitic phase-change, which can be temperature induced (*shape memory effect*) or stress induced (*superelastic effect*).

In this study, the cyclical behavior of NiTi, a binary shape memory alloy, is compared to the cyclical behavior of NiTiCr, a ternary SMA. The purpose of this study is to compare the behavior of a 0.085-in. diameter NiTiCr wire with the behavior of the same size NiTi wire to determine whether ternary SMAs are more viable ways to take advantage of the unique properties of SMAs for seismic applications. The experimental results showing the superelastic behavior of these alloys under cyclical tensile loading are summarized with attention to the effects of annealing temperature, strain rate, and cyclical training on the stress-strain hysteresis, maximum recoverable strain and equivalent viscous damping.

CHAPTER 1

INTRODUCTION

Shape memory alloys are a class of alloys that display several unique characteristics: Young's modulus-temperature relations, shape memory effects, superelastic effects, and high damping characteristics. Unlike plastically deforming metals, the nonlinear deformation is metallurgically reversible. This unique "shape memory" characteristic is a result of a martensitic phase-change, which can be temperature induced (*shape memory effect*) or stress induced (*superelastic effect*).

These unique properties have resulted in numerous technical breakthroughs via applications in the biomedical, commercial, and engineering fields. These same properties are ideal for applications in the field of earthquake resistant design and retrofit. Many structures in the United States and around the world are vulnerable to moderate and strong ground motions. Although the loss of life in severe earthquakes has decreased significantly in the developed countries, the cost of repairing damage and rebuilding structures, such as bridges and buildings, has not decreased. In fact, recent earthquakes in the US and Japan have resulted in billions of dollars in economic losses. The focus of earthquake engineering is now shifting from a strength based design, which focused on protecting life to a more performance based design, allowing a building to be occupied immediately following an earthquake event. One way to accomplish these goals is to provide structures with passive energy dissipation and/or seismic isolation devices.

Passive energy dissipation devices include friction, metallic, viscoelastic, and viscous dampers, as well as tuned mass dampers and tuned liquid dampers. Many of

these devices have proven effective in protecting structures against damage from earthquakes, but there exists some drawbacks to using these devices. These drawbacks include susceptibility to corrosion, decreased effectiveness with increased ambient temperature, maintenance requirements, and the presence of permanent offsets after an earthquake (Sadek et al., 1996). Seismic isolation devices include elastomeric bearings and roller bearings. These devices provide a reduction in acceleration, but do not significantly reduce displacements. There is a need to implement devices that provide additional damping to the structure while also providing recentering capabilities. Shape memory alloys are good candidates for this task based on their general behavior and properties.

Currently, binary NiTi SMAs have shown potential as passive energy dissipation devices and recentering devices in structures during earthquakes. Binary NiTi, also known as Nitinol, is an equiatomic alloy consisting of approximately equal parts of nickel and titanium. NiTi has some limitations, including high cost, degradation of the damping and recentering capabilities if exposed to cyclical strains greater than 6%, and lack of an adequate understanding of the relation between thermomechanical processing and properties. Furthermore, metallurgists are finding that the properties of NiTi can potentially be improved by adding small quantities of a third element such as copper, aluminum, cobalt, vanadium, zirconium, niobium, chromium, or iron. The purpose of this study is to evaluate the cyclic properties of binary NiTi SMAs and compare these properties with that of ternary NiTiCr. In particular, the properties to be evaluated include loading and unloading plateau stress, equivalent viscous damping, and residual strain.

Outline of Thesis

- Chapter 2 provides a literature review that details the microstructure of SMAs including detailed descriptions of the shape memory and superelastic effects, the non-seismic and seismic applications of SMAs, the different types of SMAs and their main characteristics, and advantages and disadvantages of the different SMAs.
- Chapter 3 describes the test setup used for the experiments in this study, as well as an annealing temperature study used to determine the ideal annealing temperature that would minimize the residual strain in the SMA while still providing adequate energy dissipation during cyclic loading.
- Chapter 4 presents a strain rate study that evaluates the effect of increased strain rate and increased loading frequency on the superelastic properties of both types of SMAs, including loading and unloading plateau stress, force transmission properties, equivalent viscous damping, and residual strain.
- Chapter 5 presents a training study which determines the effects of training in stabilizing the degradation of the superelastic properties of SMAs with increased cyclic loading.
- Chapter 6 provides conclusions from this study and suggestions for future research.

CHAPTER 2

LITERATURE REVIEW

This chapter presents a literature review of previous studies focusing on shape memory alloys (SMAs). First, an overview of the general behavior, microstructure, shape memory effect and superelastic effect associated with SMAs will be discussed. Next, the different types of SMAs will be presented, including binary NiTi (commonly referred to as Nitinol), ternary NiTi-X, Cu-base, and other alloys. The damping characteristics of SMAs, their behavior under cyclical testing and applications using SMAs will also be discussed.

Shape memory alloys are a class of metallic alloys that display several unique characteristics, such as shape memory effects, Young's modulus-temperature relations, and high damping characteristics. Unlike plastically deforming metals, the nonlinear deformation is metallurgically reversible. Large deformations can be recovered by either applying heat (*shape memory effect*) or by removing the stress causing the deformation (*superelastic effect*). The ability to recover deformation (shape memory) was first observed 70 years ago by Chang and Reid with an alloy consisting of Au-47.5 Cd at% (Otsuka and Wayman, 1998). Over the last 30 years, there has been an increase in the number of applications of shape memory alloys in fields such as medicine, commercial technology, and engineering.

This study will focus on stress induced shape memory alloys which present superelastic (or pseudo-elastic) properties that are considered more adequately suited for seismic rehabilitation of structures based on their characteristic behavior. These

characteristics include: (1) excellent recentering capabilities; (2) hysteretic damping; (3) highly reliable energy dissipation; (4) force transmissions; and (5) superior corrosion resistance.

Microstructure of Shape Memory Alloys

The atomic changes in SMAs are displacive in nature. This means that the atoms are rearranged into a more stable crystal structure during phase changes, but the chemical composition of the matrix remains the same (Duerig et al., 1990). The following provides a brief discussion on the microscopic changes that allow the shape memory and superelastic effects to occur.

There are two independent phases in shape memory alloys: martensite and austenite. The martensite phase has two stable structures: the twinned form and the deformed or de-twinned form. Martensite exhibits a rhombic geometry, and is more stable at low temperature and at high stresses. It also tends to be softer and more ductile. Austenite is highly symmetric and exhibits a body centered cubic geometry. It is more stable at high temperatures and low stresses, and tends to be harder and stronger. Figure 2.1 shows the microstructure of the martensite and austenite phases.

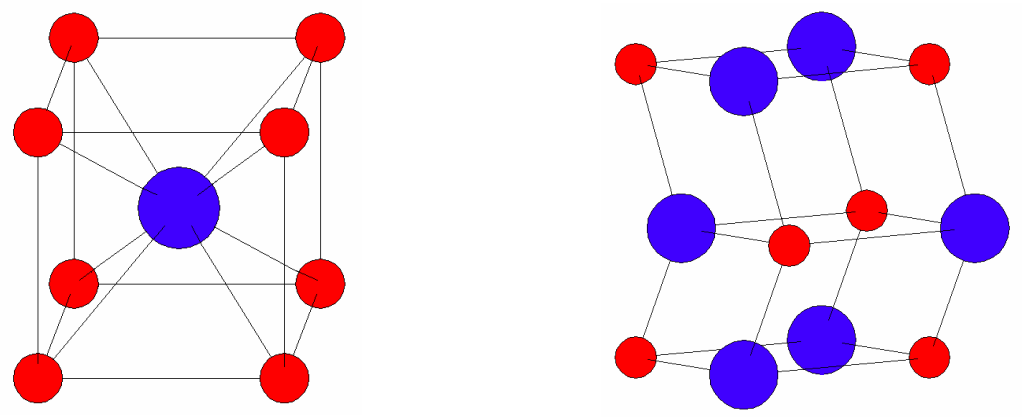

(a) **(b)**

Figure 2.1. Three dimensional microstructure of SMAs: (a) austenite and (b) twinned martensite. Large spheres represent nickel and small spheres represent titanium.

Shape Memory Effect

The shape memory characteristic refers to the ability of the alloy to retain its original shape through heating after undergoing deformation. To understand the shape memory effect and the overall behavior of SMAs, it is important to explain four basic terms: M_s, M_f, A_s, and A_f. M_s and A_s refer to the martensite and austenite start temperatures or when martensite and austenite begin to form. M_f and A_f refer to the martensite and austenite finish temperatures, respectively (Tadaki et al., 1988). The difference in the temperatures between the transformations is known as the hysteresis. The area under the hysteresis loop is the amount of energy that is dissipated by the SMA as it undergoes its phase transformations. Figure 2.2 shows the relationship between the transformation temperatures in SMAs.

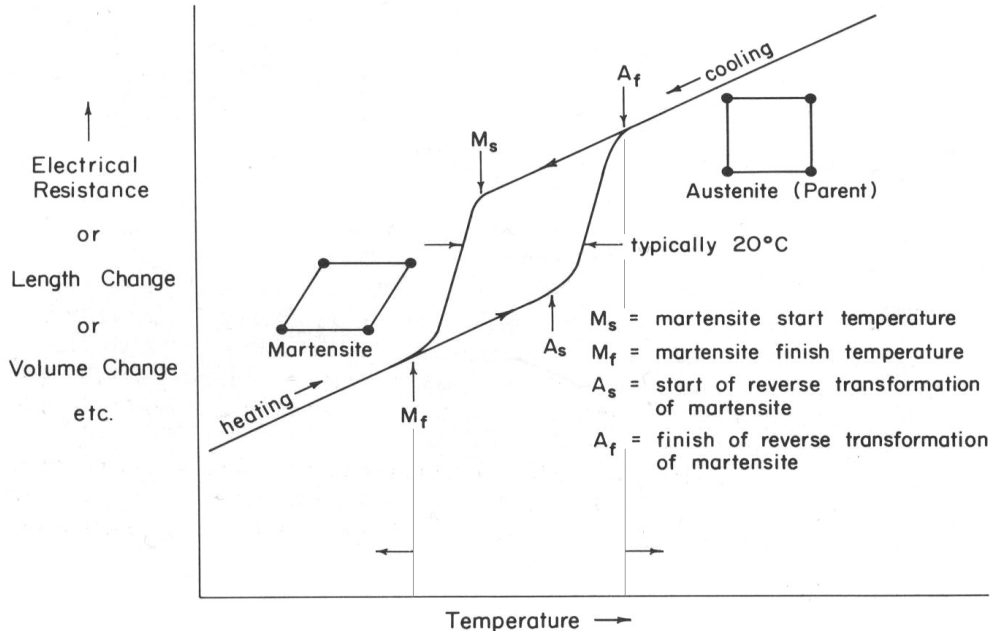

Figure 2.2. Relationships between the phases start and finish temperatures in a typical SMA. Also shown is the hysteresis loop (Duerig et al., 1990).

If a material is cooled below M_f, and undergoes deformations, the material experiences de-twinning resulting in a change from a twinned martensite to a de-twinned martensite. This state allows the maximum elongation or compression strains in the material. The deformations remain because martensite is stable below M_f (Tadaki et al., 1988). When the material is heated to a temperature above A_f, the structure of the SMA reverts to its complete austenite phase, which displays the original cubic atomic arrangement. When the material cools, its temperature drops again below M_f, and the original twinned martensite arrangement appears. Figure 2.3 shows the microstructure change of an SMA exhibiting the shape memory effect.

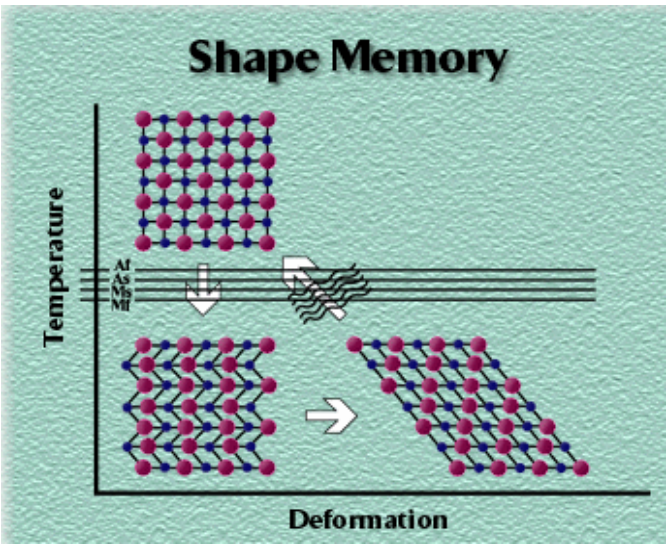

Figure 2.3. Microscopic process associated with the shape memory effect (NDC, 2001).

Superelastic Effect

The superelastic (or pseudo-elastic) effect refers to the ability of the material to regain its original shape after the removal of the stress which induced the deformation, with little residual effects (Barnes, 1999). For this to occur, the material must be at a temperature above A_f resulting in an austenitic material upon loading. When a stress is applied, the material experiences a phase transformation from austenite to stress-induced de-twinned martensite. The application of stress is equivalent to a decrease in temperature; however, the martensite is not stable in this state. As soon as the stress is removed, the material reverts back to the more stable high temperature austenite phase. Figure 2.4 (a) illustrates the superelastic effect. Figure 2.4 (b) shows an idealized stress-strain plot for a superelastic SMA showing the loading plateau stress (σ_L), the unloading plateau stress (σ_{UL}), the elastic or Young's modulus (E), the slope of the loading plateau

for the first 6% strain cycle, between 2% strain and 6% strain (K), and the residual strain (ε_r).

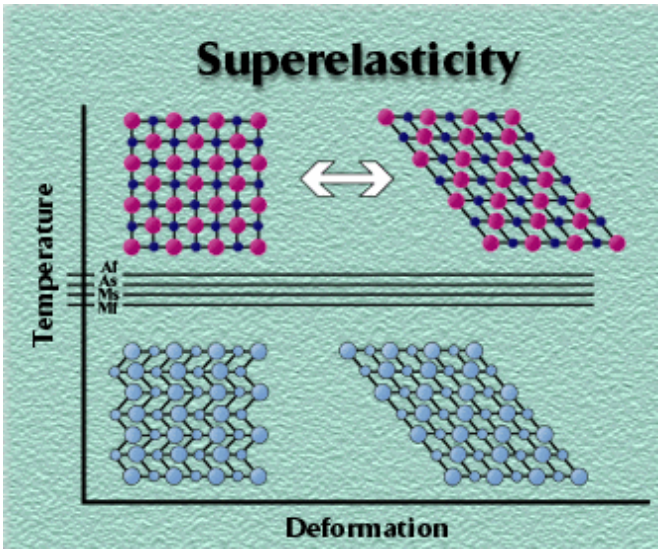

Figure 2.4 (a). Microscopic process associated with the superelastic effect (NDC, 2001).

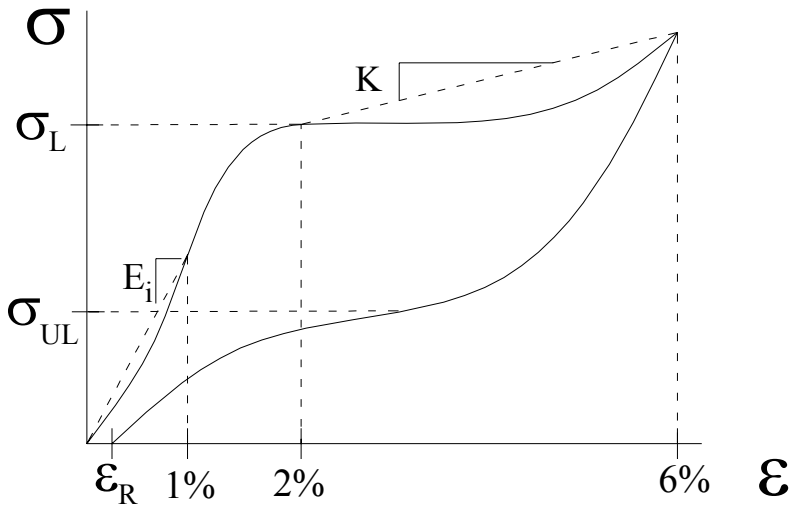

Figure 2.4 (b). Idealized stress-strain plot for superelastic SMAs.

Stress-Strain Relationship in Shape Memory Alloys

Unlike traditional materials, the behavior of shape memory alloys does not depend on stress and strain alone. Temperature is an important factor affecting the mechanical behavior of SMAs. Depending on the temperature, the behavior of the material can be characterized as linear superelastic, shape memory, or superelastic. If the temperature of the material is above M_d, above which martensite cannot be stress induced, it will exhibit higher strength and stiffness, but a smaller strain range where the material remains elastic resulting in permanent deformation upon unloading. Figure 2.5 shows the relationship between stress, strain and temperature with respect to the three behaviors associated with SMAs. The y-axis of the graph in the figure represents strain in %, the z-axis represents stress in MPa or ksi, and the x-axis represents temperature. The stress-strain curve on the left shows the behavior known as linear superelasticity, where the temperature of the material is greater than M_d. If the temperature of the material is in the austenite range (above A_f), the material exhibits superelasticity caused by the stress induced martensite. The shape of the stress-strain curve resembles a flag. If the temperature of the material is in the martensite range (below M_f), then the shape memory effect is present. Deformations can only be recovered by heating the material above A_f.

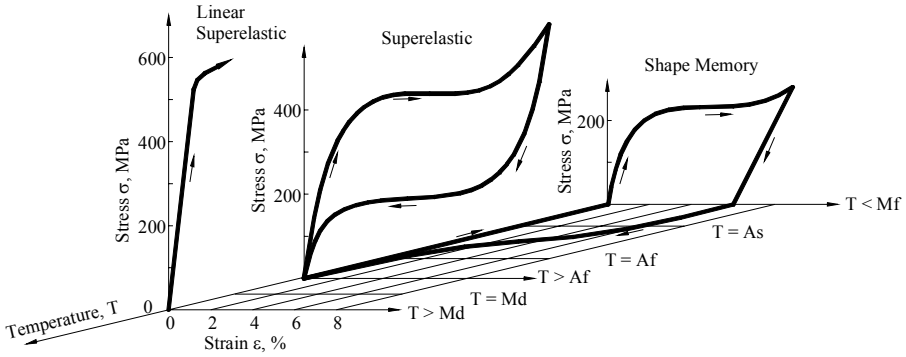

Figure 2.5. Typical stress vs. strain vs. temperature curves for Shape Memory Alloys (reproduced from Duerig et al., 1990).

Applications of Shape Memory Alloys

Shape memory alloys have found many applications in every day life. For the purposes of this study, the applications of SMAs have been divided into two main categories: non-seismic applications of SMAs and seismic applications of SMAs.

Non-Seismic Applications

There have been an increasing number of non-seismic SMA applications in the past decade. This can be attributed to a decrease in cost of SMAs, and an increase in reliability, availability, and research projects focusing on the use of SMAs for biomedical, aerospace, and commercial industries.

SMAs are being used in arterial stents, which are at a lower temperature when inserted into the artery and expand due to body heat. The stents are used to support and enlarge blocked arteries. They are also being used as orthodontic wire because they provide a constant corrective force on teeth (Asai and Suzuki, 2000). Figure 2.6 illustrates both applications. In the commercial industry, the superelastic properties of

SMAs have made them excellent materials to use in eyeglass frames, cell phone antennas and golf clubs, as shown in Figure 2.7 (Asai and Suzuki, 2000, Hsu et al., 2000, Takaoka et al., 2002). The aerospace industry has used SMAs in helicopter blades and aircraft wings to reduce noise and vibrations (Beauchamp et al., 1992; Chandra, 2001). Figure 2.8 illustrates these applications.

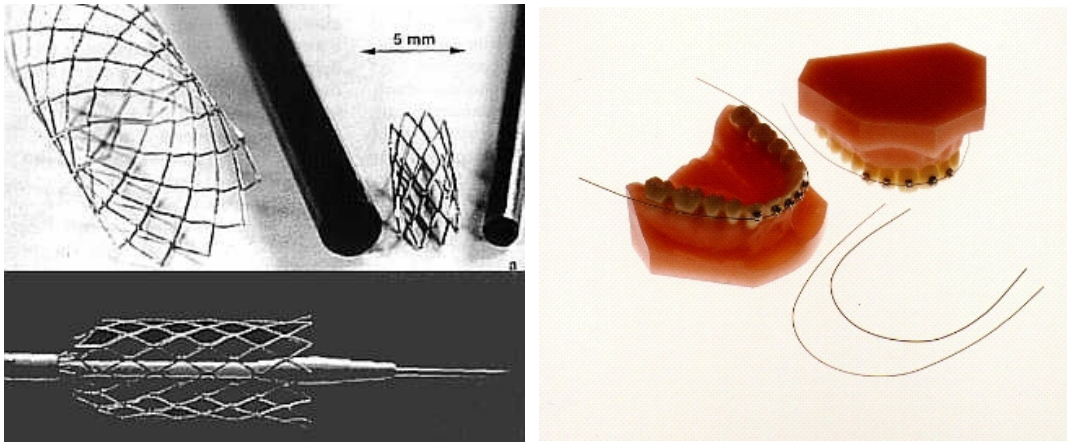

Figure 2.6. SMAs used in arterial stents and orthodontic braces (NDC, 2001).

Figure 2.7. Applications of SMAs: eyeglass frames, cell phone antennas, and golf clubs (NDC, 2001).

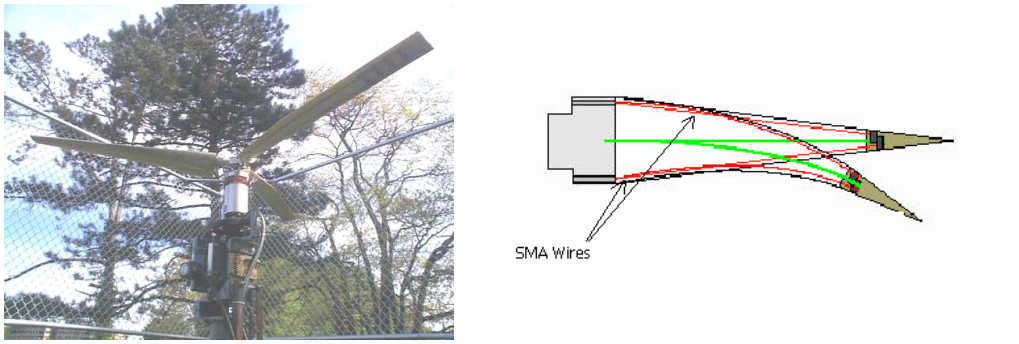

Figure 2.8. SMAs in aerospace industry: helicopter blades (Continuum Dynamics, 2000) and Smart aircraft wing (eSMART, 2002).

Taking advantage of the shape memory effect, SMAs are being used in anti-scalding valves and thermostatic mixing valves. The temperature dependence of SMAs allows them to control the amount of cold or hot water that is delivered to the user (Asai and Suzuki, 2000).

Seismic Applications

Because of their excellent energy dissipation capabilities and their recentering properties, SMAs show promise for use in seismic isolation. A study by Graesser and Cozzarelli (1991) identified the key characteristics that a damping material used in seismic isolation should exhibit: increased stiffness at large levels of strain, a significant energy-absorbing effect at low strains, and optimal damping properties for increased levels of strain and strain rate which are consistent with SMA properties. In the martensitic form, the shape memory effect produces a high damping capacity. In the austenitic form, the superelastic response provides an energy-absorbing effect with zero residual strain upon unloading (recentering capability). Although the strain rates applied

in this experiment are lower than those experienced during an earthquake, SMAs like NiTi can endure deformation to large strain levels without experiencing damage from plastic deformation. This results in an optimal recentering capability.

Many current studies are investigating the application of the damping properties and recentering potential of SMAs to seismic resistant design and retrofit. Dolce and Marnetto have developed a device where the SMA wire is always in tension (DesRoches and Smith, 2004). The NiTi wires provide recentering capabilities and the steel elements provide the energy dissipation effect (Dolce and Marnetto, 1999). Figure 2.9 shows the schematics of this device. Wesolowsky and Wilson (2004) discovered that systems implementing lead-rubber type bearings for isolation experience lower stresses and strains than systems that use SMAs for seismic protection. However, SMAs exhibit automatic recentering, which makes them a desirable alternative to lead-rubber type isolators (Wesolowsky and Wilson, 2004). A study by Ocel et al. (2002) investigated the use of martensitic NiTi rods to provide the primary moment-resisting capacity in a beam-column connection. After quasi-static and dynamic testing, the connection was found to exhibit a stable hysteresis for cyclical loads up to 4% interstory drift, which corresponds to a strain of 5% in the SMA. After the test, the NiTi rods were heated for approximately 8 minutes at 300°C. The rods recovered approximately 76% of their undeformed shape, and after being retested they showed a nearly-identical behavior to the original connection (Ocel et al., 2002). Figure 2.10 shows the test setup for this study.

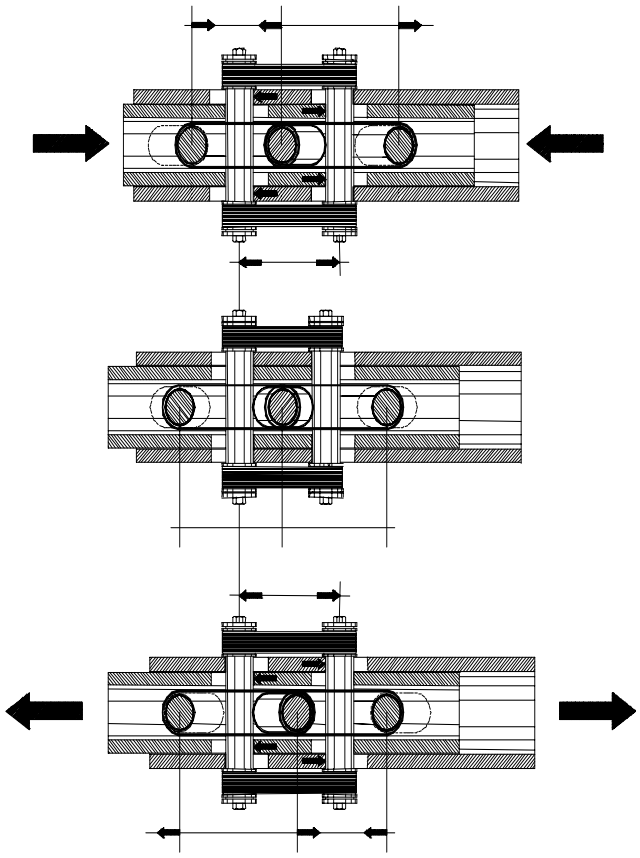

Figure 2.9. Schematics of SMA seismic device providing recentering and energy dissipation capabilities (Dolce and Marnetto, 1999).

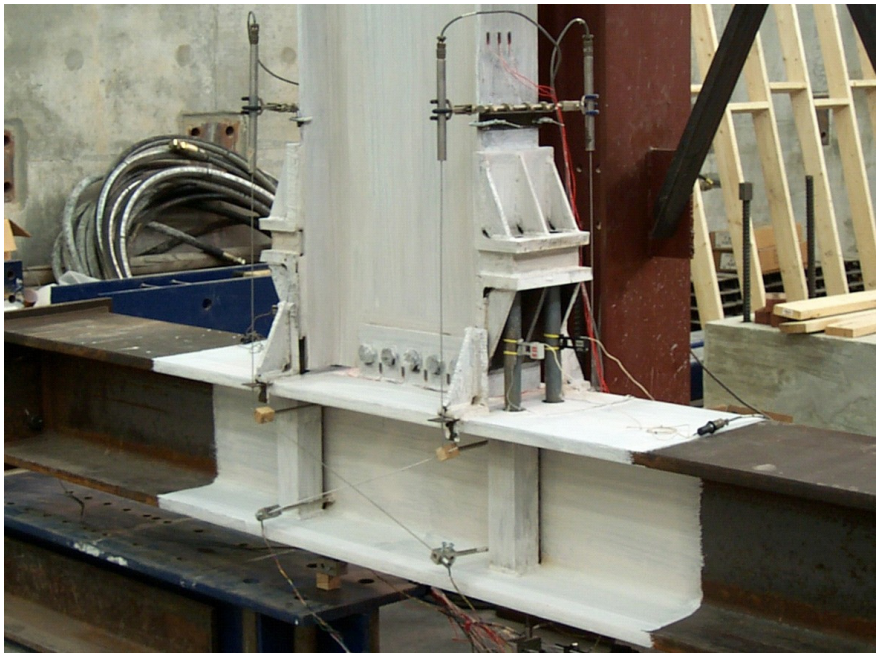

Figure 2.10. SMA beam-column connection test setup (Ocel et al., 2002).

Adachi and Unjoh (1999) subjected a simple NiTi plate to cyclical loading. It was found that the equivalent damping of the plate exhibiting the shape memory effect was 15%. The same experiment was performed with a superelastic NiTi plate, and the equivalent damping was reduced to less than 10%. The purpose of this study was to develop and test an SMA device that can absorb seismic energy and reduce seismic forces on a bridge. Another advantage of using SMAs as isolators is that their equivalent damping increases with an increase in loading amplitude, and that the energy is dissipated in the pseudo-elastic range (Adachi and Unjoh, 1999).

Currently, SMAs have been used for seismic isolation purposes in the rehabilitation of the S. Giorgio Church bell tower, the façade of the S. Feliciano Cathedral, and the Basilica of S. Francesco in Assisi, all located in Italy. These represent

the first efforts in the world to make use of SMA technology in seismic retrofit and rehabilitation of masonry structures (Indirli et al., 2001).

The S. Giorgio Church in Trignano, Italy was damaged following the Reggio Emilia and Modena earthquake on October 15, 1996. To increase the flexural resistance of the structure, four vertical prestressing tie bars containing SMA devices were placed in the interior corners of the bell tower (DesRoches and Smith, 2004). These devices limited the force applied to the masonry and maintained a constant compressive force on the masonry walls. In June 18, 2000, the church experienced another earthquake of similar magnitude as the previous one that damaged the structure in 1996. However, the structure remained intact because of the SMA restrainers. Figure 2.11 shows the SMA tendons used in the rehabilitation of the S. Giorgio Church bell tower.

Figure 2.11. Prestressed tendons used to retrofit the S. Giorgio Church bell tower (Castellano et al., 2001).

Shape memory alloys were used to repair the tympanums of the Basilica of S. Francesco after the September, 1997 earthquake. To reduce the seismic forces transmitted to the tympanums, they were connected to the roof with SMAs (Croci, 2001). Under high horizontal loads, the SMA stiffness reduces to allow controlled displacement of the masonry walls, but the stiffness increases if the structure is subjected to intense horizontal forces in order to prevent collapse (Croci, 2001).

Even though the use of SMAs in seismic resistant applications is still in its infancy, more studies are being performed with promising results. With sufficient evidence that SMAs are a good alternative to the traditional passive systems being used today, the near future promises many commercially available SMA devices developed

and marketed specifically for their use in seismic resistant design, rehabilitation, and retrofit.

Types of Shape Memory Alloys

The most widely studied SMAs have been Ni-based, Cu-based, and Fe-based alloys. Each of these types of alloys has desirable qualities, the most sought-after being cost-effectiveness while maintaining the key SMA properties of shape memory and superelasticity.

Nickel-Titanium Shape Memory Alloys

The most commonly used shape memory alloy in the U.S. is the binary NiTi alloy. This alloy has many valuable characteristics, including large recoverable strain capabilities, corrosion resistance, large hysteresis, stability, biocompatibility and exhibits excellent shape memory and superelastic functions (Barnes, 1999, Miyazaki and Kohl, 1998). The main drawbacks to NiTi alloys are their high manufacturing cost and the fact that they are difficult to manufacture and machine.

The most well-known type of NiTi SMA is Nitinol, which was developed in the 1960's by Buhler and Wiley of the U.S. Naval Ordnance Laboratory. This equi-atomic alloy consists of approximately 55% nickel and 45% titanium by weight. Since this type of alloy has been widely used in medicine and orthodontics, its properties are well documented. Table 2.1 presents a summary of the properties of Nitinol SMAs in both the austenite and martensite form.

Table 2.1. Properties of Nitinol SMAs.

Property	NiTi SMA	
	Austenite	Martensite
Physical Properties		
Melting Point	1240-1310^{o}C	
Density	6.45 g/cm^{3}	
Thermal Coefficient	0.28 W/cm^{o}C	0.14 W/cm^{o}C
Thermal Expansion Coeff.	11.3 x 10^{-6}/^{o}C	6.6 x 10^{-6}/^{o}C
Mechanical Properties		
Recoverable Elongation	up to 8%	
Young's Modulus	30-83 GPa	21-41 GPa
Yield Strength	195-690 MPa	70-140 MPa
Ultimate Tensile Strength	895-1900 MPa	
Elongation at Failure	5-50% (typically 25%)	
Poisson's Ratio	0.33	
Hot Workability	Quite good	
Cold Workability	Difficult due to rapid work hardening	
Machinability	Difficult, abrasive techniques preferred	
Hardness	30-60 Rc	
Weldability	Quite Good	
Electrical Properties		
Resistivity	100 μΩcm	80 μΩcm
Chemical Properties		
Corrosion Performance	Excellent (similar to stainless steel)	

NiTi SMAs are available in a number of manufacturing methods: rolling, sputtering, tubing, and drawing among others (Miyazaki and Kohl, 1998).

Ternary Nickel-Titanium Based Shape Memory Alloys

To reduce the cost of NiTi and improve its properties, a third metal is often added to the binary alloy (Barnes, 1999). Some of these metals include copper, aluminum, cobalt, vanadium, zirconium, niobium, chromium, and iron.

The addition of copper increases the workability of the alloy and its internal friction, decreases the Young's modulus (E), reduces the ageing effect, narrows the stress hysteresis, and stabilizes the transformation temperature – no large-scale shift in M_s is observed (Barnes, 1999, Bricknell et al., 1979, Gil and Planell, 1999, Mercier et al., 1982, Ranucci et al., 2000). With the addition of 10% copper, the alloy still exhibits the shape memory effect at low temperatures, and is pseudo-elastic at higher temperatures (Hsu et al., 2000).

Studies by Hsieh and Wu (1997) have shown that adding Al to Ni-rich NiTi alloys can prevent the growth of precipitants during ageing. Also, the maximum shape recovery increases with ageing time, and it is achieved on the specimen that exhibits the highest hardening. On this type of alloy, the permanent strains during deformation are reduced (Hsieh and Wu, 1997).

According to Hsu et al. (2000), TiNiCoV retains the shape memory effect at low temperatures and is superelastic at room temperature. It also exhibits good workability at different strain rates with higher temperatures. Adding cobalt and vanadium to NiTi

lowers the transformation temperature, which is dependent on the nickel content and the atomic percentage of vanadium (Hsu et al., 2000).

If zirconium is added to NiTi, the transformation temperature decreases initially, and then increases with an increase in Zr content. This alloy exhibits improved mechanical and shape memory properties when the Zr content is between 1 to 2 atomic %. Figure 2.12 shows the comparison in recovery rate between NiTi and NiTiZr. However, the alloy is too brittle for hot-forging and hot-rolling processing (Feng et al., 2002).

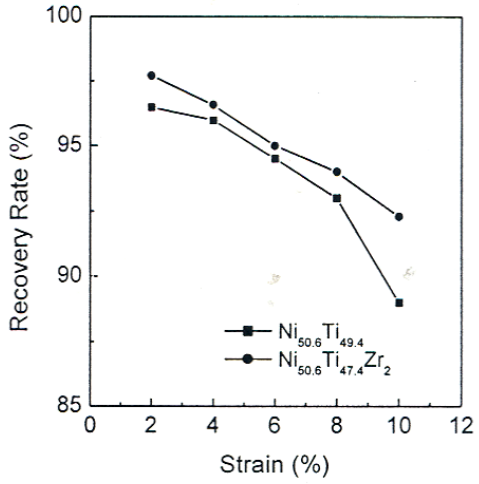

Figure 2.12. Recovery rate vs. strain for NiTi and NiTiZr alloys (Feng et al., 2002).

Adding Nb to binary NiTi increases the peak to peak transformation hysteresis (Siegert et al., 2002). This increase is directly proportional to the Nb content as shown in Figure 2.13.

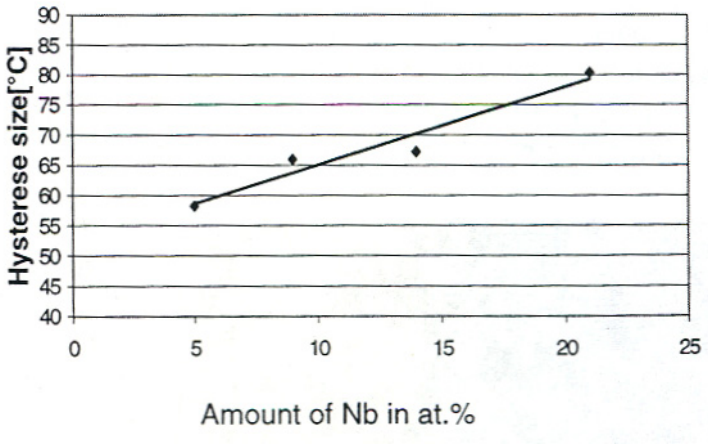

Figure 2.13. Width of peak to peak hysteresis vs. percent of Nb in a NiTiNb alloy (Siegert et al., 2002).

When 3% Fe is substituted for Ni in the binary NiTi alloy, there is an increase in the shape memory strain, the recovery rate, and the slip strength. There is also a reduction in the ductility and the transformation temperature (Hwang and Wayman, 1983, Jiang and Xu, 2000).

Copper Based Shape Memory Alloys

The most common copper based SMAs include CuZnAl, CuAlNi and CuAlMn. When compared to NiTi, the main advantage of these alloys is that they are relatively inexpensive, and that they can be fabricated using conventional metallurgical methods. Copper based SMAs are suitable for use in actuators, safety valves, and pipe couplings (AZoM.com). The good rigidity and high damping capacity of copper-based SMAs make them suitable for passive vibration control (Gotthardt et al., 2000). Properties of copper based SMAs have not been widely reported, but the Young's modulus and the yield strength increase for the high-temperature phase of the alloy (AZoM.com).

CuZnAl has a main advantage of low cost. However, the shape memory properties only allow for a maximum recoverable strain up to approximately 5% (Barnes, 1999). Alloys with lower aluminum content can be cold worked using interpass annealing. With increased aluminum content, the cold working process becomes more difficult. Also, this alloy can suffer from stabilization of the martensite if it is quenched rapidly in the martensite phase, therefore negating the shape memory effect (AZoM.com). Table 2.2 summarizes the main properties of CuZnAl.

Table 2.2. Properties of CuZnAl SMAs (from Perkins, 1981).

Property	**CuZnAl SMA**	
	Austenite	Martensite
Physical Properties		
Melting Point	$1000^{o}C$	
Density	$7.6\ g/cm^{3}$	
Thermal Expansion Coeff.	---	$16.6 \times 10^{-6}/^{o}C$
Mechanical Properties		
Recoverable Elongation	5 – 10%	
Young's Modulus	200 GPa	130 GPa
Yield Strength	200 MPa	120 MPa
Ultimate Tensile Strength	650 MPa	
Electrical Properties		
Resistivity	---	18 μΩcm

Some advantages of CuAlNi SMAs include a wide range of useful transformation temperatures, stability at higher temperatures, small hysteresis, and low cost

(AZoM.com, Barnes, 1999). CuAlMn is difficult to process, and can only be hot-worked.

Due to the large grain size, CuZnAl and CuAlNi tend to be brittle. Adding small quantities of other metals like boron, cesium, and cobalt can control this problem. However, caution must be exercised because this addition can compromise the shape memory characteristics (AZoM.com).

Iron Based Shape Memory Alloys

Among iron based SMAs, the most common are FeNi-based alloys and FeMnSiCrNi (also referred to as shape memory stainless steels). A study by Koval and Monastyrsky (1995) quantified the effects of adding several elements to FeNi-based alloys. The addition of Ti, Al, Nb, and Ta all lowered the martensite start temperature (Ms) and increased the hysteresis and the hardness. The addition of Co actually increased the M_s temperature and had no noticeable effect on the hysteresis and hardness. The addition of Co allows these alloys to become useful in practical applications (Koval and Monastyrsky, 1995).

Shape memory stainless steels offer good SME, mechanical properties, machinability and weldability. They are relatively inexpensive and provide good corrosion resistance. Their main drawback is that they only provide 2% - 3% reversible strain, which is adequate for pipe coupling applications but not sufficient enough for large-scale applications (Zhao, 2001).

Table 2.4 presents a summary of the advantages and disadvantages of the different SMAs.

Table 2.4. Advantages and disadvantages of different SMAs.

Alloy Type	Advantages	Disadvantages
Ni-based		
NiTi (Nitinol)	Large recoverable strain capabilities, corrosion resistance, biocompatibility, large hysteresis.	High manufacturing cost, difficult to manufacture and machine.
NiTiCu	Increased workability, stable transformation temperatures, reduced ageing effect, narrower stress hysteresis (good for recentering).	Decreased Young's modulus (E).
NiTiAl	Prevents growth of precipitants during ageing, reduced permanent deformation strains.	Shape memory effect decreases gradually in over-aged specimens.
TiNiCoV	Superelastic at room temperature, good workability, lower transformation temperature.	
NiTiZr	Improved mechanical and shape memory properties with Zr content between 1 – 2 at %.	Too brittle for hot-forging and hot-rolling processing.
NiTiNb	Increased peak to peak transformation hysteresis.	N/A
TiNiFe	Increased shape memory strain, recovery rate, and slip strength. Reduced transformation temperature.	Reduced ductility.
Cu-based		
CuZnAl	Low cost, can be fabricated using conventional metallurgical methods, good rigidity, high damping capacity.	Maximum recoverable strain up to approximately 5%, martensite stabilization possible, difficult to cold work if it has high Al content.
CuAlNi	Wide range of transformation temperatures, stability at higher temperatures, high damping capacity, low cost.	Difficult to process, can only be hot-worked, brittle.
Fe-based		
FeNiTi FeNiAl	Lower Ms, increased hysteresis, increased hardness	N/A
FeNiCo	Higher Ms.	Accelerated decomposition
FeMnSiCrNi	Good shape memory effect, good mechanical properties, easier to machine and weld, relatively inexpensive, corrosion resistant.	Reversible strain only 2% - 3%, not suitable for large-scale applications.

CHAPTER 3

TEST SETUP AND ANNEALING OF SPECIMENS

The purpose of this study was to compare the cyclic behavior of superelastic binary NiTi SMAs with that of superelastic ternary NiTiCr SMAs. The NiTi specimens were cold drawn and 40% cold worked. The surface was an oxide free pickled surface. The NiTiCr specimens were also cold drawn and 40% cold worked with an oxide free pickled surface. They contained 0.25 wt % Cr. All the specimens were obtained from Special Metals Corporation (http://www.specialmetals.com).

All testing was performed on specimens that are 0.085-in. in diameter, 6.5-in. in length, with a gauge length of 2.5-in. The testing apparatus consisted of a MTS 55 kip hydraulic testing machine fitted with circular MTS 647 hydraulic wedge grips as shown in Figure 3.1. In order to better facilitate gripping of the wire specimens, the SMA specimens were held in place by custom-made steel grips that are 2-in. in length, 0.75-in. in diameter, and have a circular groove in the middle that is 0.082-in. in diameter. Figure 3.2 shows a close-up of the specimen in the MTS testing apparatus. Figure 3.3 shows the grips and the specimen ready to be placed in the testing apparatus, and Figure 3.4 shows a close-up of the open grips.

Figure 3.1. MTS hydraulic testing machine.

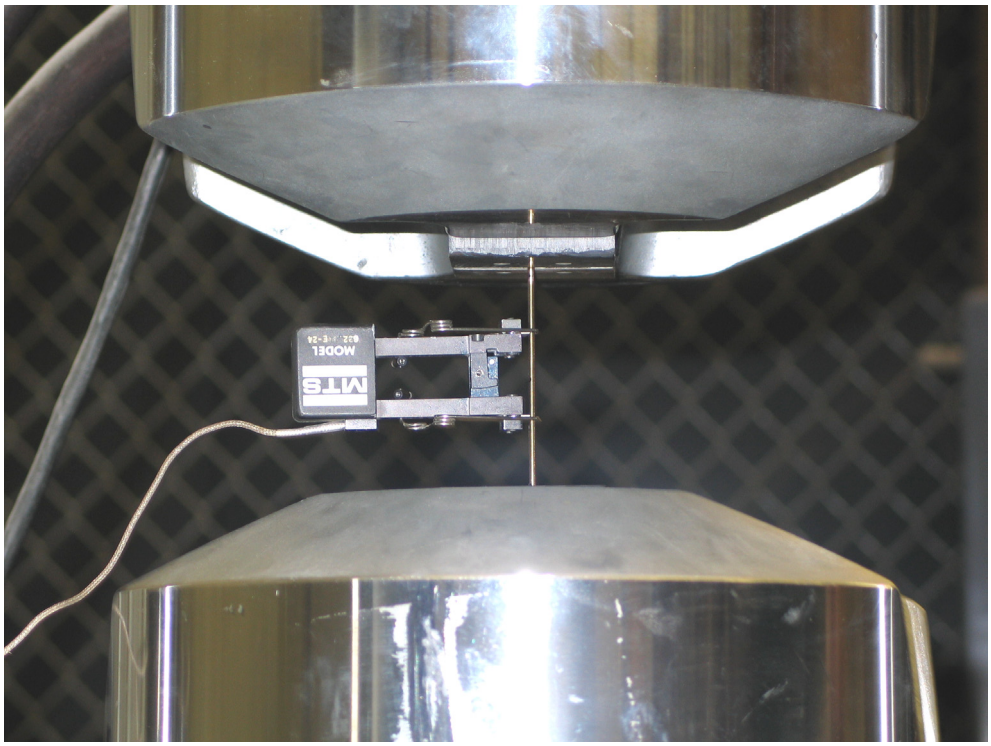

Figure 3.2. Close-up of SMA specimen in MTS testing apparatus.

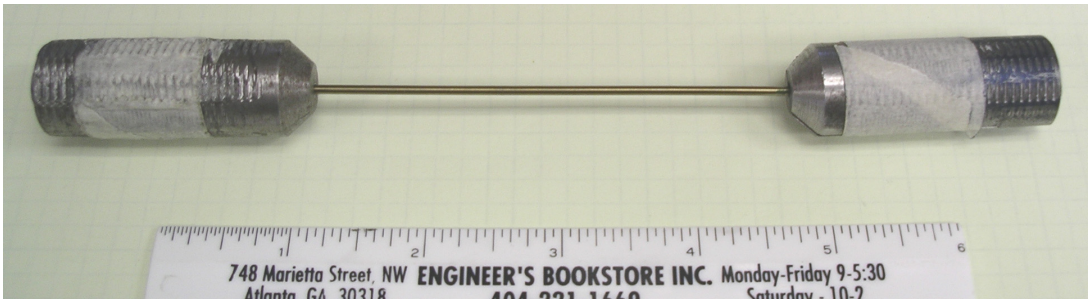

Figure 3.3. SMA specimen with grips.

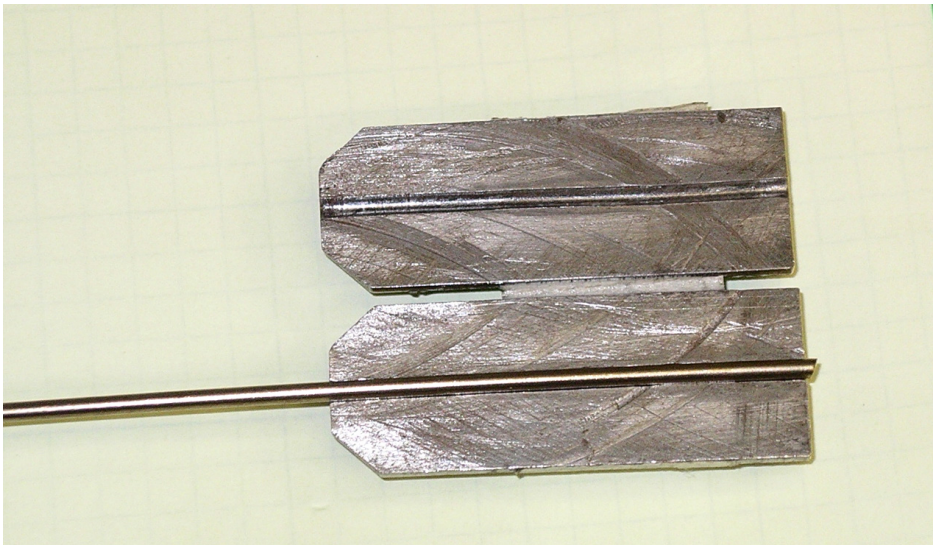

Figure 3.4. Close-up of SMA specimen in open grips.

The 55 kip internal load cell of the MTS testing apparatus was used to measure the load applied to the specimen. Cross head displacement provided a measure of the displacement. A 1.0-in. gage length extensometer was used to measure the strain in the specimen. The extensometer was placed in the mid-span of the specimen. The tests were run using an MTS TestStar controller running TestWare software and the loading protocol was as follows: all specimens were subjected to one cycle of 0.5%, 1%, 2%, 3%, 4%, and 5% strain. Then, six 6% strain cycles followed. Figure 3.5 shows the loading protocol for the SMA tests. For the annealing temperature tests, the specimens were loaded quasi-statically at 0.025 Hz (0.3%/s). An OPTIM Electronics system was used with TCS software for the data acquisition.

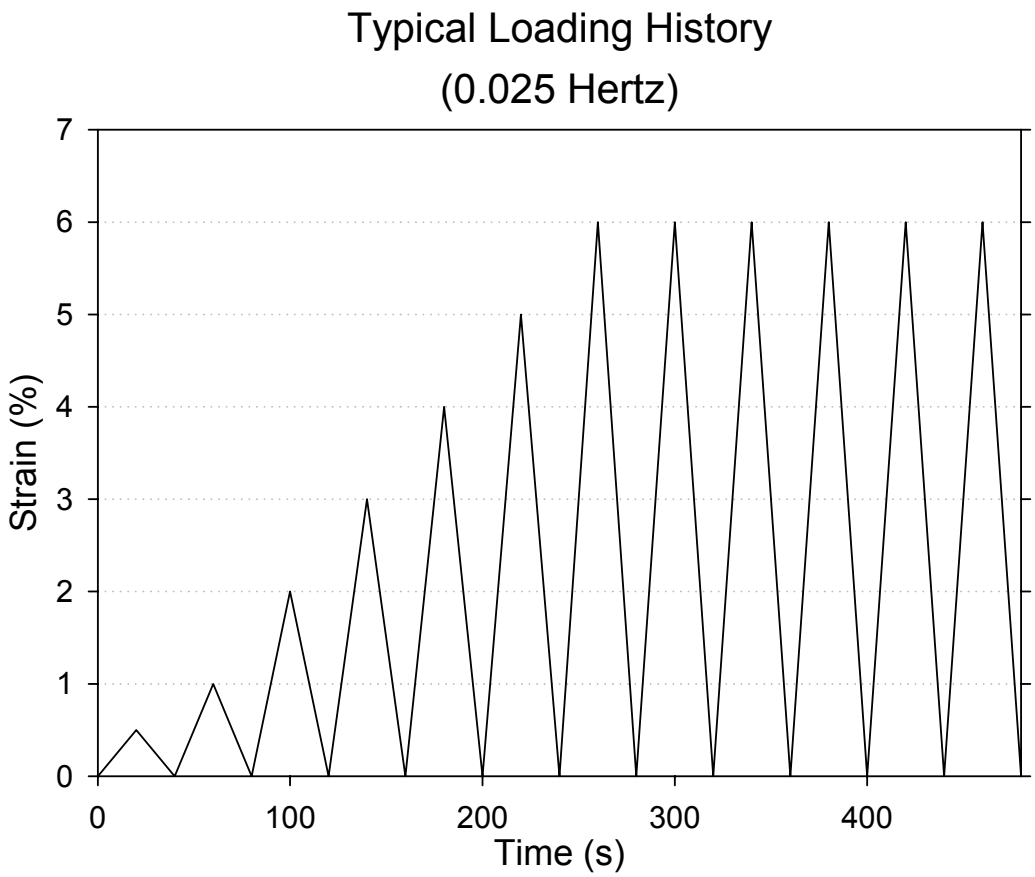

Figure 3.5. Typical loading history for SMA specimens (0.025 Hz).

Annealing Temperature Study

There is an observable effect of annealing temperature on the superelastic behavior of the alloy. Studies show that changes in annealing temperature can cause changes in the tensile properties of SMAs. Van Humbeeck and Liu (2000) researched the effect of annealing temperature on the damping capacity of NiTi. According to their study, the internal friction of NiTi at a low strain amplitude (3×10^{-5}) increases with increased annealing temperature up to 550°C, and then decreases. Therefore, the maximum damping capacity of the alloy in the martensite phase can be obtained by annealing the specimens at 550°C (Van Humbeeck and Liu, 2000). Huang and Liu

(2001) noted that the increase in annealing temperature produced a continuous decrease in the loading stress plateau. Figure 3.6 shows this decrease in loading stress plateau versus the annealing temperature. For a specimen that is 50.58% Ti and 49.42% Ni, the lowest plateau strain was obtained at an annealing temperature of 673 K (946º C) (Huang and Liu, 2001).

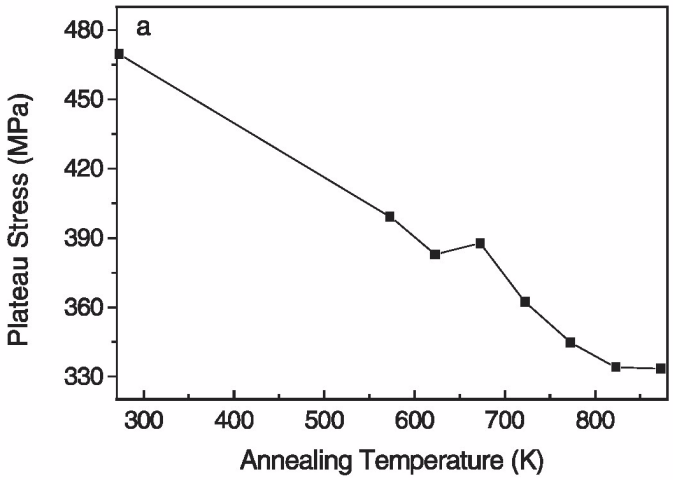

Figure 3.6. Decreased plateau stress vs. increasing annealing temperature (Huang and Liu, 2001).

A goal of the study was to determine the optimum annealing temperature for each alloy. The optimal annealing temperature was chosen such that it would minimize the residual strain in the specimen while still providing adequate energy dissipation during cyclic loading. The specimens were annealed in an oven and then immediately water quenched. Three new specimens for each type of alloy were tested at each of the different annealing temperatures to determine which was the most effective.

NiTi Annealing Study

The NiTi specimens were annealed for 30 minutes at 300°C, 350°C, 400°C, and 450°C. Figure 3.7 shows the stress-strain strain plots for each annealing temperature for one of the three specimens. The specimen annealed at 300°C does not exhibit the typical "flag-shaped" stress-strain curve associated with superelastic SMAs. This flag shape becomes more apparent in the specimens annealed at higher temperatures. With increased annealing temperature, the slope of the loading plateau for the first 6% strain cycle, between 2% strain and 6% strain (K), decreases. This decrease in slope is important because it lowers the stress in the SMA at higher strains, which in turn limits the forces in the structure.

With increasing annealing temperature, the residual strain increases as well. However, it is worth noting that the residual strain for all specimens remained under 1%, which is suitable for seismic applications that take advantage of the recentering capabilities of SMAs. Also shown in Figure 3.7 is the residual strain (ε_r) and the equivalent viscous damping (ζ_{eq}) for the first 6% strain cycle. The equivalent viscous damping is the amount of damping that accounts for all the energy dissipated by the system. A method for finding the equivalent viscous damping is to consider the energy dissipated in one strain cycle (Chopra, 2001). Equation 3.1 shows the method used to calculate the equivalent viscous damping in this study:

$$\zeta_{eq} = \frac{E_D}{4\pi E_{So}} \tag{3.1}$$

where E_D represents the energy dissipated by viscous damping in one cycle and E_{So} represents the strain energy (Chopra, 2001).

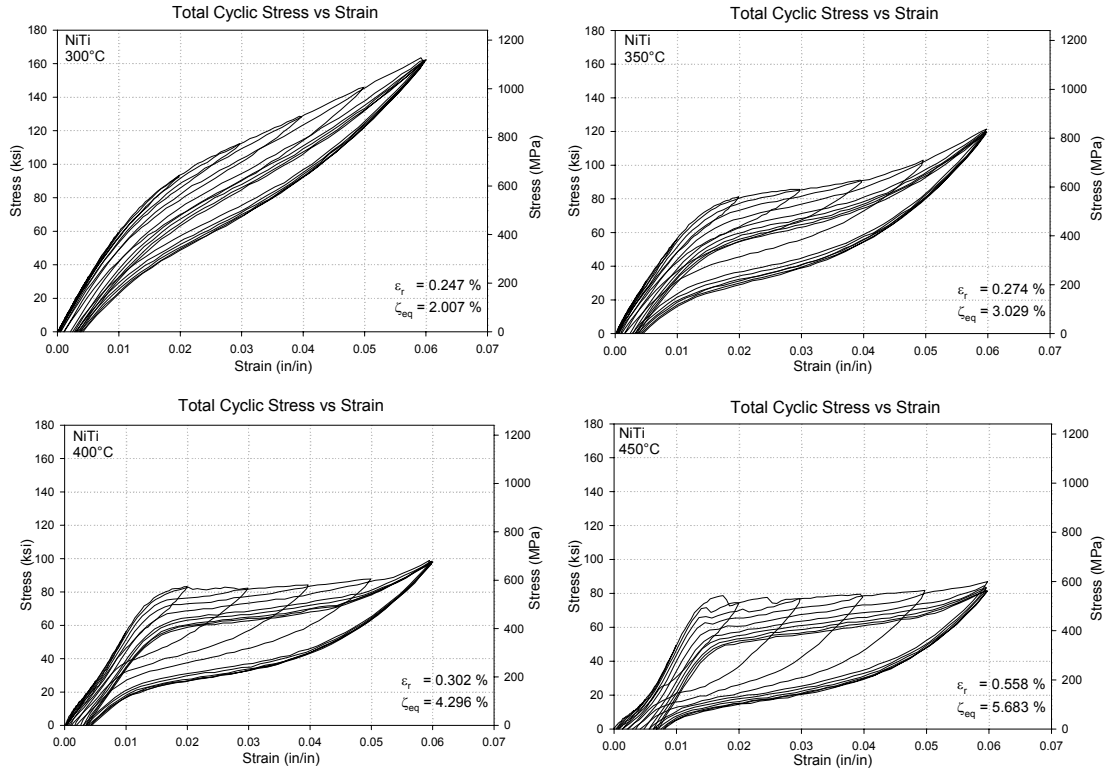

Figure 3.7. NiTi stress-strain plots for 300°C, 350°C, 400°C, and 450°C.

The maximum stress in the specimen decreased with an increase in annealing temperature, from approximately 160 ksi (1103 MPa) to approximately 87 ksi (600 MPa). This again happens because K decreases from 19.50 ksi/% strain for the NiTi specimen annealed at 300°C, to 12.50 ksi/% strain for the specimen annealed at 350°C, to 7.25 ksi/% strain for the specimen annealed at 400°C, to 6.50 ksi/% strain for the specimen annealed at 450°C. The size of the stress hysteresis (the area inside the stress-strain curve) tended to increase with increased annealing temperature. This indicates an increase in the energy dissipated by the specimen with an increase in annealing temperature.

The elastic modulus (Young's modulus E) was calculated for each cycle. Table 3.1 shows the average elastic modulus at 2% strain for each annealing temperature. It does not appear that there is a correlation between annealing temperature and elastic modulus.

Table 3.1. NiTi Average Elastic Modulus (E).

Annealing Temperature (°C)	**Average Elastic Modulus @ 2% Strain (ksi)**
300	6021
350	5532
400	5329
450	5534

The residual strain (ε_r) and equivalent viscous damping (ζ_{eq}) were calculated at each strain cycle for each specimen at the different annealing temperatures. Figure 3.8 shows the residual strain plots for each annealing temperature for all three specimens. From the results, it is clear that the specimens annealed at 300°C and 350°C retain the least amount of residual strain: less than 0.5% while the specimens annealed at 400°C and 450°C exhibit 0.7% and 0.8% residual strain, respectively.

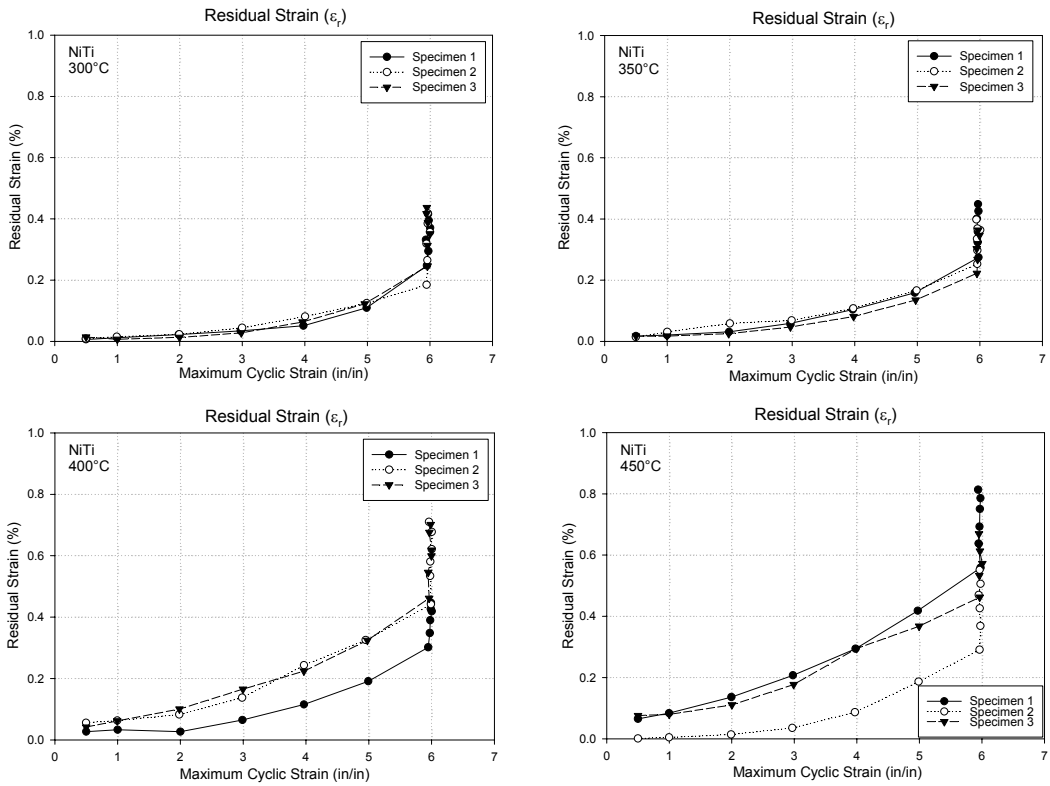

Figure 3.8. NiTi residual strain plots for all annealing temperatures.

For the purposes of this study, we are focusing on the development of residual strain in the specimen. However, it is also important for the SMA specimen to have good damping capabilities. Figure 3.9 shows the equivalent viscous damping plots for all the annealing temperatures. All specimens provide good damping, but the higher annealing temperatures provide more damping capacity. If only damping was being considered, the 450°C annealing temperature would be considered optimal with approximately 6% maximum equivalent viscous damping. However, this annealing temperature exhibits approximately 0.8% residual strain. The optimal annealing temperature chosen for this study is 350°C. It provides the least amount of residual strain while still maintaining a

good damping capacity and a classic flag-shaped hysteresis. This annealing temperature is used for all the specimens tested dynamically.

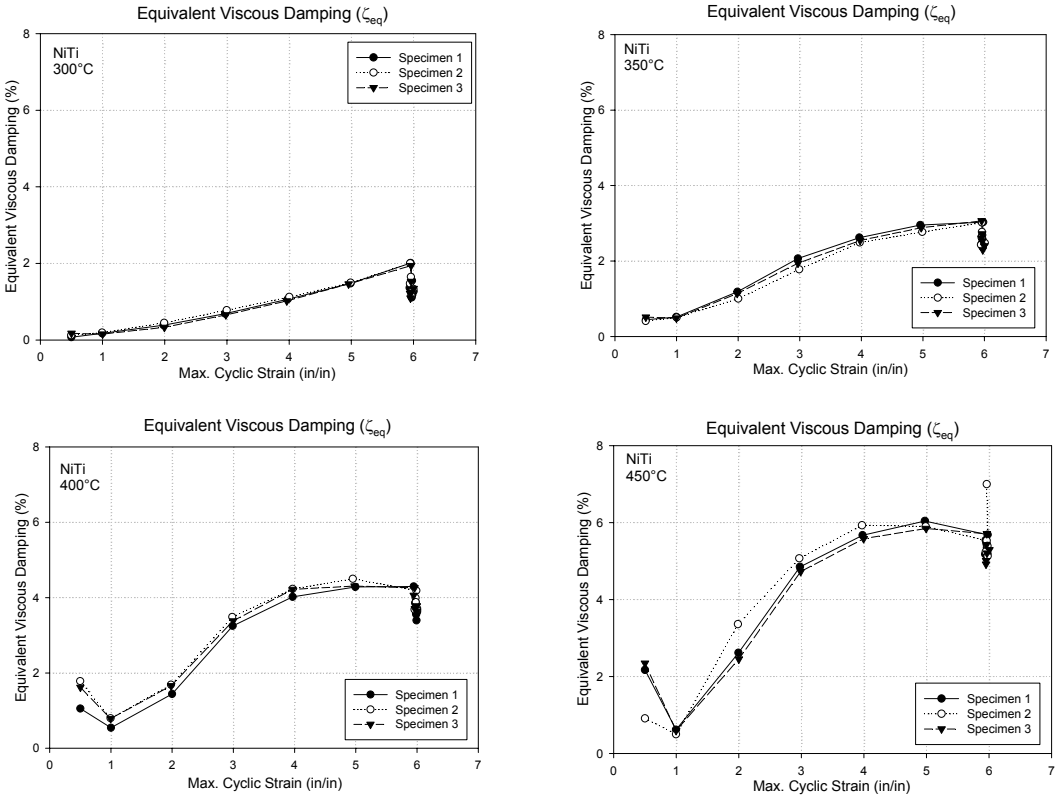

Figure 3.9. NiTi equivalent viscous damping plots for all annealing temperatures.

NiTiCr Annealing Study

The NiTiCr specimens were annealed for 15 minutes at 300°C, 350°C, 400°C, 450°C, and 500°C. After annealing, the specimens were immediately water quenched. Due to the loss of data during the testing of the second specimen annealed at 450°C, only two specimens were used for this annealing temperature. Figure 3.10 shows the stress-strain plots for one of the three specimens (two specimens for 450°C) for each annealing temperature, along with the residual strain (ε_r) and the equivalent viscous damping (ζ_{eq})

for the first 6% strain cycle. The specimens annealed at 300°C and 350°C do not display a sufficiently large stress hysteresis and retain a larger residual strain than the specimens annealed at 400°C, 450°C, and 500°C. Unlike NiTi specimens, the residual strains tend to decrease initially with increasing annealing temperature, but then increase again as the annealing temperature is increased past 450°C.

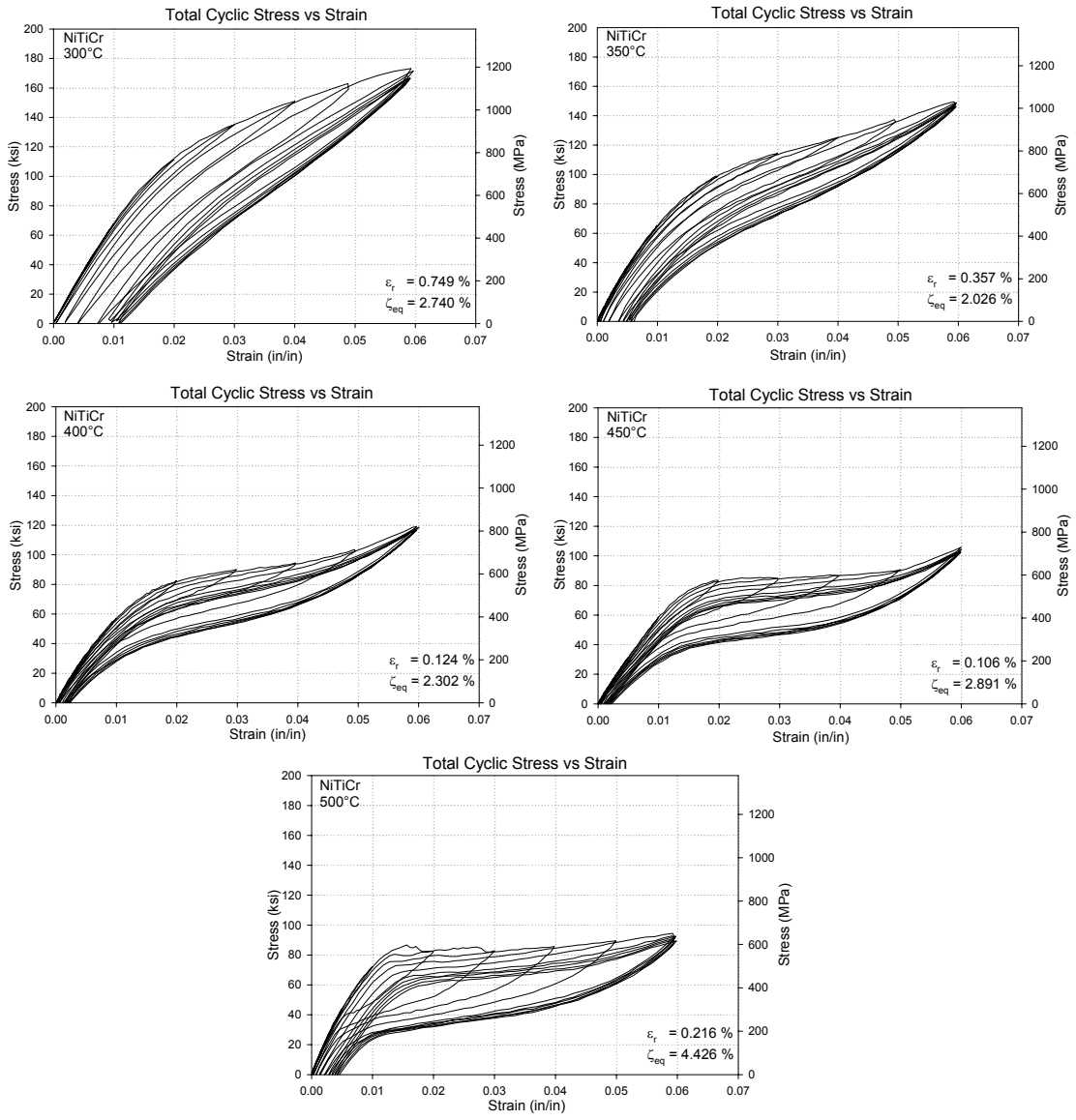

Figure 3.10. NiTiCr stress-strain plots for 300°C, 350°C, 400°C, 450°C, and 500°C.

As with NiTi specimens, the maximum stress in the specimen decreased with an increase in annealing temperature, from approximately 175 ksi (1206 MPa) to 95 ksi (655 MPa) for the 300°C case and the 500°C case respectively. This happens because K decreases from 21.75 ksi/% strain for the NiTiCr specimen annealed at 300°C, to 15.50 ksi/%strain for the specimen annealed at 350°C, to 11.75 ksi/% strain for the specimen annealed at 400°C, to 9.00 ksi/% strain for the specimen annealed at 450°C, to 6.25 ksi/%strain for the specimen annealed at 500°C. The maximum stress in the NiTiCr specimens was approximately 8% less than in the NiTi specimens.

The elastic or Young's modulus (E) was also calculated for the NiTiCr specimens, for each cycle at 2% strain. Table 3.2 shows a comparison of the average elastic modulus for each annealing temperature, for both NiTi and NiTiCr.

Table 3.2. NiTi and NiTiCr Average Elastic Modulus (E).

Annealing Temperature (°C)	**NiTi Average Elastic Modulus @ 2% Strain (ksi)**	**NiTiCr Average Elastic Modulus @ 2% Strain (ksi)**
300	6021	6778
350	5532	6327
400	5329	5732
450	5534	5942
500	N/A	7047

On average, the elastic modulus of NiTiCr appears to be slightly larger than the elastic modulus of NiTi. As with the NiTi specimens, there does not appear to be a direct correlation between annealing temperature and the average elastic modulus at 2% strain.

For NiTiCr, the residual strain (ε_r) and equivalent viscous damping (ζ_{eq}) were calculated at each strain cycle for each specimen at the different annealing temperatures.

Figure 3.11 shows the residual strain plots for each annealing temperature for all three specimens at a given annealing temperature (two specimens for 450°C). The specimens that exhibit the most residual strain are those annealed at 300°C, 350°, and 500°C, with a residual strain of 1%, 0.65% and 0.55% after four cycles of 6% strain, respectively. The lower residual strains were shown by the specimens annealed at 400°C and 450°C, with residual strains of 0.27% and 0.23% respectively. Based on the residual strain results, an annealing temperature of 450°C was selected as the optimal temperature for this research study.

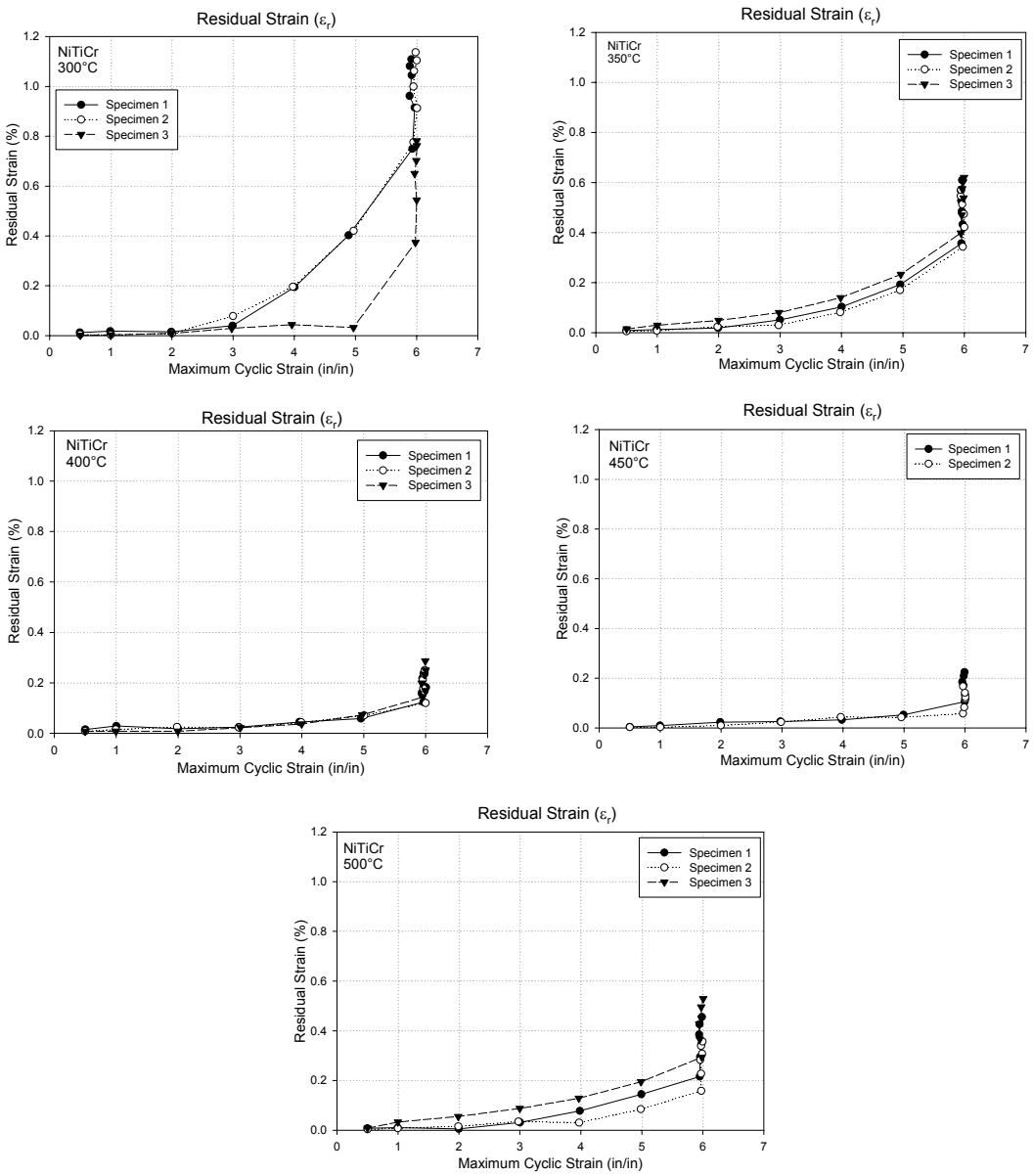

Figure 3.11. NiTiCr residual strain plots for all annealing temperatures.

While the annealing temperature that results in the lowest residual strain in the specimen was selected as the optimal temperature, it is important to check the damping capacity of all specimens. Figure 3.12 shows the equivalent viscous damping plots for all annealing temperatures with respect to loading cycle.

The highest damping is provided by the specimens annealed at 500°C. However, these specimens also exhibit large residual strains ranging from approximately 0.5% - 0.6%. The specimens annealed at 450°C, the annealing temperature selected for this study, exhibit approximately 2.5% equivalent viscous damping, which is in the same order as the damping provided by NiTi specimens annealed at 350°C.

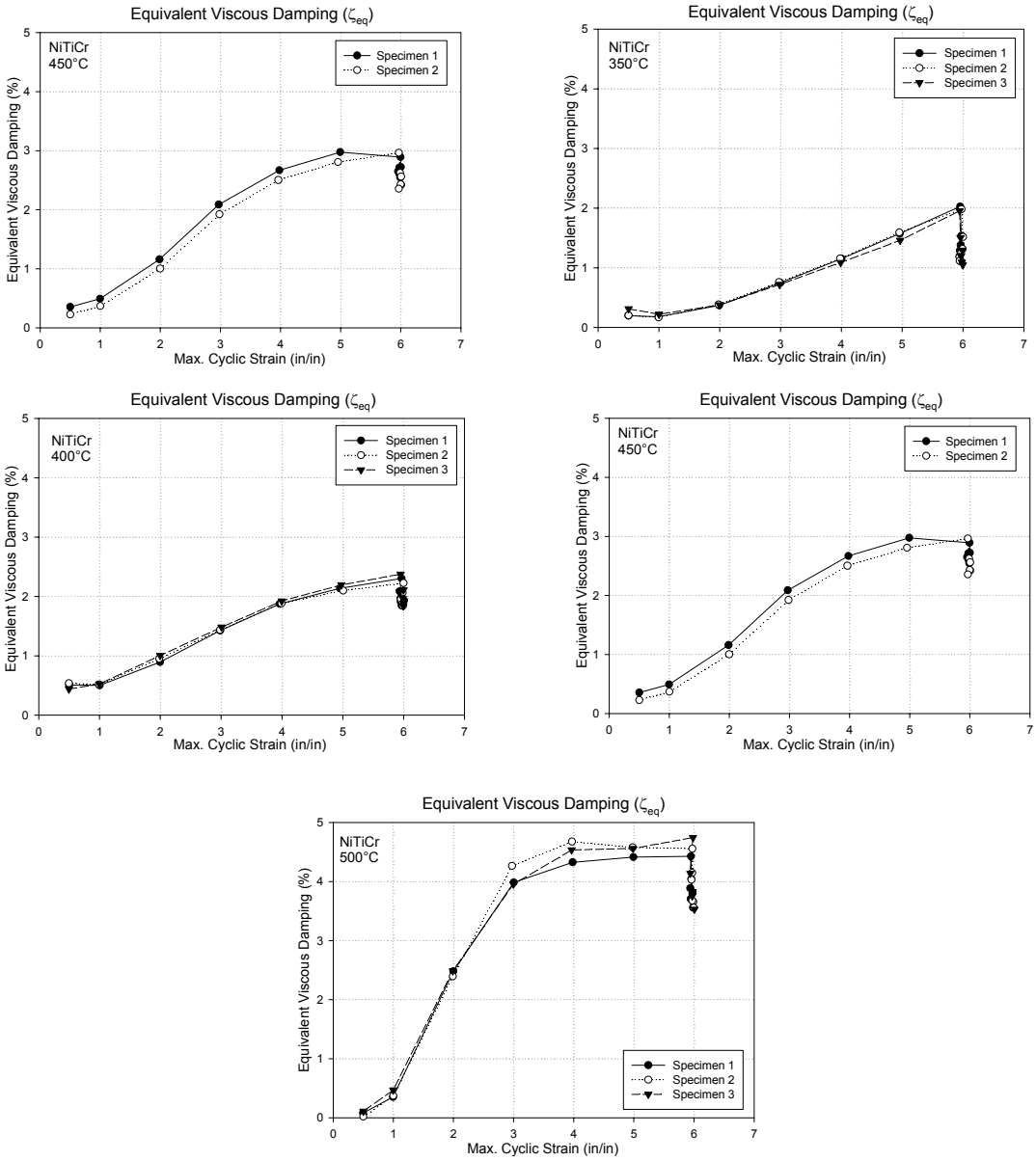

Figure 3.12. NiTiCr equivalent viscous damping plots for all annealing temperatures.

Properties of Annealed NiTi and NiTiCr

This section presents a comparison of the properties of NiTi and NiTiCr after annealing. The properties analyzed for the purposes of this study are elastic modulus (E), force transmission (K) loading plateau stress (σ_L), unloading plateau stress (σ_{UL}), equivalent viscous damping (ζ_{eq}), and residual strain (ε_r). These properties were obtained after testing the specimens quasi-statically at 0.025 Hz.

Elastic Modulus

The elastic modulus (E) was calculated at the 2% strain cycle for the average of the three NiTi specimens annealed at 350°C for 30 minutes and the average of the two NiTiCr specimens annealed at 450°C for 15 minutes. The average elastic modulus for NiTi was found to be 5532 ksi, while the average elastic modulus for NiTiCr was found to be 5942 ksi. The difference is approximately 7% and is not significant.

Loading and Unloading Plateau Stresses

The loading plateau stress, also known as the forward transformation stress, was calculated by determining the stress at 2% strain during loading representing the onset of the phase transformation. The unloading plateau stress was obtained by determining the stress at 3% strain during unloading representing the inflection point on the unloading curve. Figure 3.13 shows the average loading plateau for the three NiTi specimens annealed at 350°C for 30 minutes and the average loading plateau for the two NiTiCr specimens annealed at 450°C for 15 minutes. The NiTiCr specimens exhibit a higher loading plateau stress than the NiTi specimens. The slope of the loading plateau for the

first 6% strain cycle, between 2% strain and 6% strain (K), is 9.0 ksi/% strain for the NiTiCr specimens and 12.5 ksi/% strain for the NiTi specimens. This means that the NiTiCr specimens have a flatter loading plateau when compared with the NiTi specimens.

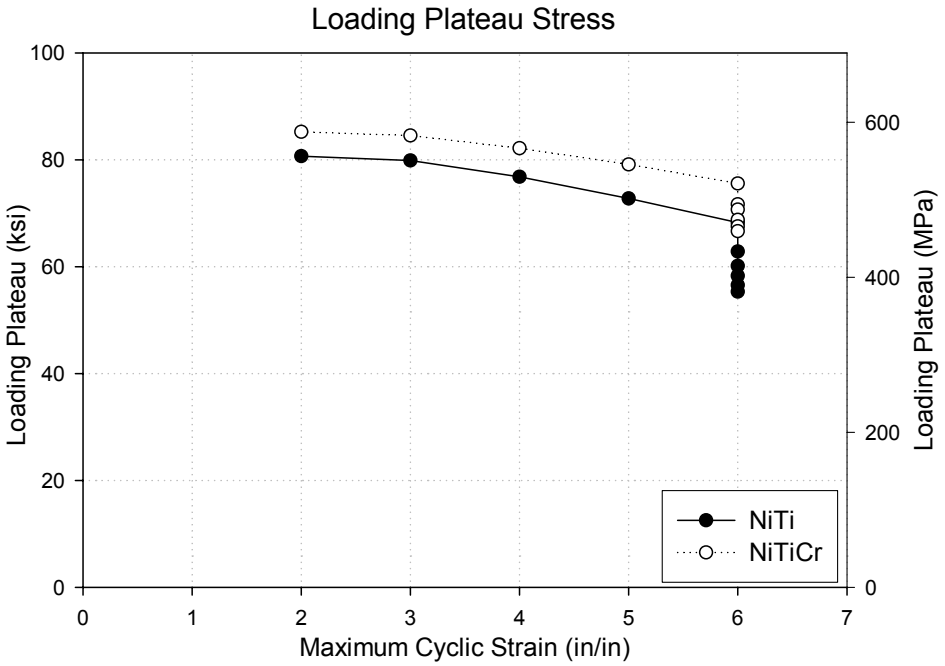

Figure 3.13. Loading plateau stress for NiTi and NiTiCr loaded at 0.025 Hz.

Figure 3.14 shows the average unloading plateau for the three NiTi specimens annealed at 350°C for 30 minutes, and the average unloading plateau for the two NiTiCr specimens annealed at 450°C for 15 minutes. The unloading plateau is almost identical for both the NiTi and the NiTiCr specimens for the 3% and 4% strain cycles. After the 4% strain cycle, the NiTiCr specimens exhibit a higher unloading plateau stress than the NiTi specimens.

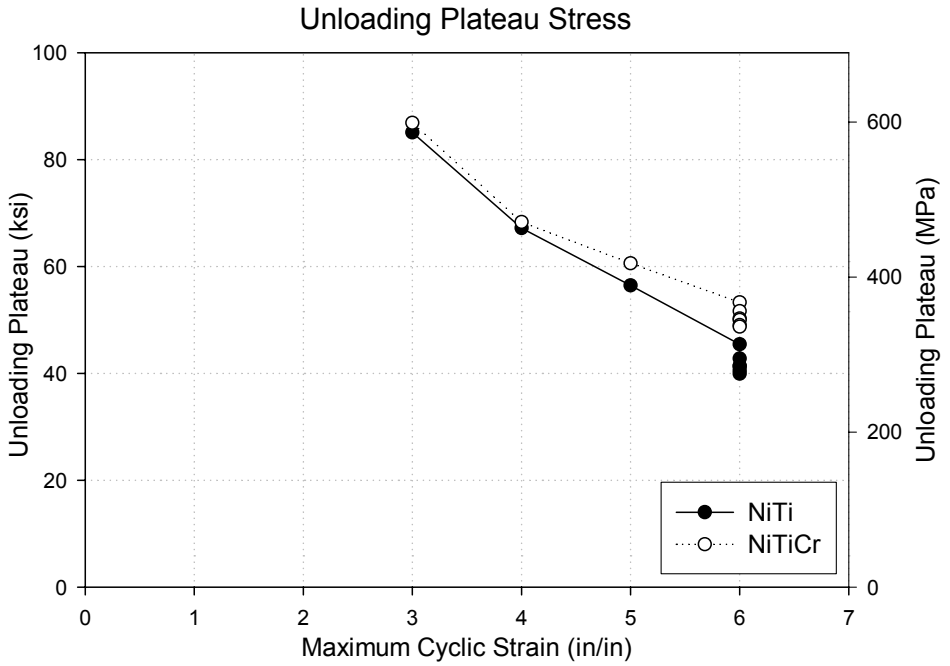

Figure 3.14. Unloading plateau stress for NiTi and NiTiCr loaded at 0.025 Hz.

Equivalent Viscous Damping

The equivalent viscous damping was calculated as described previously in Equation 3.1. The equivalent viscous damping was calculated starting with the 2% strain cycle, since at strains smaller than 2% specimens are essentially elastic and have no damping associated with them. Figure 3.15 shows the equivalent viscous damping for an average of the three NiTi specimens annealed at 350°C for 30 minutes, and an average of the three NiTiCr specimens annealed at 450°C for 15 minutes. It is worth noting that the equivalent viscous damping of NiTi and NiTiCr are essentially identical at approximately 3% for the first 6% strain cycle, and at approximately 2.5% for the final 6% strain cycle.

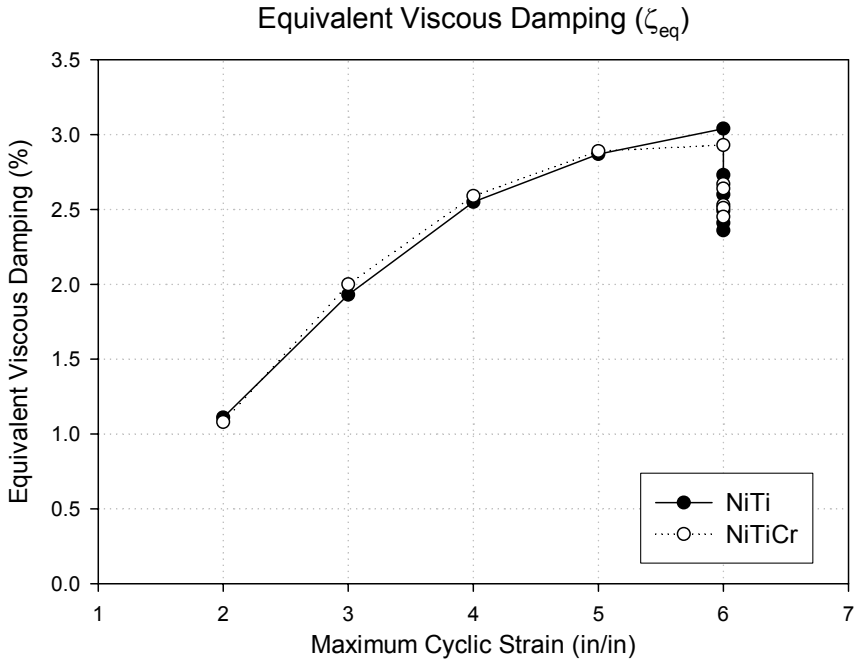

Figure 3.15. Comparison of equivalent viscous damping for NiTi and NiTiCr.

Residual Strain

When comparing the NiTi specimens annealed at 350°C with the NiTiCr specimens annealed at 450°C, it is worth noting that the NiTiCr specimens present slightly smaller (~0.2%) residual strains than the NiTi specimens (~0.4%) as shown in Figure 3.16. Up to the 2% strain cycle, the residual strains are very similar for both NiTi and NiTiCr specimens. However, starting with the 3% strain cycle, the increase in residual strain is more rapid for the NiTi specimens than for the NiTiCr specimens. In this figure, the residual strain values are shown for the average of the three NiTi specimens annealed at 350°C, and the two NiTiCr specimens annealed at 450°C.

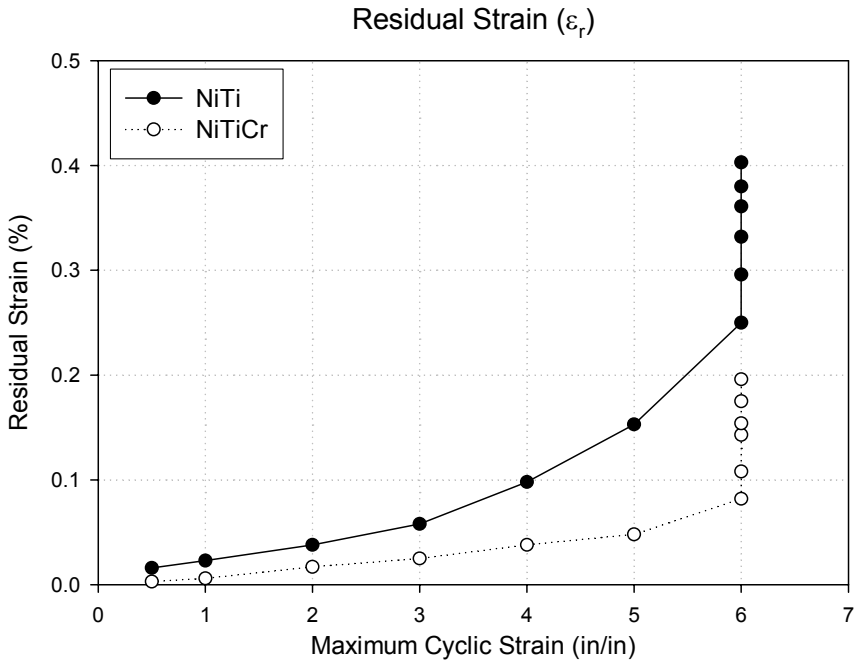

Figure 3.16. Comparison of residual strain for NiTi and NiTiCr.

In summary, NiTi and NiTiCr exhibit very similar behaviors when the specimens are annealed to each alloy's optimal temperature. The loading and unloading plateau stresses for both NiTi and NiTiCr were very close, with the NiTiCr specimens exhibiting slightly higher values for the loading and unloading plateaus. The equivalent viscous damping was essentially identical for both NiTi and NiTiCr. The only significant difference is in residual strain. NiTi specimens exhibit larger residual strains than NiTiCr specimens. It is possible that this difference is due to the fact that for NiTi specimens, the residual strain increases with increased annealing temperature, but for NiTiCr specimens, the residual strain decreases with increased annealing temperature up to an annealing temperature of 450°C. The behavior of the two different alloys can be used to explain the differences in residual strain.

CHAPTER 4

INFLUENCE OF STRAIN RATE ON PROPERTIES

This chapter presents the results of the study investigating the influence of strain rate on the superelastic properties of NiTi and NiTiCr shape memory alloys (SMAs). First, an overview of previous studies determining the influence of strain rate on SMA mechanical properties is presented. Next, the results of a comprehensive strain rate study are presented and compared to the results from previous studies.

Several studies have tried to quantify the influence of various strain rates on the different properties of SMAs. Those properties found to be affected by strain rate are the loading plateau, unloading plateau, equivalent viscous damping, and residual strain. Studies by Tobushi et al. (1998), Kolomytsev et al. (1998), Piedboeuf et al. (1998), and DesRoches et al. (2004) have found that an increase in strain rate leads to an increase in both the loading and unloading stress with the increase in the unloading stress being the most pronounced. This, in turn, leads to a narrowing in the stress hysteresis and an overall reduction in the energy dissipated when compared with the energy dissipated during quasi-static loading. Figure 4.1 shows a comparison of stress-strain plots for a 7.1-mm (0.28-in.) rod loaded quasi-statically at 0.025 Hz (0.3%/s), and dynamically at 0.5 Hz (6.0%/s) and 1.0 Hz (12%/s).

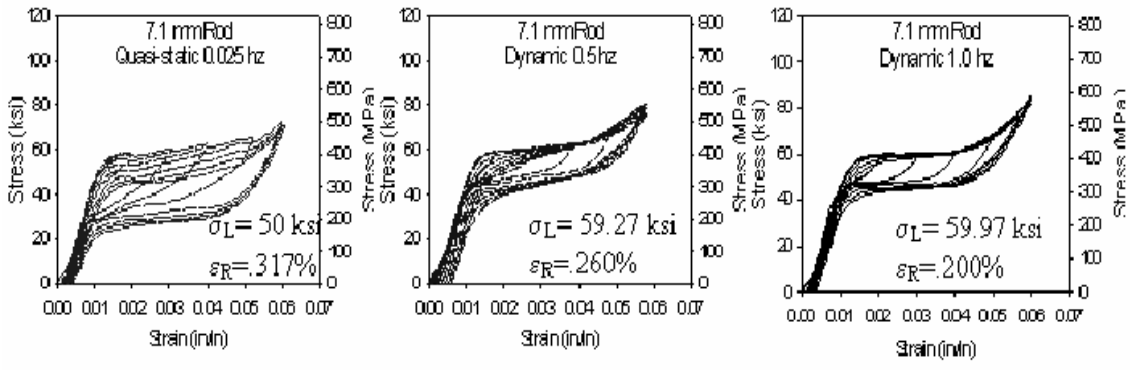

Figure 4.1. Stress-strain plots for 7.1-mm NiTi rod tested at 0.025 Hz, 0.5 Hz and 1.0 Hz (DesRoches et al., 2004).

Similarly, Dolce and Cardone (2001) and Wolons et al. (1998) observed that for frequencies higher than 0.1 Hz (1.0%/s) the energy dissipated decreased as the frequency was increased. However, at frequencies lower than 1.0%/s the energy dissipated increases initially.

Studies by Leo et al. (1993) found that an increase in strain rate leads to an increase in the hysteresis due to an increase in the temperature affecting the transition stresses. However, a study by Wu et al. (1996) found that when wires are tested in liquid to ensure that self-heating and self-cooling of the specimen does not occur during cyclic testing, the stress-strain hysteresis is not affected by strain rates between 0.01%/s and 1%/s. It is believed that the change in properties with increased strain rate is a function of the increased temperature in the specimen during the dynamic loading due to the exothermal and endothermal phase transformations during cycling (DesRoches et al., 2004). However, since most current applications of SMAs do not prevent an increase in temperature from occurring during dynamic loading, it is important to know how varying strain rates affect the mechanical properties of SMAs.

Test Setup

All of the specimens in this study were tested at room temperature (26°C) using a MTS 55 kip hydraulic testing machine fitted with circular MTS 647 hydraulic wedge grips as explained in Chapter 3. Two specimens of each type (NiTi and NiTiCr) were tested at the following dynamic strain rates: 6%/s (0.5 Hz), 12%/s (1.0 Hz), and 24%/s (2.0 Hz). These frequencies simulate those that are expected to occur during an earthquake.

The loading protocol used for the strain rate study was the same that was used for the annealing temperature study in Chapter 3. All specimens were subjected to one cycle of 0.5%, 1%, 2%, 3%, 4%, and 5% strain, followed by six 6% strain cycles.

Effect of Strain Rate on the Loading and Unloading Plateau

As previously discussed, it was expected that an increase in strain rate would cause a narrowing of the stress hysteresis. To quantify this behavior, the loading plateau, also known as the forward transformation stress, was calculated by determining the stress at 2% strain during loading representing the onset of the phase transformation. The unloading plateau for each cycle was obtained by determining the stress at 3% strain during unloading representing the inflection point on the unloading curve.

NiTi Loading and Unloading Plateau

For the NiTi specimens, a narrowing of the stress-strain hysteresis was observed. The loading plateau was calculated as the average of the three specimens tested at 0.025 Hz, the average of the two specimens tested at 1.0 Hz and 2.0 Hz, and only for the second

specimen tested at 0.5 Hz. Only one specimen tested at 0.5 Hz yielded usable results, since the first specimen experienced slipping in the grips while being tested. Figure 4.2 shows the average loading plateau stress at each cycle starting with the 2% strain cycle, for the 0.025 Hz, 1.0 Hz and 2.0 Hz loading rates, and the loading plateau stress for the second specimen tested at 0.5 Hz. Comparing the 0.025 Hz and 0.5 Hz cases, the loading plateau decreased slightly up to the 5% cycle, but then increased for each of the 6% cycles. A reason for this is that increased cycles tend to stabilize the properties of the SMA.

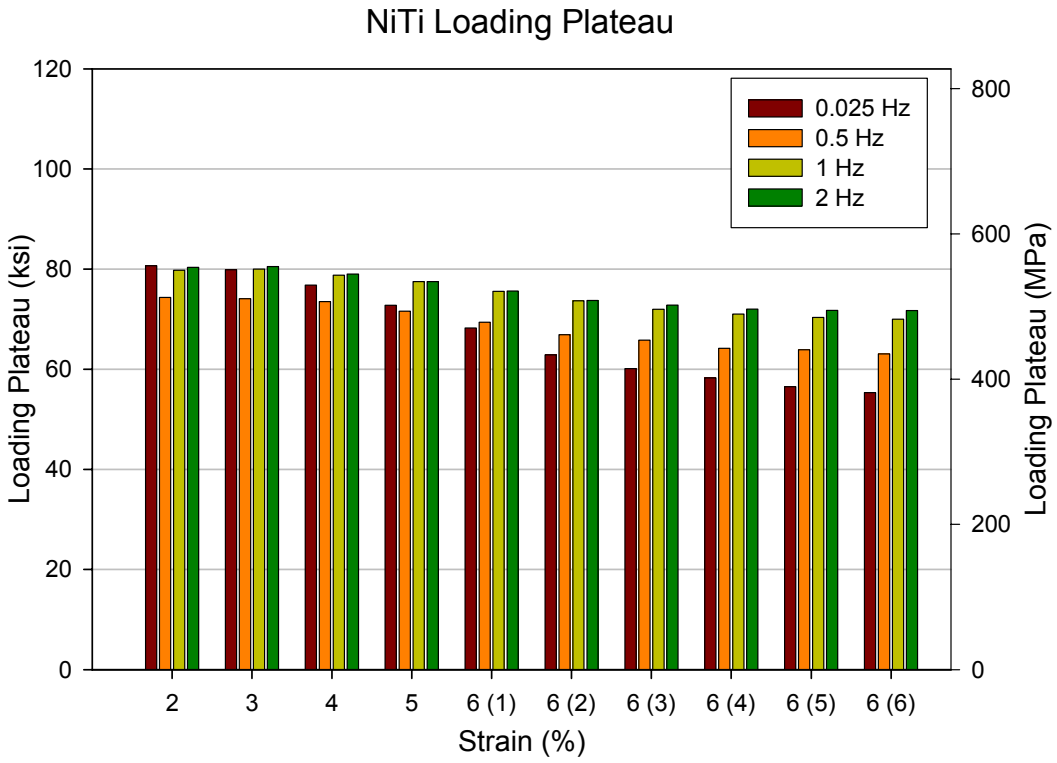

Figure 4.2. NiTi average loading plateau.

It is worth noting that for all strain cycles, the increase in loading plateau is less than 2% when going from 1.0 Hz to 2.0 Hz dynamic loading. This may be occurring because the effects of the temperature increase may not be influencing the behavior due to the higher loading rate. The overall increase in the loading plateau agrees with the findings from other studies as discussed above. Figure 4.3 shows the stress-strain plots for one of the specimens tested at 0.5 Hz, 1.0 Hz and 2.0 Hz at room temperature. The residual strain and the equivalent viscous damping shown in the stress-strain plots were calculated for the first 6% strain cycle.

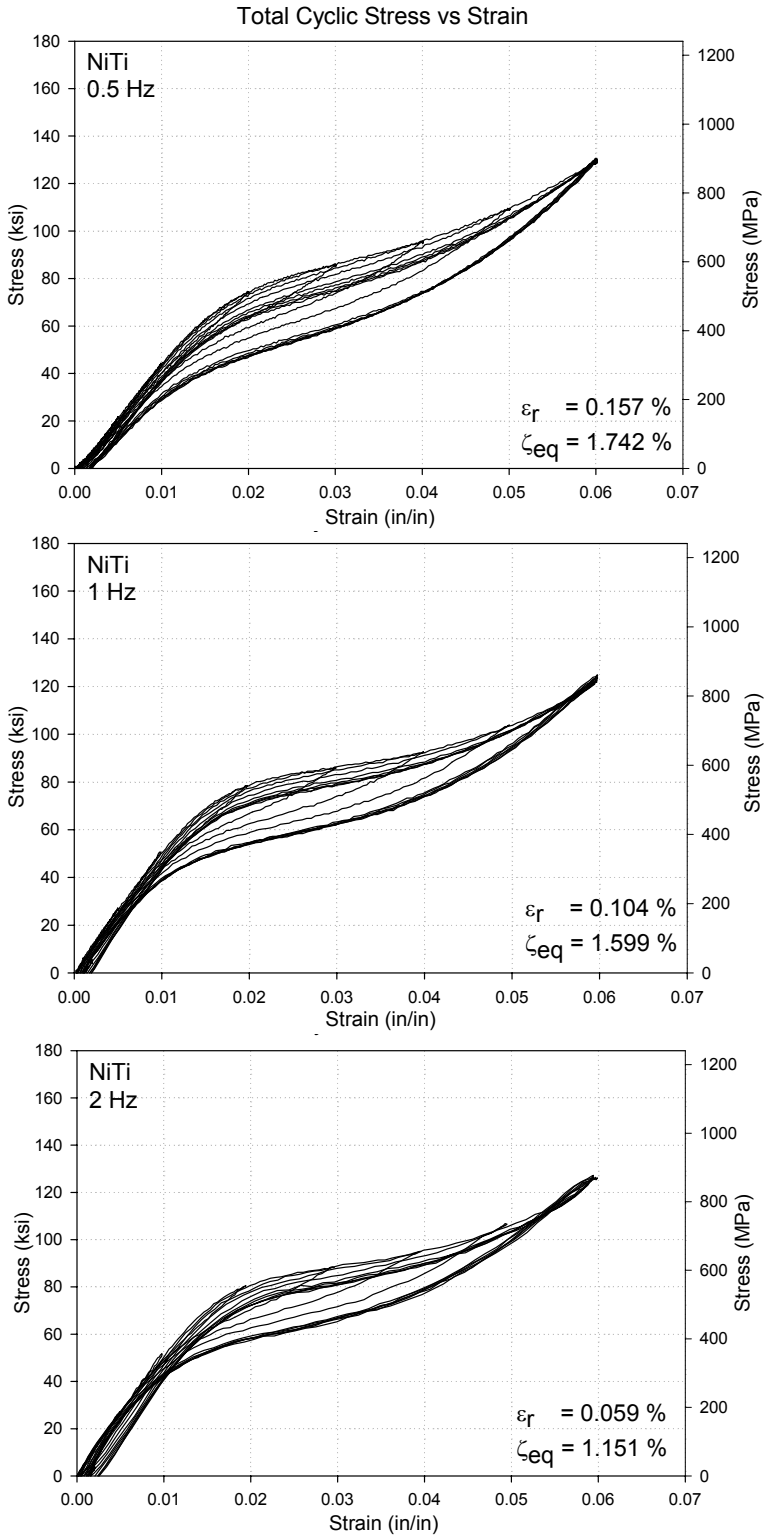

Figure 4.3. Stress-strain curves for NiTi loaded dynamically at 0.5 Hz, 1.0 Hz and 2.0 Hz.

The unloading plateau stress also increases with increased loading rates. However, the increase appears to be more rapid than that associated with the loading plateau stress. This results in a narrowing of the hysteresis observed in the stress-strain plots shown in Figure 4.3. Figure 4.4 shows the average unloading plateau at each cycle starting with the 3% strain cycle, for 0.025 Hz, 1.0 Hz and 2.0 Hz loading rates, and the loading plateau for the second specimen tested at 0.5 Hz. Between 0.025 Hz and 2.0 Hz, the unloading plateau increased slightly for the 3% cycle, with a significant increase in the unloading plateau stress with higher strain rates for the rest of the strain cycles.

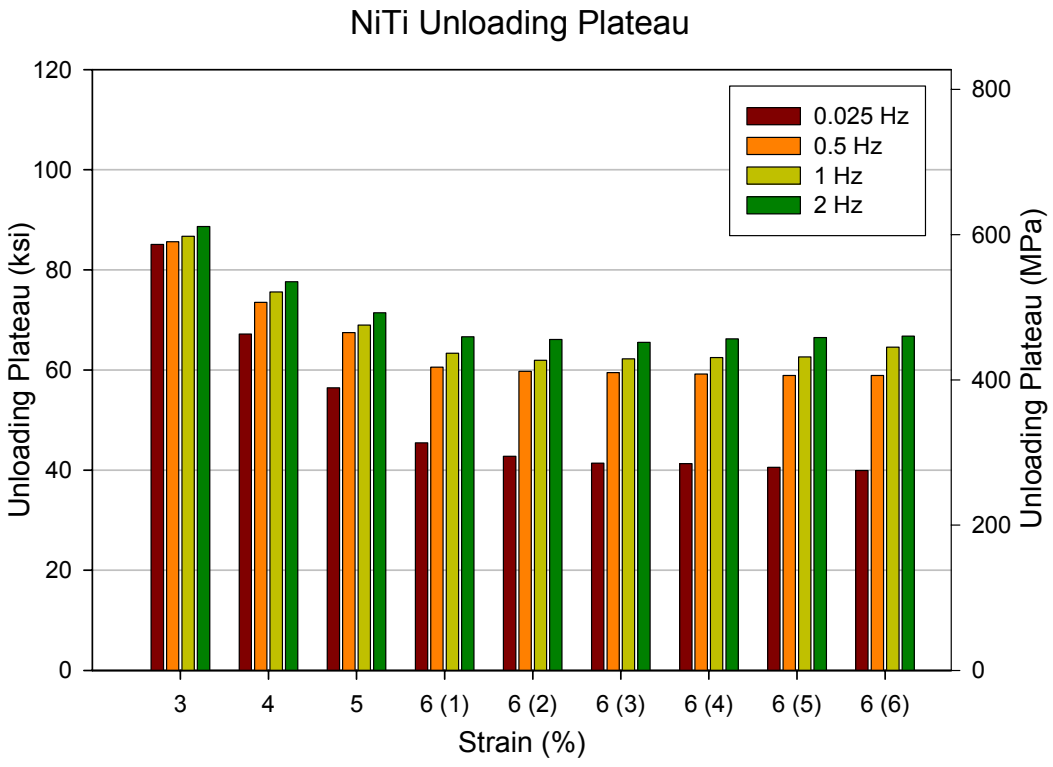

Figure 4.4. NiTi average unloading plateau.

Between the 0.025 Hz and 2.0 Hz cases, the loading plateau increased by 27 % for the last 6% strain cycle. However, the unloading plateau increased by 60%. This rapid increase in unloading plateau causes the narrowing of the stress hysteresis, and agrees with the expected results.

NiTiCr Loading and Unloading Plateau

For the NiTiCr specimens, the loading plateau was calculated for the average of the three specimens tested at 0.025 Hz, the average of the two specimens tested at 0.5 Hz and 2.0 Hz, and only for the second specimen tested at 1.0 Hz. Only one specimen tested at 1.0 Hz yielded usable results, since the first specimen only experienced three 6% strain cycles as opposed to six 6% strain cycles. Figure 4.5 shows the average loading plateau stress at each cycle starting with 2%, for the 0.025 Hz, 1.0 Hz and 2.0 Hz loading rates, and the loading plateau for the second specimen tested at 0.5 Hz. The loading plateau increased between the 0.025 Hz and the 1.0 Hz loading rates at each strain level, but then decreased slightly between the 1.0 Hz and the 2.0 Hz loading rates. Between the 1.0 Hz and 2.0 Hz dynamic test, the loading plateau decreases by approximately 1% - 2%. It is possible that the increased loading speed when testing at 2.0 Hz test prevents the effects from the increased specimen temperature from significantly affecting the mechanical behavior.

Figure 4.6 shows the stress-strain plots for one of the specimens tested at 0.5 Hz, 1.0 Hz and 2.0 Hz at room temperature. The residual strain and the equivalent viscous damping shown in the stress-strain plots were calculated for the first 6% strain cycle.

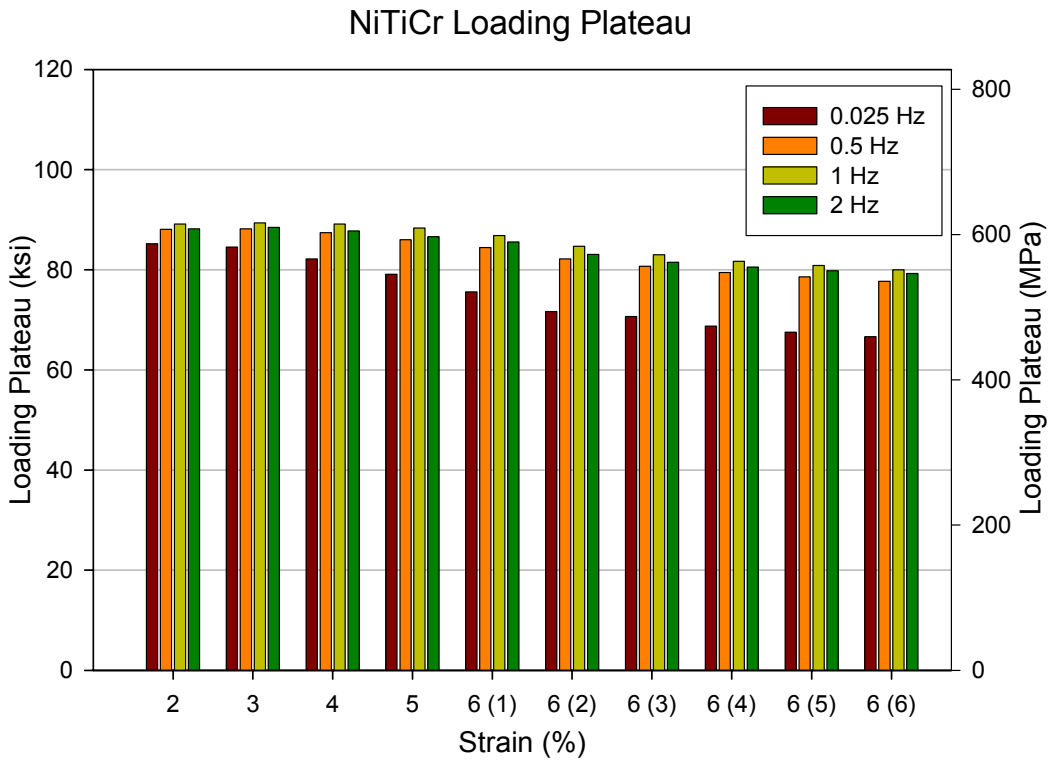

Figure 4.5. NiTiCr average loading plateau.

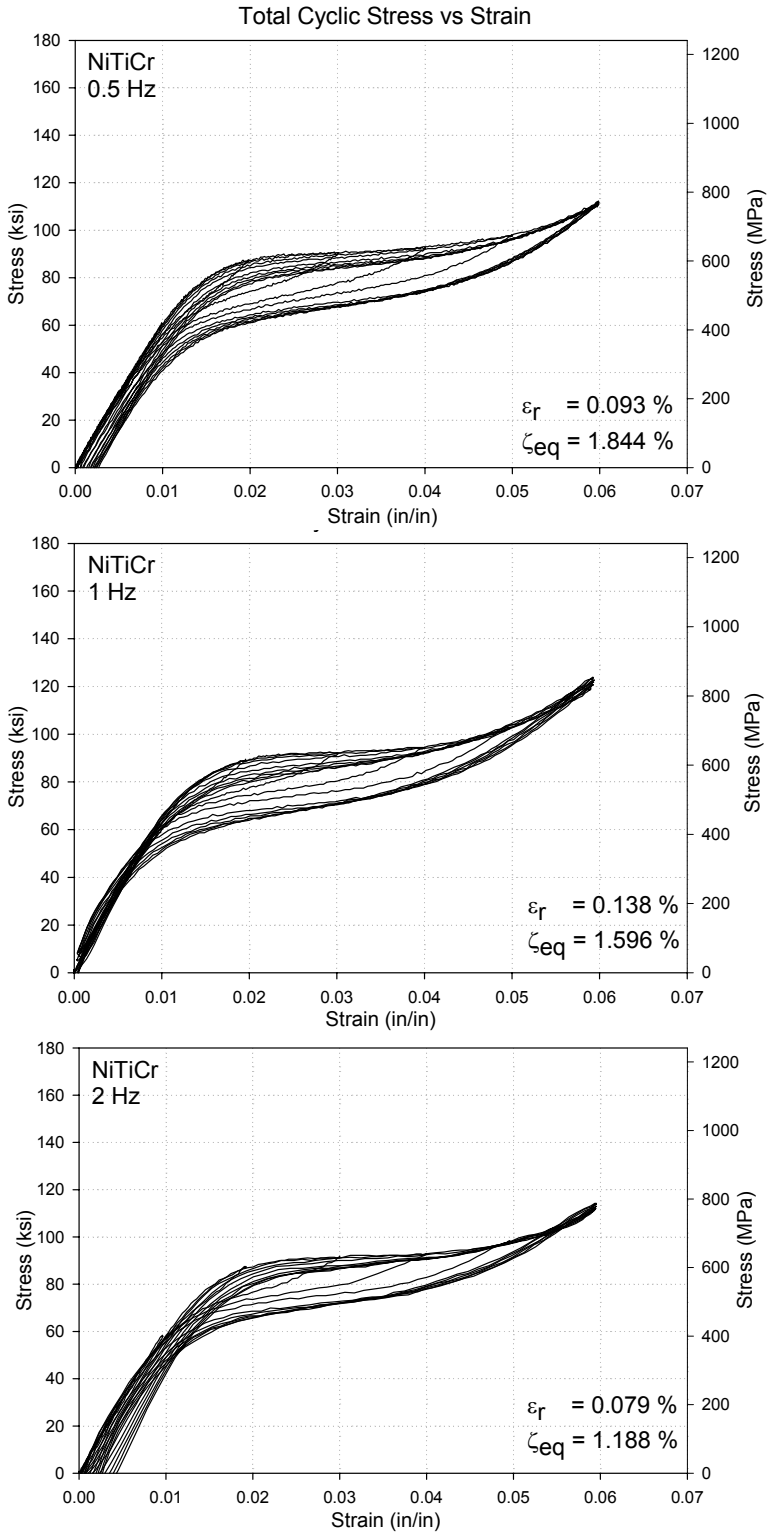

Figure 4.6. Stress-strain curves for NiTiCr loaded dynamically at 0.5 Hz, 1.0 Hz and 2.0 Hz.

The unloading plateau also increases with increased loading frequency, but the increase appears to be more rapid compared with the increase in the loading plateau as was seen with the NiTi specimens. This causes the narrowing of the hysteresis observed in the stress-strain plots shown in Figure 4.6. The average unloading plateau at each cycle starting with 3%, for the 0.025 Hz, 1.0 Hz and 2.0 Hz loading rates, and the loading plateau for the second specimen tested at 0.5 Hz are shown in Figure 4.7. Between 0.025 Hz and 2.0 Hz, the unloading plateau increased slightly for the 3% strain cycle with further increases found during the subsequent strain cycles.

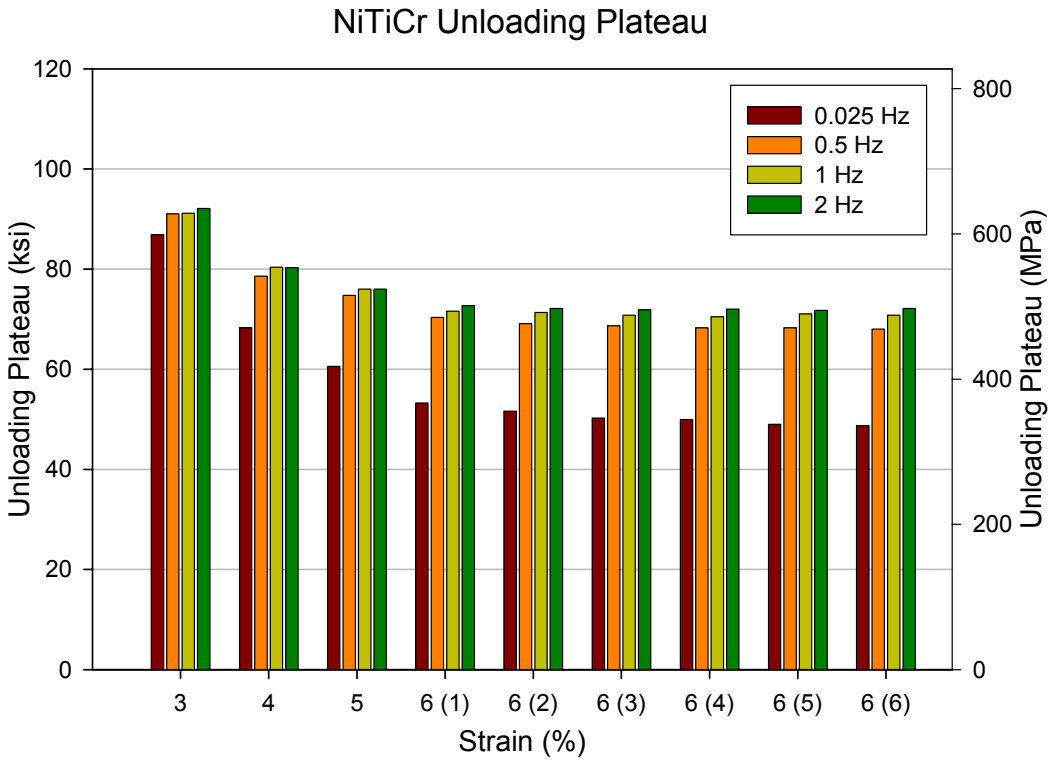

Figure 4.7. NiTiCr average unloading plateau.

Comparing the change in loading plateau versus the change in unloading plateau, it is obvious that the unloading plateau increases much more rapidly (~ 45%) than the loading plateau (~ 18%) between the 0.025 Hz loading rate and the 2.0 Hz loading rate, for the last 6% strain cycle. This results in a narrowing of the stress hysteresis, which results in a decrease in the energy dissipated by the sample. The effect of strain rate on energy dissipation is discussed later in the chapter.

Changes in Loading and Unloading Plateau: NiTi vs. NiTiCr

Comparing the changes in loading plateau stress between the NiTi specimens and the NiTiCr specimens between the 0.025 Hz and 2.0 Hz loading rates, one can observe that the increase in the loading plateau with increased loading frequency is more pronounced for the NiTi specimens starting with the second 6% strain cycle. Overall, the loading plateau increases by 30% between the 0.025 Hz and 2.0 Hz loading frequencies, for the NiTi specimen in the last 6% strain cycle, while the loading plateau increase by approximately 19% for the NiTiCr specimen in the last 6% cycle between 0.025 Hz and 2.0 Hz. Figure 4.8 presents a comparison of the percent change in loading plateau for the NiTi specimens and the NiTiCr specimens for the six 6% strain cycles, calculated between the 0.025 Hz quasi-static loading and the 2.0 Hz dynamic loading.

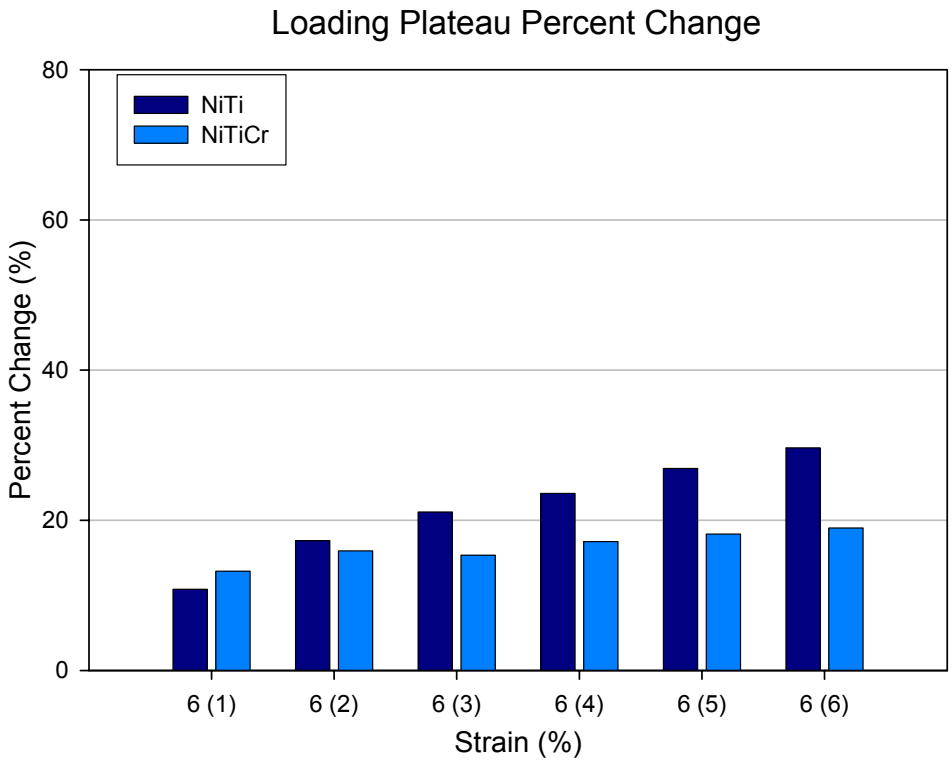

Figure 4.8. NiTi and NiTiCr loading plateau percent change between 0.025 Hz and 2.0 Hz cases.

For the unloading plateau, the difference between the NiTi specimens and the NiTiCr specimens is even more pronounced. Overall, the unloading plateau increases by 67% for the NiTi specimen in the last 6% strain cycle, while the unloading plateau increased by about 48% for the NiTiCr specimen in the last 6% cycle. Figure 4.9 shows a comparison of the percent change in unloading plateau for the NiTi specimens and the NiTiCr specimens for the six 6% strain cycles. From these results, it is expected that the NiTi specimens will have a greater reduction in equivalent viscous damping with increased strain rate.

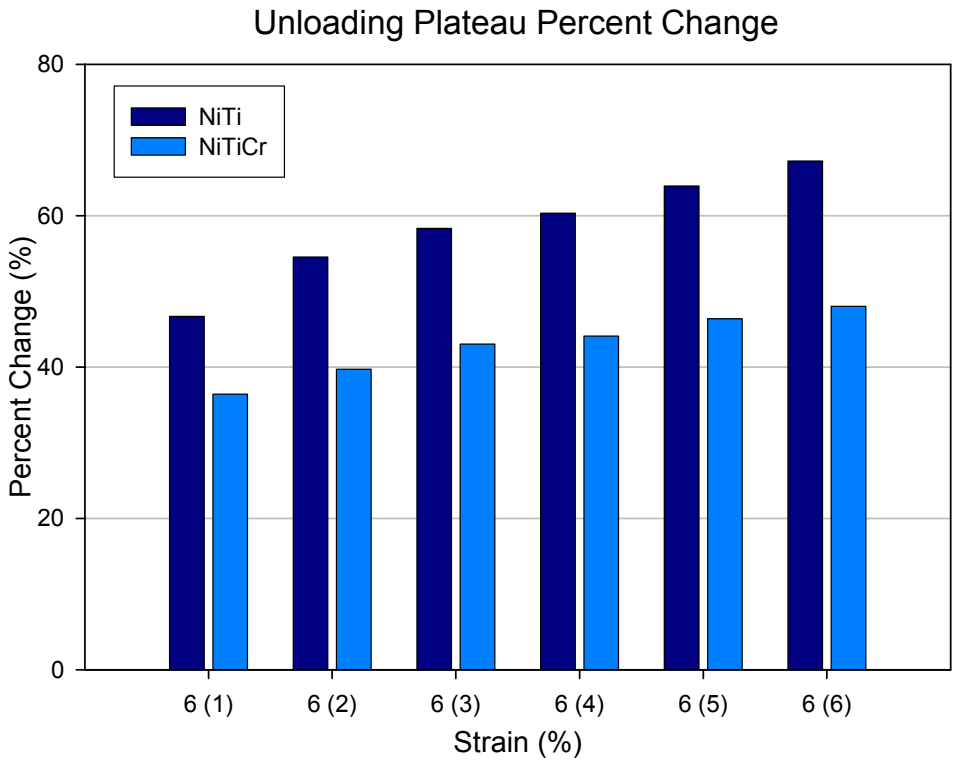

Figure 4.9. NiTi and NiTiCr unloading plateau percent change between 0.025 Hz and 2.0 Hz cases.

Effect of Strain Rate on Equivalent Viscous Damping

The energy dissipated by the system decreases due to the narrowing of the stress hysteresis with an increase in strain rate. This means that at higher loading frequencies, the equivalent viscous damping is less.

NiTi Equivalent Viscous Damping

The equivalent viscous damping (ζ_{eq}) was calculated as described in Chapter 3, and was calculated for the average of the three specimens tested at 0.025 Hz, the average of the two specimens tested at 1.0 Hz and 2.0 Hz, and only for the second specimen tested at 0.5 Hz, as explained earlier in the chapter. The equivalent viscous damping was

only calculated starting with the 2% strain cycle, since before the material is strained to 2%, it is essentially elastic and provides no real hysteretic behavior. As expected, the equivalent viscous damping decreases significantly with increased strain rate, as shown in Figure 4.10. For the second specimen tested at 1.0 Hz, the equivalent viscous damping does not follow the trend expected, which can be attributed to the specimen experiencing slipping in the grips during testing.

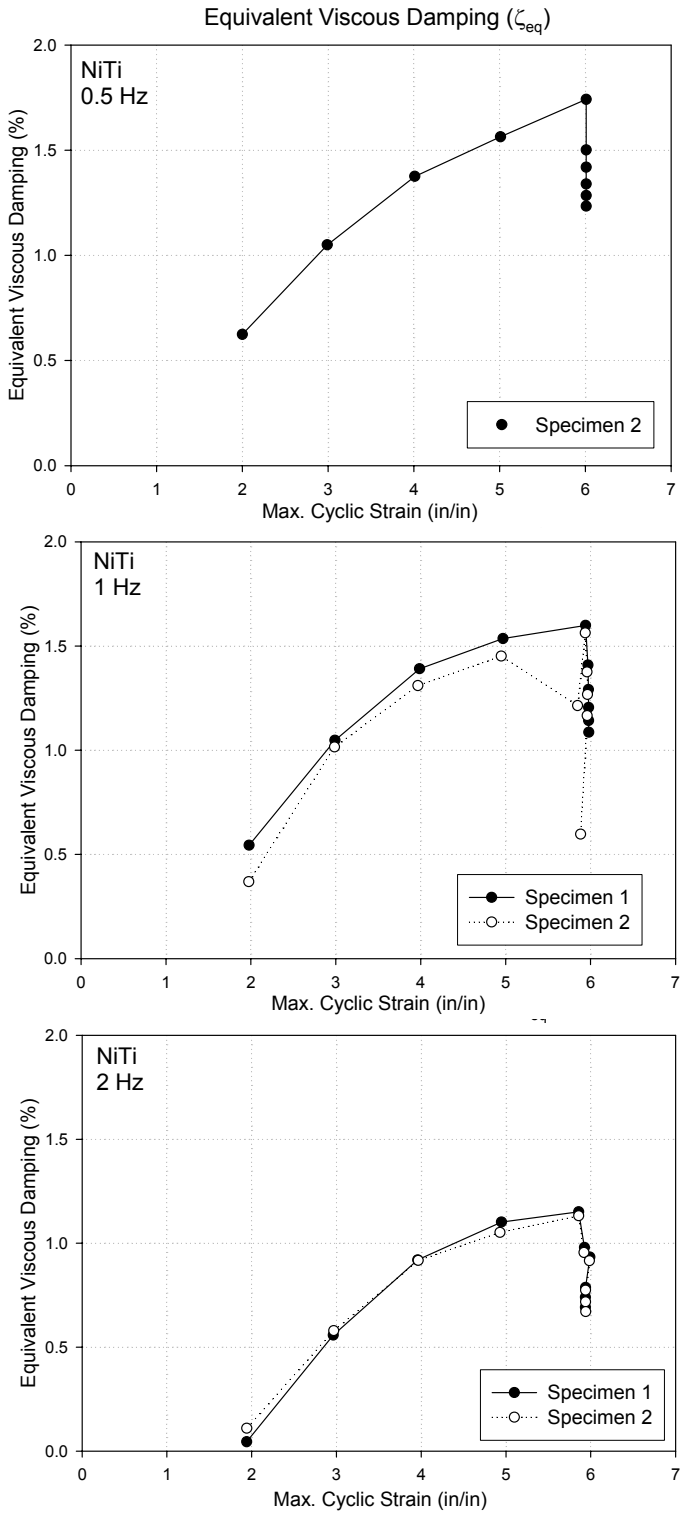

Figure 4.10. Equivalent viscous damping for NiTi loaded dynamically at 0.5 Hz, 1.0 Hz and 2.0 Hz.

Figure 4.11 shows the equivalent viscous damping values at each strain cycle starting with 2%, for 0.025 Hz, 1.0 Hz and 2.0 Hz, and the equivalent viscous damping values for the second specimen tested at 0.5 Hz. As discussed above, the equivalent viscous damping was only calculated starting with the 2% strain cycle. The decrease in equivalent viscous damping with increased loading strain rate agrees with previous results.

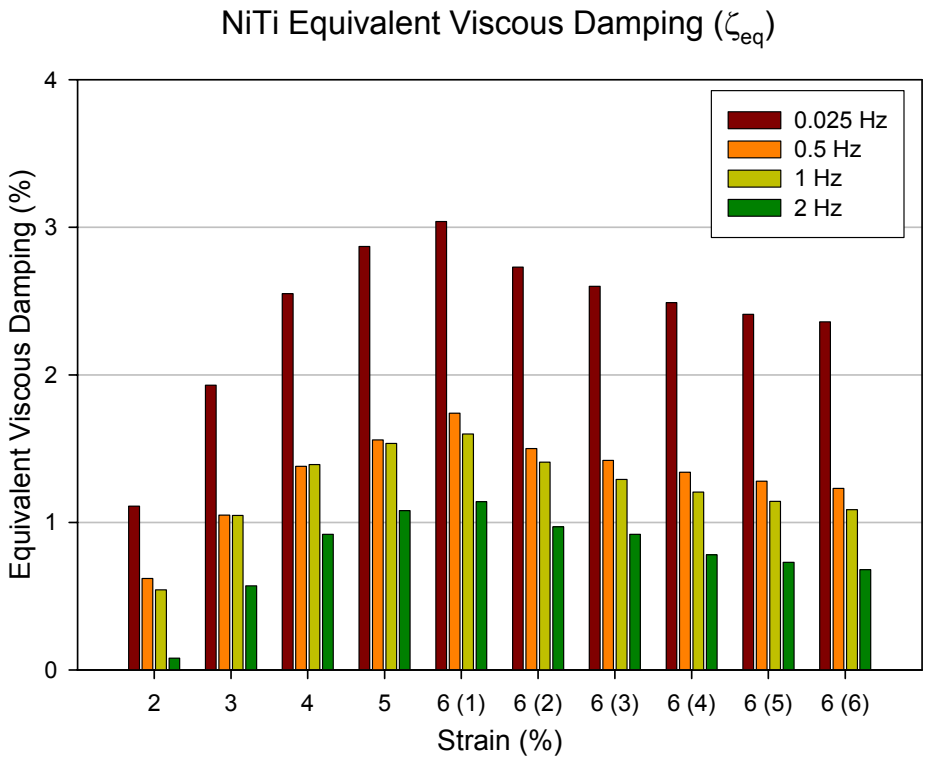

Figure 4.11. NiTi average equivalent viscous damping.

Between the 0.025 Hz and the 0.5 Hz dynamic loadings, the decrease in ζ_{eq} is very consistent (~ 45%) for all strain cycles. The lowest percent change occurs between the 0.5 Hz and 1.0 Hz dynamic loadings. There is a moderate drop between the 1.0 Hz

and 2.0 Hz dynamic loadings. The sharp decrease in equivalent viscous damping with increased strain rate agrees with the findings from other studies as discussed above.

NiTiCr Equivalent Viscous Damping

As with the NiTi specimens, the equivalent viscous damping (ζ_{eq}) decreases with increased strain rate. Figure 4.12 shows the equivalent viscous damping for the two specimens loaded at 0.5 Hz, 1.0 Hz, and 2.0 Hz. The first specimen loaded at 1.0 Hz experienced only three 6% strain cycles before the machine interlocks were triggered. However, the data up to the third 6% strain cycle is good. As with the NiTi specimens, the equivalent viscous damping was only calculated starting with the 2% strain cycle, since before the material is strained to 2%, it is essentially elastic and provides no damping capabilities.

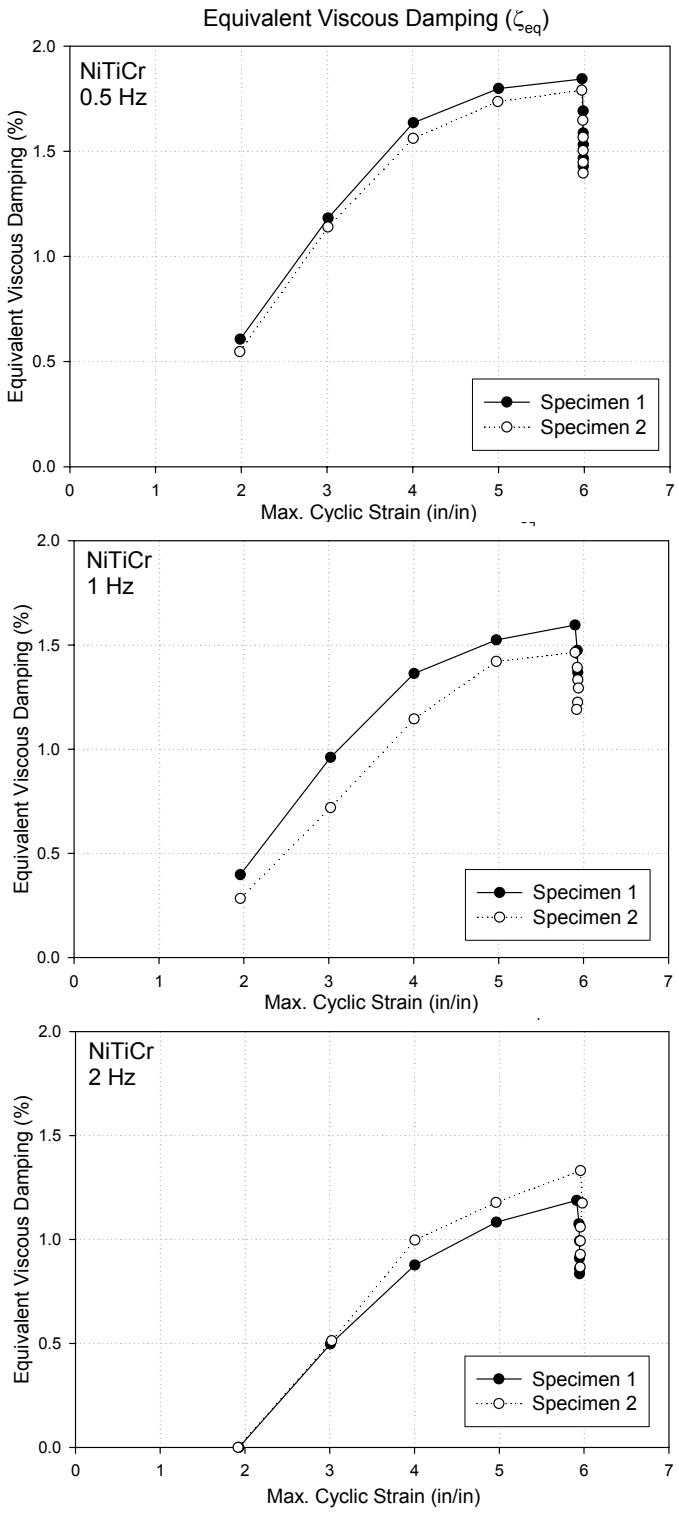

Figure 4.12. Equivalent viscous damping for NiTiCr loaded dynamically at 0.5 Hz, 1.0 Hz and 2.0 Hz.

Figure 4.13 shows the equivalent viscous damping at each cycle starting with 2% strain cycle, for the 0.025 Hz, 0.5 Hz, 1.0 Hz, and 2.0 Hz loading rates. Between the 0.025 Hz quasi-static loading and the 0.5 Hz dynamic loading, the decrease in ζ_{eq} is very consistent (~ 40%) for all strain cycles. The smallest change occurs between the 0.5 Hz and 1.0 Hz dynamic loadings. However, between the 1.0 Hz and 2.0 Hz dynamic loadings, there is a 28% decrease in ζ_{eq}. The sharp decrease in equivalent viscous damping with increased strain rate agrees with the findings from other studies as discussed above. For the 2% strain cycle, the equivalent viscous damping for the 2.0 Hz loading rate is essentially zero.

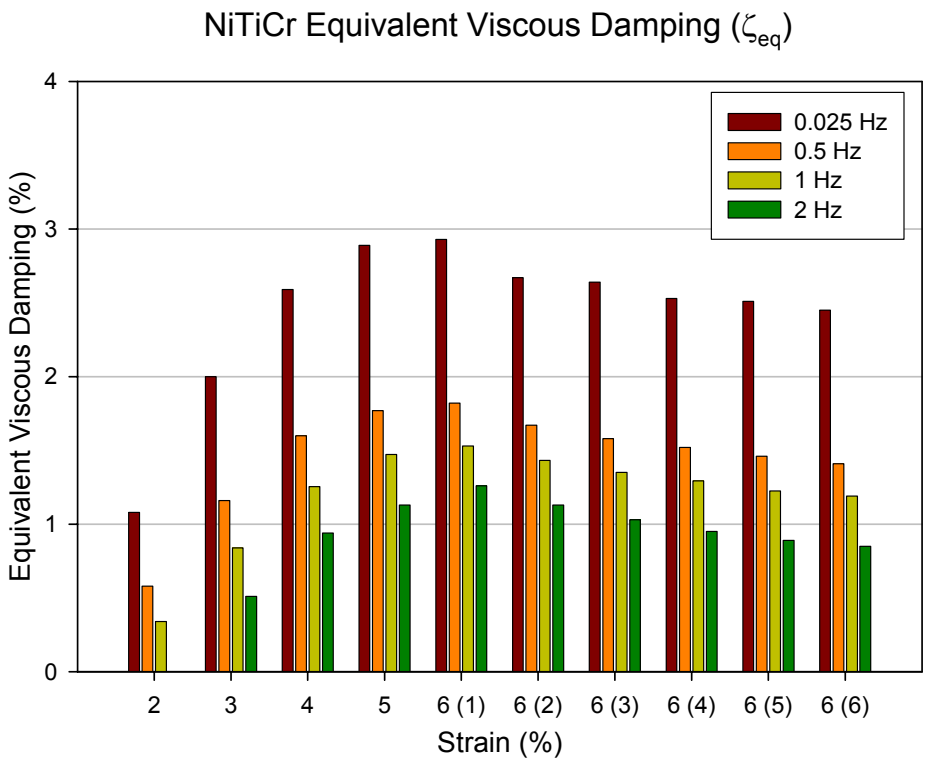

Figure 4.13. NiTiCr average equivalent viscous damping.

Changes in Equivalent Viscous Damping: NiTi vs. NiTiCr

Comparing the decrease in equivalent viscous damping between the NiTi specimens and the NiTiCr specimens between the 0.025 Hz quasi-static loading and the 2.0 Hz dynamic loading, one can observe that the decrease in equivalent viscous damping with increased strain rate is slightly more pronounced for the NiTi specimens starting with the 4% strain cycle. Overall, the equivalent viscous damping decreases by 71% for the NiTi specimen in the last 6% strain cycle, while the decrease of the equivalent viscous damping is about 65% for the NiTiCr specimen in the last 6% strain cycle. There appears to be no significant difference in the behavior of NiTi versus NiTiCr when it comes to a decrease in equivalent viscous damping with increased strain rate. Figure 4.15 shows a comparison of the percent change in equivalent viscous damping between the 0.025 Hz and 2.0 Hz loading rates for the NiTi specimens and the NiTiCr specimens for the 2%, 3%, 4%, 5%, and the six 6% strain cycles.

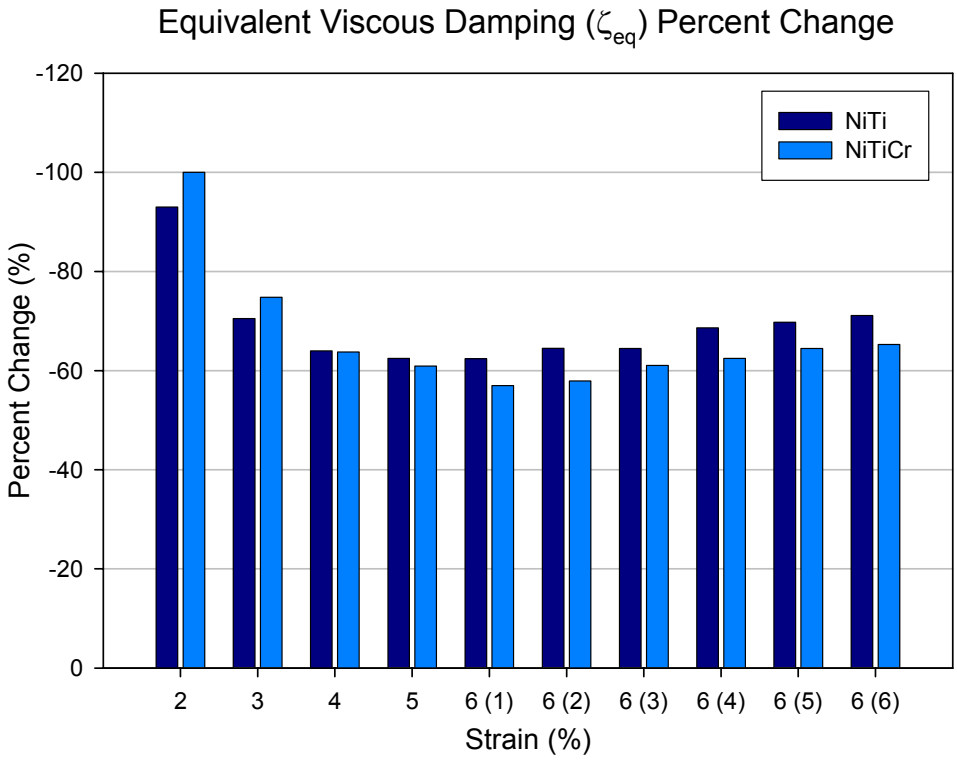

Figure 4.15. NiTi and NiTiCr equivalent viscous damping percent change between 0.025Hz and 2.0 Hz.

Effect of Strain Rate on Residual Strain

For this study, we are focusing on the development of residual strains during and after loading. It is important to know how an increase in the frequency of the dynamic loading will affect the accumulation of residual strain. Since SMAs are being used for seismic resistant designs and retrofits, it necessary that they maintain a low residual strain at high loading strain rates in order to ensure their recentering capability during an earthquake.

NiTi Residual Strain

The residual strain was calculated for the average of the three specimens tested at 0.025 Hz, the average of the two specimens tested at 1.0 Hz and 2.0 Hz, and only for the second specimen tested at 0.5 Hz, as explained earlier in the chapter. The residual strain appears to decrease with an increase in strain rate starting with the 4% strain cycle. as shown in Figure 4.16. On the sixth 6% strain cycle, the residual strain decreases from 0.403% for the 0.025 Hz quasi-static loading to 0.205% for the 2.0 Hz dynamic loading. This represents a decrease of approximately 50%. Figure 4.17 shows the plots of the residual strain versus maximum cyclical strain for one specimen loaded dynamically at 0.5 Hz, and the two specimens loaded dynamically at 1.0 Hz and 2.0 Hz.

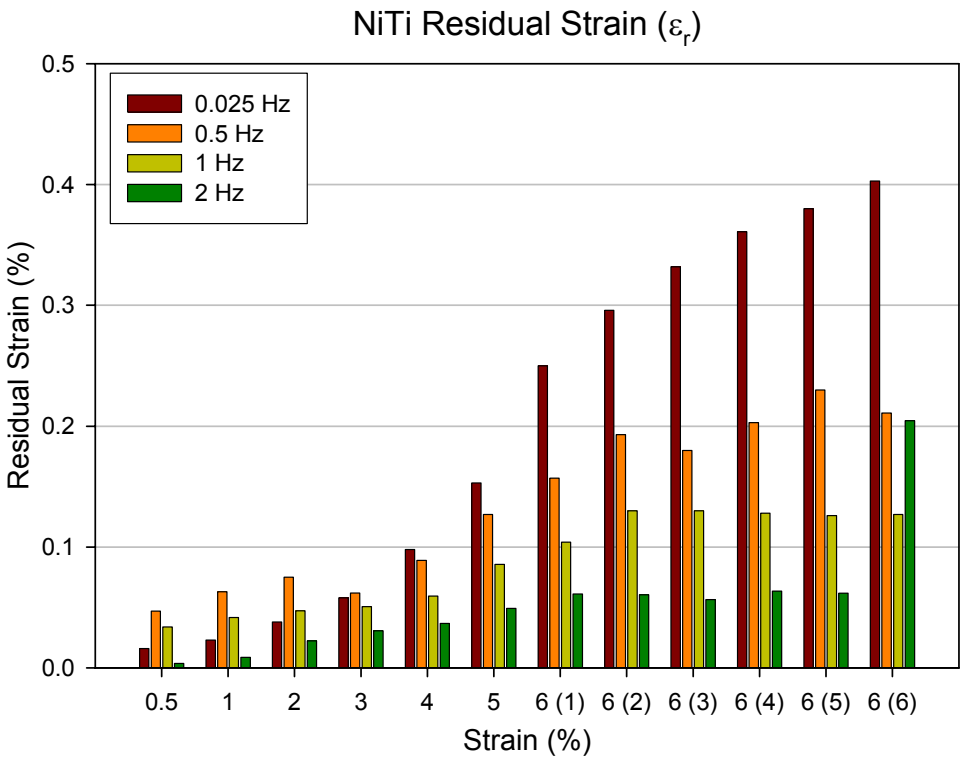

Figure 4.16. NiTi average residual strain.

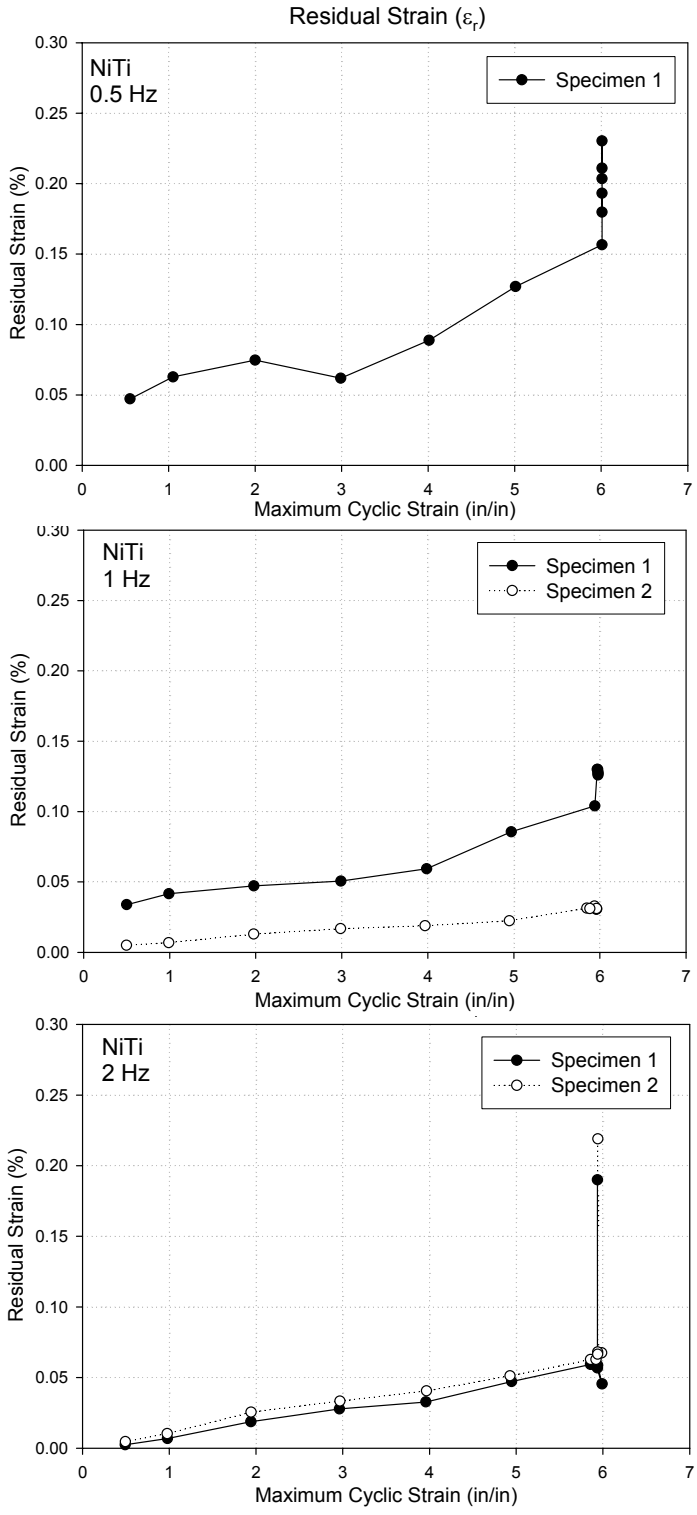

Figure 4.17. Residual strain for NiTi loaded dynamically at 0.5 Hz, 1.0 Hz and 2.0 Hz.

NiTiCr Residual Strain

The residual strain was calculated for the average of the three specimens tested at 0.025 Hz, the average of the two specimens tested at 0.5 Hz and 2.0 Hz, and only for the second specimen tested at 1.0 Hz, as explained earlier in the chapter. The residual strain appears to increase with an increase in loading frequency up to 1.0 Hz, but then decreases for the 2.0 Hz loading frequency as shown in Figure 4.18. On the sixth 6% strain cycle, the residual strain decreases from 0.196% for the 0.025 Hz quasi-static loading to 0.174% for the 2.0 Hz dynamic loading. This represents a decrease of approximately 11%. Figure 4.19 shows the plots of the residual strain versus maximum cyclical strain for one specimen loaded dynamically at 0.5 Hz, and the two specimens loaded dynamically at 1.0 Hz and 2.0 Hz.

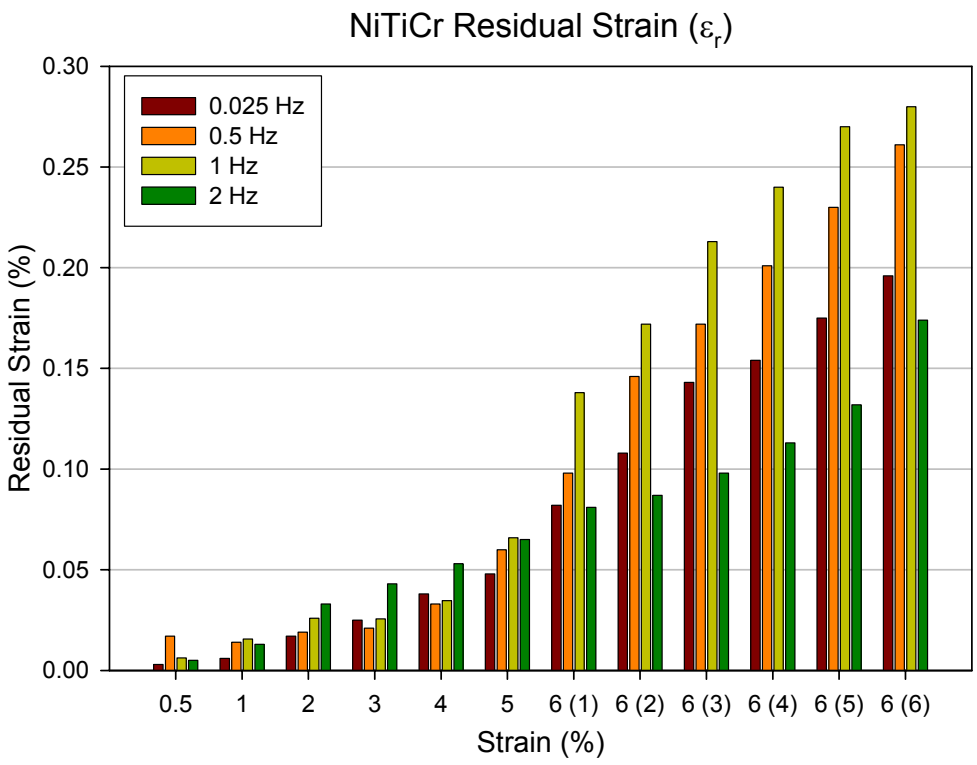

Figure 4.18. NiTiCr average residual strain.

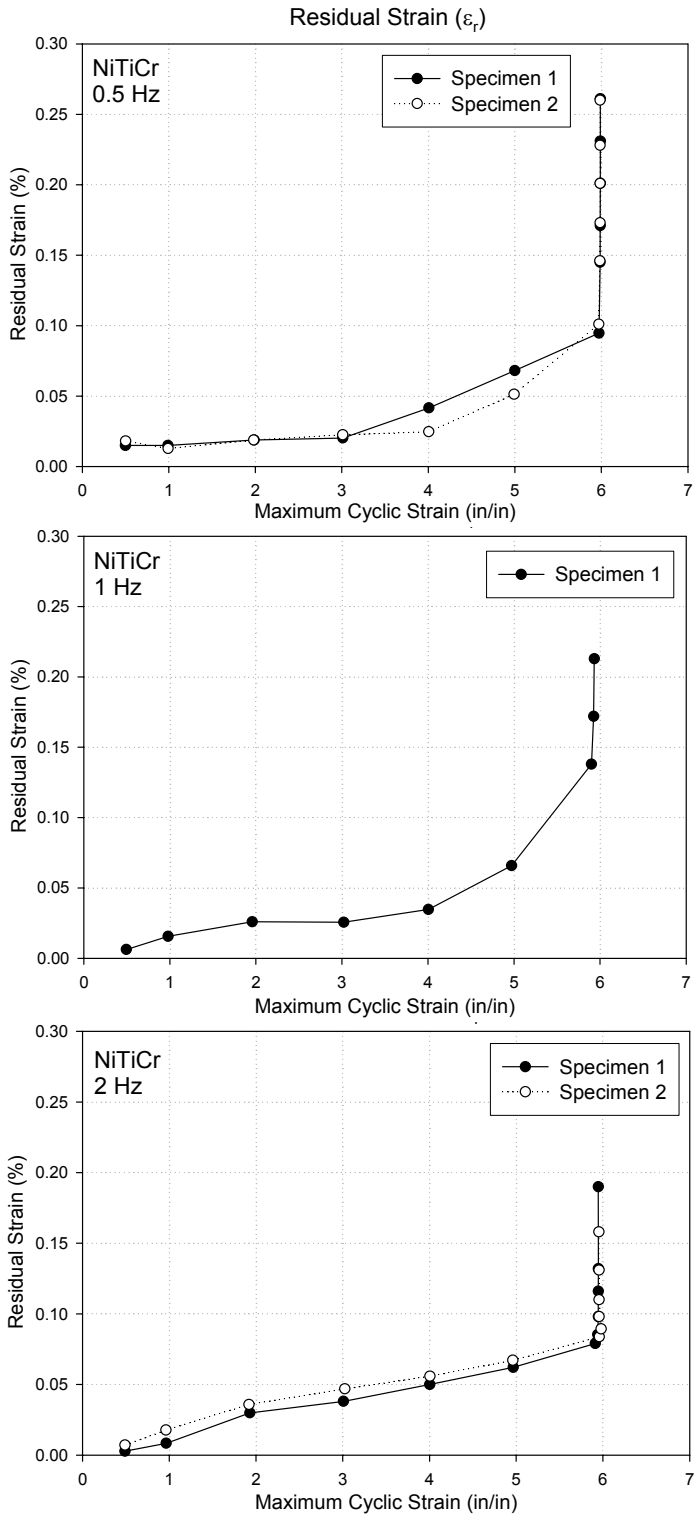

Figure 4.19. Residual strain for NiTiCr loaded dynamically at 0.5 Hz, 1.0 Hz and 2.0 Hz.

Lowest Residual Strain: NiTi vs. NiTiCr

The largest residual strains are found, on average, in the sixth 6% strain cycle. Figure 4.20 shows the residual strains at the final 6% strain cycle for the NiTi and NiTiCr specimens at all four loading frequencies: 0.025 Hz, 0.5 Hz, 1.0 Hz, and 2.0 Hz. Comparing the residual strains between the NiTi specimens and the NiTiCr specimens for the 0.025 Hz dynamic loading and the 2.0 Hz dynamic loading, one can observe that at very low frequencies (~ 0.025 Hz) and at high frequencies (~ 2.0 Hz), the NiTiCr specimens exhibit smaller residual strains than the NiTi specimens for the sixth 6% strain cycle. However, at intermediate frequencies, between 0.5 Hz and 1.0 Hz, the NiTi specimens exhibit smaller residual strains than the NiTiCr specimens. The results thus show that the accumulation of residual strain and the recentering capability have no real loading rate effect or specimen type effect associated with them. It is worth noting that maximum residual strain exhibited by either specimen for the last 6% strain cycle is 0.4%, which is still very small. For this reason, either NiTi or NiTiCr SMAs achieve the small residual strains suitable for seismic applications.

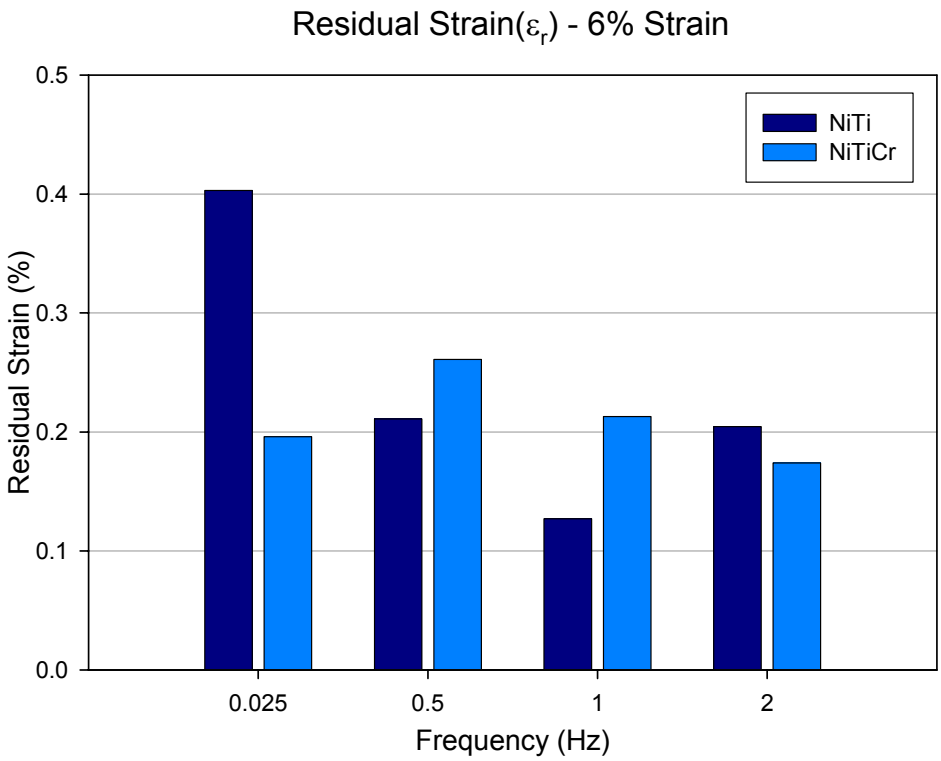

Figure 4.20. Maximum residual strain – NiTi vs. NiTiCr.

CHAPTER 5

TRAINING STUDY

As shown in the previous section, the properties of SMAs tend to degrade with increased cycling, including the residual strains, the equivalent viscous damping, and the loading and unloading plateau stresses. The cause of the degradation is the development of dislocations which tend to assist the forward and reverse transformation and lead to the accumulation of residual strains. Researchers recommend training the SMA specimens to stabilize the degradations in properties prior to their implementation into seismic applications. Wu et al. (1996) stabilized the properties with 100 thermal cycles before loading, as did Scherngell and Kneissl (1999). However, the results of these studies are not relevant to our research since they did not focus on mechanical training.

Among studies that have focused on mechanical training of SMA specimens, Wolons et al. (1998) found that un-cycled wires presented a larger value of energy dissipated per cycle than wires that had been stabilized. Tobushi et al. (1998) applied 20 loading and unloading cycles to wire specimens. It was observed that increased cycling decreased the forward and reverse transformation stresses, and increased the residual strain. Studies by Dolce and Cardone (2001) arrived at similar conclusions. The available research concerning training of SMA wires is limited. The purpose of this section is to determine the number of cycles or the strain level necessary to obtain stable cyclical behavior. This study will also help determine whether a full flag-shaped hysteresis (cycling up to 5% strain) is necessary for stabilization to occur.

Training Protocol

The NiTi specimens annealed at 350°C for 30 minutes and the NiTiCr specimens annealed at 450°C for 15 minutes were subjected to four different training regimes: 20 cycles strained to 3% strain, 20 cycles strained to 5% strain, 60 cycles strained to 3% strain, and 60 cycles strained to 5% strain. Table 5.1 shows the testing matrix for both NiTi and NiTiCr SMAs. Figure 5.1 shows sample stress-strain plots for the NiTi specimens trained for 20 cycles at 3% and 5% strain. Figure 5.2 shows sample stress-strain plots for the NiTi specimens trained for 60 cycles at 3% and 5% strain. The stress-strain plots for the NiTiCr specimens were similar to the NiTi stress-strain plots and are therefore not shown.

Table 5.1. Training matrix for NiTi and NiTiCr.

Specimen No.	Number of Cycles	Maximum Strain Level (%)
1	20	3
2	60	3
3	20	5
4	60	5

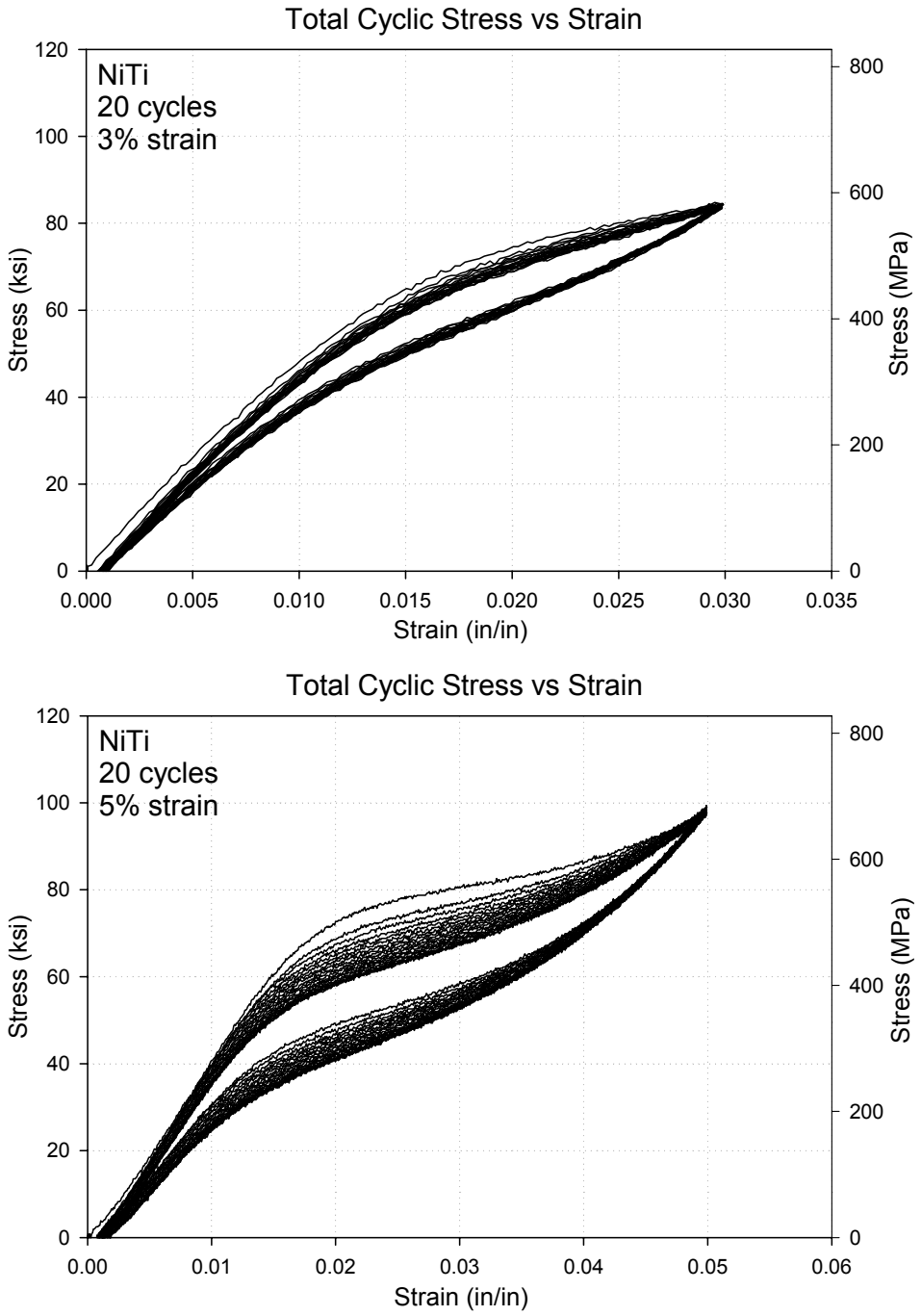

Figure 5.1. Stress-strain plots for NiTi trained for 20 cycles at 3% and 5% strain.

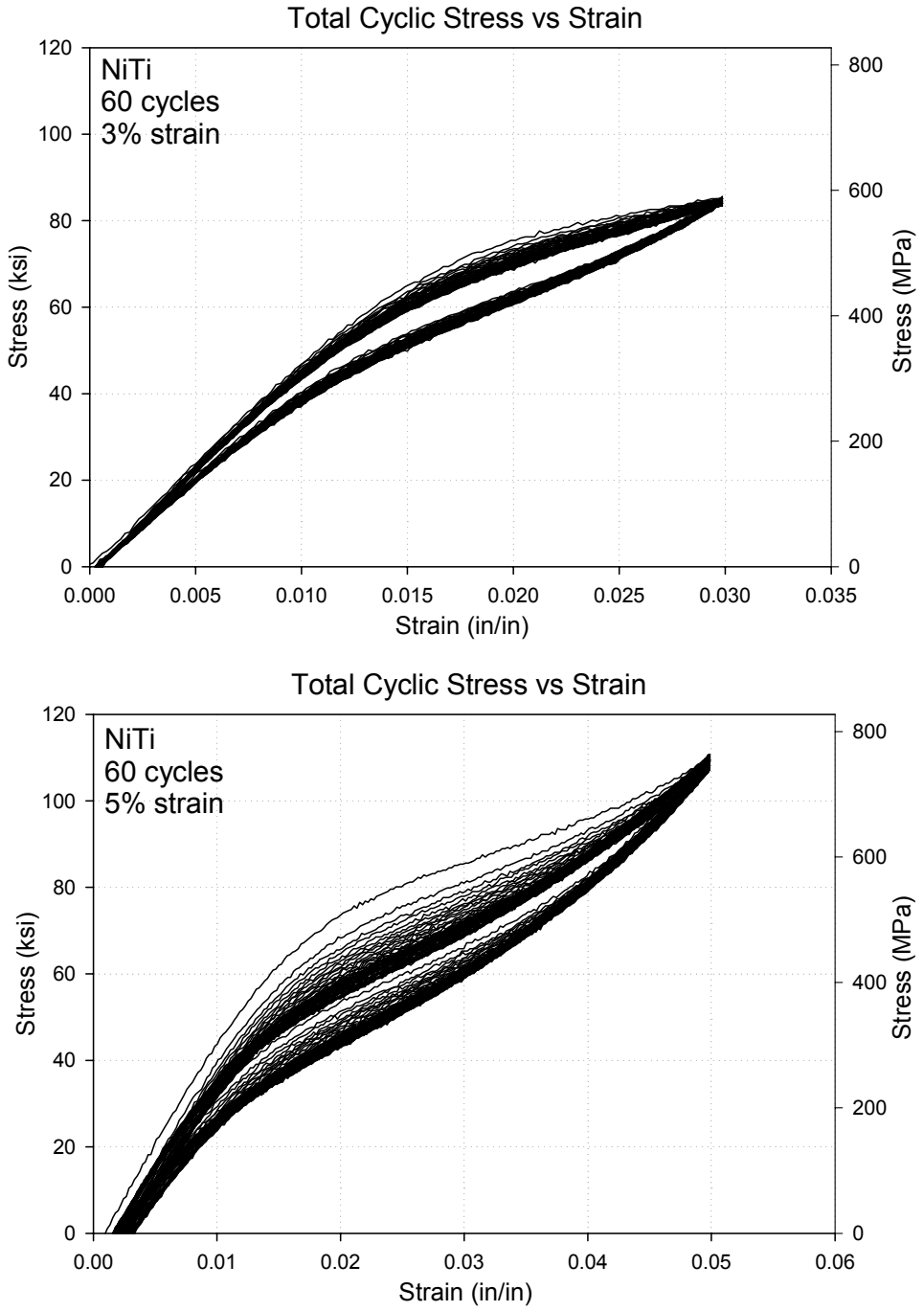

Figure 5.2. Stress-strain plots for NiTi trained for 60 cycles at 3% and 5% strain.

Training of NiTi Shape Memory Alloys

Four NiTi specimens were trained following the protocol described previously. These four specimens were tested quasi-statically at 0.025 Hz (0.3%/s) under cyclical loading as described in Chapter 3. Next, the data was analyzed and the loading plateau stress, unloading plateau stress, equivalent viscous damping, and residual strain and were calculated at each cycle for all four specimens. The results of this study were compared with the average results of the three untrained specimens annealed at 350°C for 30 minutes and tested quasi-statically at 0.025 Hz for the annealing temperature study presented in Chapter 3. Figure 5.3 shows the stress-strain plot for one of the untrained specimens tested quasi statically. Also shown on Figure 5.3 are the residual strain (ε_r) and the equivalent viscous damping (ζ_{eq}) for the first 6% strain cycle. Figure 5.4 shows the stress-strain plots for the four trained specimens. Also shown on Figure 5.4 are the residual strain (ε_r) and the equivalent viscous damping (ζ_{eq}) for the first 6% strain cycle.

Comparing the stress-strain plots for the untrained specimen with the stress-strain plots for the trained specimens, one can observe that the hysteresis narrows, the equivalent viscous damping decreases, the residual strains increase slightly, and the strain hardening slope increases. Between the untrained specimen and the specimen trained for 60 cycles at 5% strain one can observe that the loading plateau for the first 5 strain cycles decreases for the trained specimens.

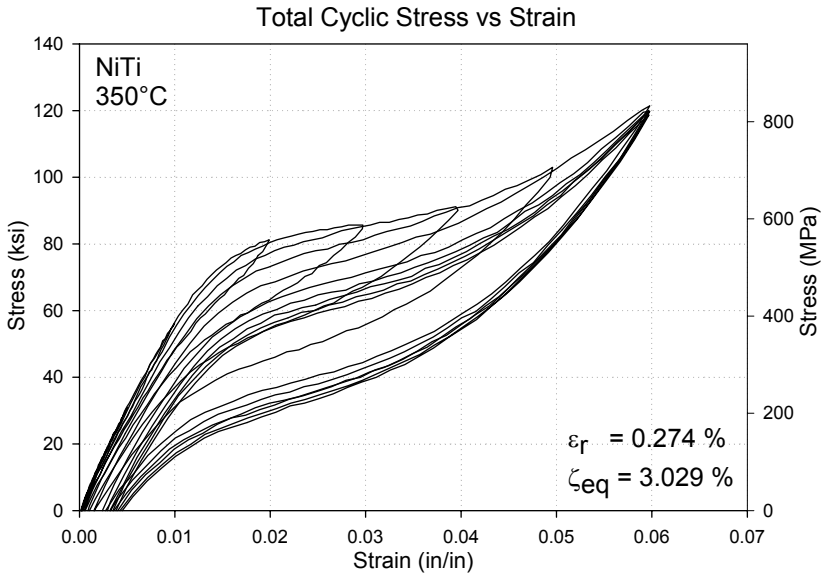

Figure 5.3. Stress-strain plot for untrained NiTi specimen

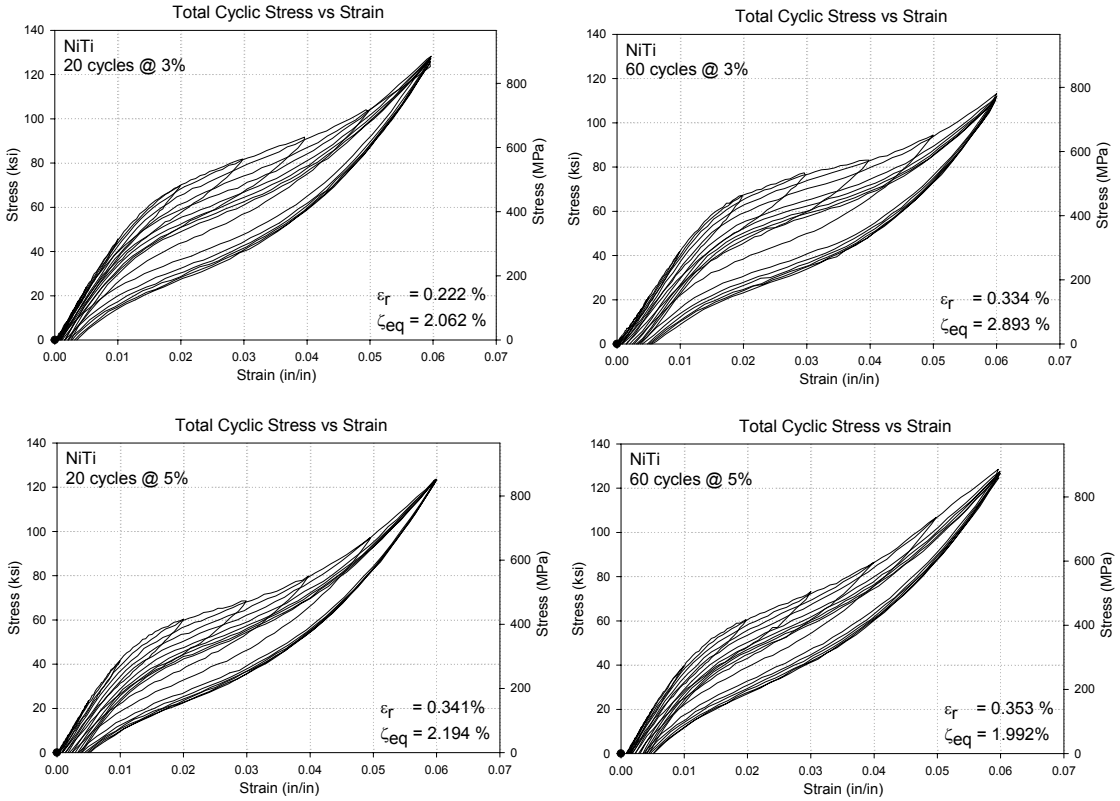

Figure 5.4. Stress-strain plots for trained NiTi specimens.

NiTi Loading and Unloading Plateau Stress

The purpose of training the NiTi wires is to determine if the decrease in loading and unloading plateau stress with increased cyclic strain can be minimized. This can be evaluated by comparing the loading and unloading plateau for the last 6% strain cycles. Figure 5.5 shows the loading plateau stress for the NiTi specimens, including the untrained and the four trained specimens. From this figure one can observe that the decrease in loading plateau is stabilized by the higher training strain, that is, the two specimens trained at 5% strain showed a smaller decrease in loading plateau with increased number of cycles than the two specimens trained at 3% strain. The specimens trained for 20 and 60 cycles at 5% strain both experienced a 16% decrease in loading plateau stress from the first 6% strain cycle to the sixth 6% strain cycle. The specimens trained for 20 and 60 cycles at 3% both experienced a 20% decrease in loading plateau stress from the first 6% strain cycle to the sixth 6% strain cycle. It appears that a full hysteresis is necessary for stabilization to occur, since the untrained specimens experienced an average decrease of 19% in loading plateau stress from the first 6% strain cycle to the sixth and final 6% strain cycle. The specimens trained for 20 and 60 cycles at 5% strain experienced a decrease of 11% between the 2% strain cycle and the sixth 6% strain cycle. The untrained specimens experienced a decrease of approximately 12% between the second 6% and the sixth 6% strain cycles. The specimens trained at 3% strain experienced a decrease of approximately 15% - 17% between the 2% strain cycle and the sixth 6% strain cycle. It is also worth noting that the loading plateau stress decreases significantly with training of specimens. Table 5.2 shows the decrease in loading plateau for the NiTi specimens.

Table 5.2. Decrease in loading plateau stress for NiTi specimens.

	Decrease in Loading Plateau Stress	
Training Protocol	**Between First and Sixth 6% Strain Cycle**	**Between Second and Sixth 6% Strain Cycle**
Untrained	19%	12%
20 cycles @ 3%	20%	17%
60 cycles @ 3%	20%	15%
20 cycles @ 5%	16%	11%
60 cycles @ 5%	16%	11%

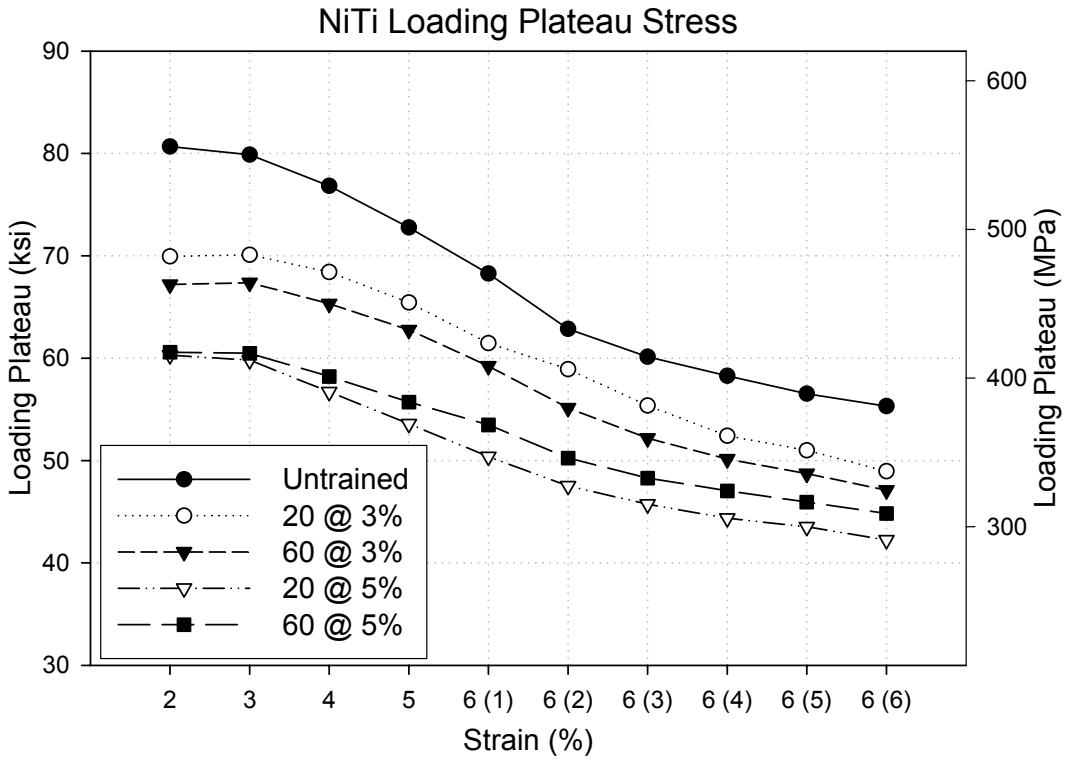

Figure 5.5. NiTi loading plateau stress after training.

Figure 5.6 shows the NiTi unloading plateau for the NiTi specimens, including the untrained and the four trained specimens. From the data shown in this figure, it appears that the unloading plateau is fairly stable for the six 6% strain cycles, and the stabilization of the unloading plateau stress is not affected by training. However, on

closer inspection, the specimens trained at 3% strain for 20 and 60 cycles experience a decrease of 19% and 17% between the first 6% strain cycle and the sixth 6% strain cycle, respectively. The untrained specimens and the specimens trained at 5% strain for 20 and 60 cycles experience an approximate decrease of 12% between the first 6% strain cycle and the sixth 6% strain cycle. The specimen trained for 20 cycles at 5% experienced the smallest decrease in unloading plateau, 10%, between the first and the sixth 6% strain cycles. It appears that the largest decrease in unloading plateau stress occurs between the first 6% and second 6% strain cycle. The decrease in the unloading plateau stress after training is not as pronounced as the decrease in the loading plateau stress after training.

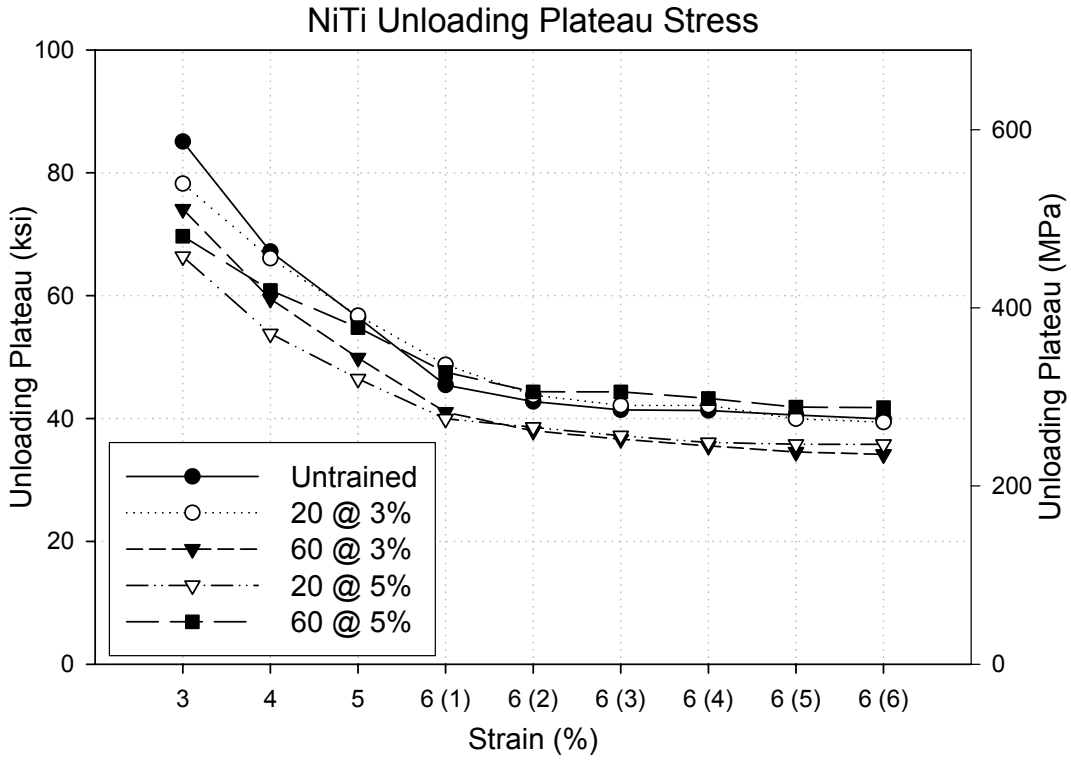

Figure 5.6. NiTi unloading plateau stress after training.

NiTi Equivalent Viscous Damping

There does not appear to be any direct correlation between training and the stabilization of the equivalent viscous damping for the NiTi specimens. However, it does seem that the specimen trained for 60 cycles at 5% strain exhibits the smallest reduction in equivalent viscous damping, 8%, between the second 6% strain cycle and the sixth 6% strain cycle. The untrained specimens, the specimens trained for 20 and 60 cycles at 3%, and the specimen trained for 20 cycles at 5% strain exhibit a reduction of approximately 13% - 16% between the second 6% strain cycle and the sixth and final 6% strain cycle. Figure 5.7 shows the equivalent viscous damping for the NiTi specimens, including the untrained specimens and the four trained specimens.

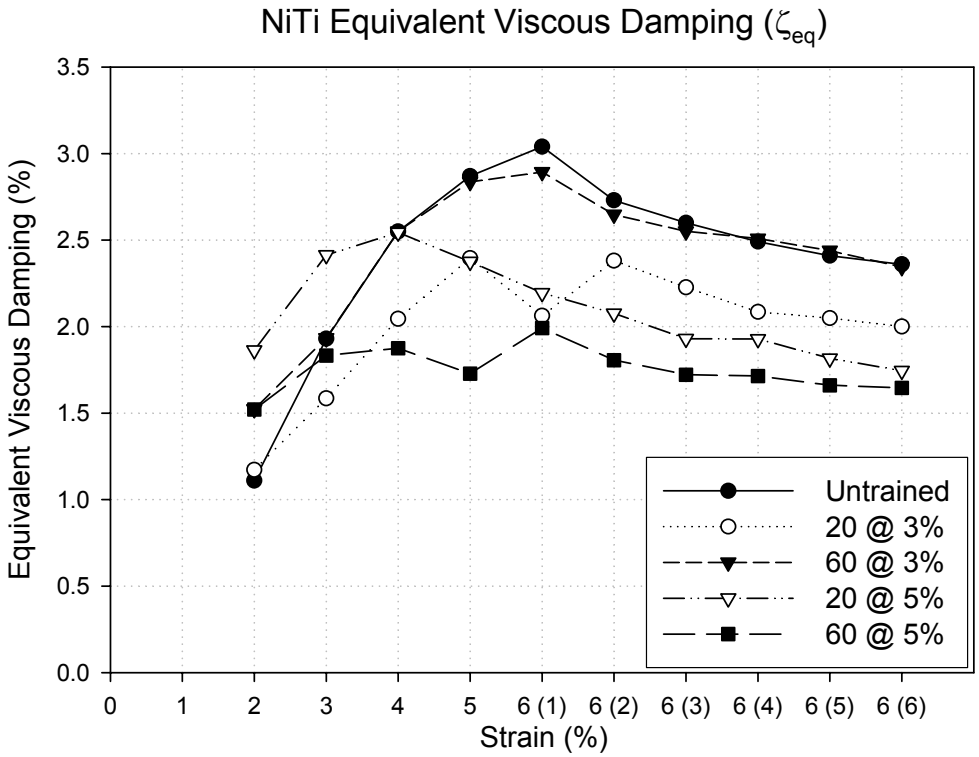

Figure 5.7. NiTi equivalent viscous damping after training.

NiTi Residual Strain

The trained specimens have larger initial residual strains when compared to the untrained specimens. The trained specimens also exhibit larger final residual strains after the sixth 6% strain cycle when compared to the untrained specimens. However, the specimen trained for 20 cycles at 3% shows lower residual strains than the untrained specimens after the sixth 6% strain cycle. Also, the specimens trained for 20 cycles at 5% strain, and for 60 cycles at 3% and 5% strain show very similar residual strains after the sixth 6% strain cycle. Overall, even after repeated training cycles, the residual strains are still in the order of 0.5%, which is small enough to consider trained NiTi SMAs for civil engineering applications. Figure 5.8 shows the residual strain for the NiTi specimens, including the untrained specimens and the four trained specimens.

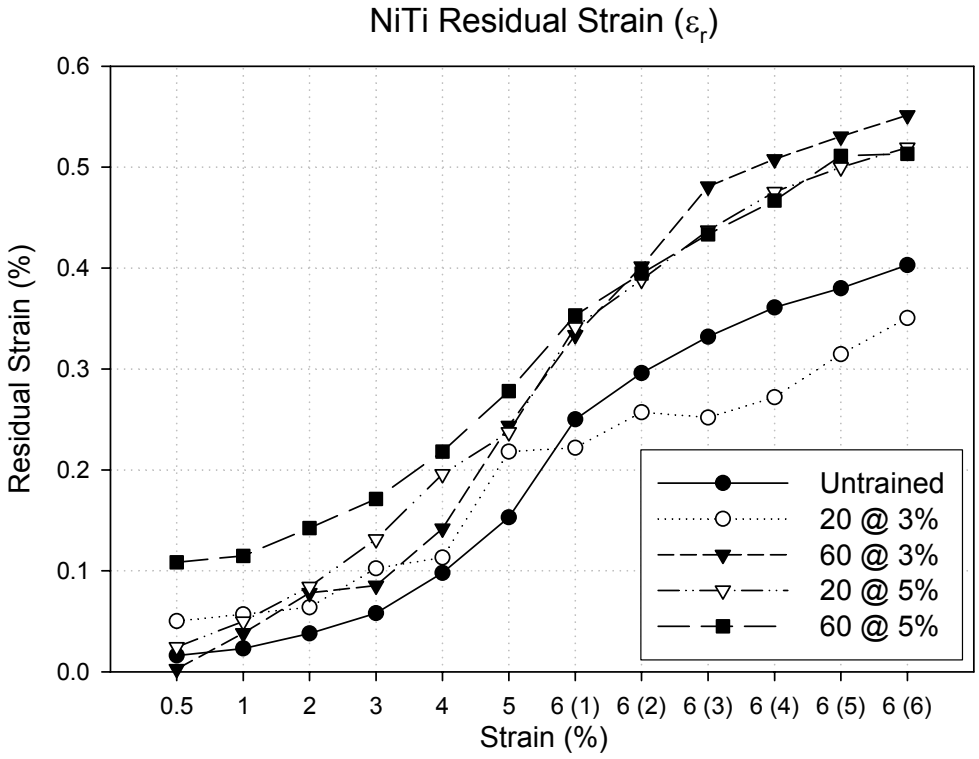

Figure 5.8. NiTi residual strains after training.

Training of NiTiCr Shape Memory Alloys

As with NiTi, four NiTiCr specimens were trained following the protocol described previously. These four specimens were tested quasi-statically at 0.025 Hz (0.3%/s) under cyclical loading as described in Chapter 3. The data was analyzed and the loading plateau stress, unloading plateau stress, equivalent viscous damping, and residual strain were calculated at each cycle for all four specimens. The results of this study were compared with the average results of the two specimens annealed at 450°C for 15 minutes and tested quasi-statically at 0.025 Hz as part of the annealing temperature study.

Figure 5.9 shows the stress-strain plots for the one of the untrained specimens. Also shown on Figure 5.9 are the residual strain (ε_r) and the equivalent viscous damping

(ζ_{eq}) for the first 6% strain cycle. Figure 5.10 shows the stress-strain plots for the four trained specimens. Also shown on Figure 5.10 are the residual strain (ε_r) and the equivalent viscous damping (ζ_{eq}) for the first 6% strain cycle. Comparing the stress-strain plots for the untrained specimen with the stress-strain plots for the trained specimens, one can observe that the hysteresis appears to widen, the equivalent viscous damping increases slightly, and the residual strains increase. Also, the loading plateau for the trained specimens appears to be more "level" than the loading plateau for the untrained specimen.

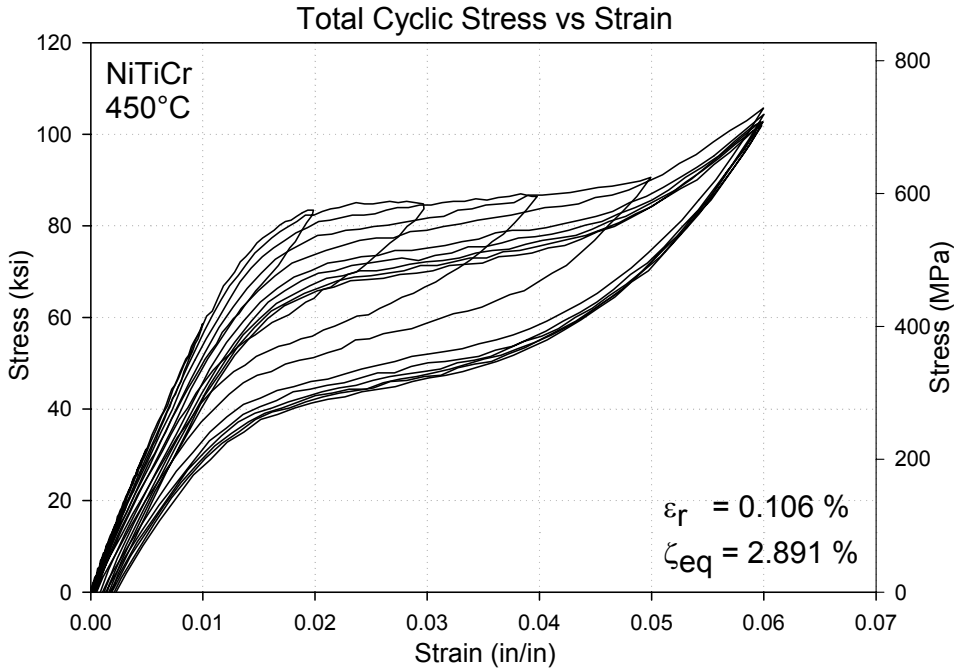

Figure 5.9. Stress-strain plot for the untrained NiTiCr specimen.

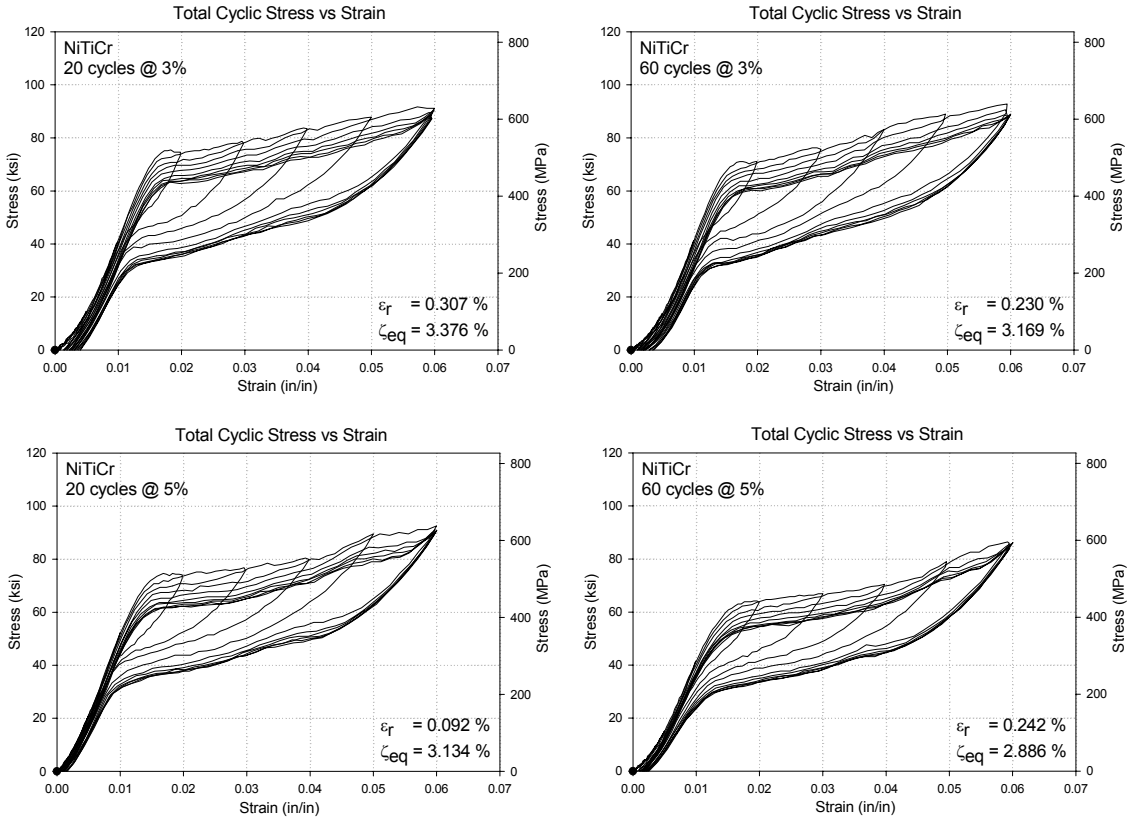

Figure 5.10. Stress-strain plots for trained NiTiCr specimens.

NiTiCr Loading and Unloading Plateau Stress

Training of NiTiCr specimens appears to stabilize the fatigue effect in the loading plateau stress. The untrained specimens experienced a decrease in the loading plateau stress of 12% between the first and sixth 6% strain cycles. The specimens trained for 20 and 60 cycles at 3% strain, as well as the specimen trained for 60 cycles at 5% strain experienced a decrease of approximately 7% between the first and sixth 6% strain cycle. The specimen trained for 60 cycles at 5% strain experienced a decrease of approximately 5.7% between the first and sixth 6% strain cycles. The largest drop in loading plateau stress occurs between the first and second 6% strain cycle. Table 5.3 shows the decrease in loading plateau stress between the second and sixth 6% strain cycle for the untrained specimens and the four trained specimens. Figure 5.11 shows the loading plateau stress for the trained NiTiCr specimens after training and testing, as well as for the untrained specimens.

Table 5.3. Decrease in loading plateau stress for NiTiCr specimens.

	Decrease in Loading Plateau Stress	
Training Protocol	**Between First and Sixth 6% Strain Cycle**	**Between Second and Sixth 6% Strain Cycle**
Untrained	12%	7.0%
20 cycles @ 3%	7.3%	4.5%
60 cycles @ 3%	6.7%	3.7%
20 cycles @ 5%	6.6%	3.5%
60 cycles @ 5%	5.7%	2.6%

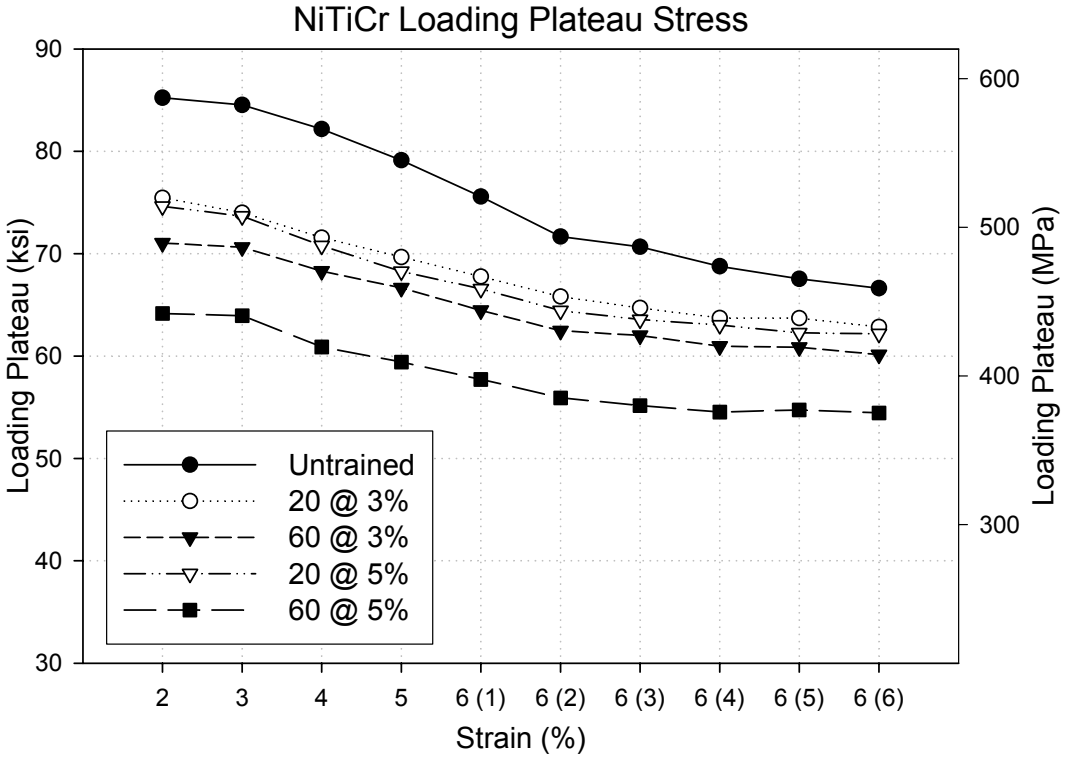

Figure 5.11. NiTiCr loading plateau stress after training.

The unloading plateau decreases with increased training, especially for the specimen trained for 60 cycles at 5% strain. The specimens trained for 20 and 60 cycles at 3% strain, and for 20 cycles at 3% strain have almost identical unloading plateau stresses. The lowest unloading plateau stress occurs in the specimen trained for 60 cycles at 5% strain. As with NiTi specimens, the unloading plateau appears to be fairly stable for the six 6% strain cycles, the stabilization of the unloading plateau stress does not appear to be affected by training. All specimens, including the untrained specimens, experienced a decrease of approximately 7% - 8% between the first and the sixth 6% strain cycle. The decrease in the unloading plateau stress is not as pronounced as the decrease in the loading plateau stress with training. Figure 5.12 shows the unloading

plateau for the NiTiCr specimens after training and testing, as well as for the untrained specimens.

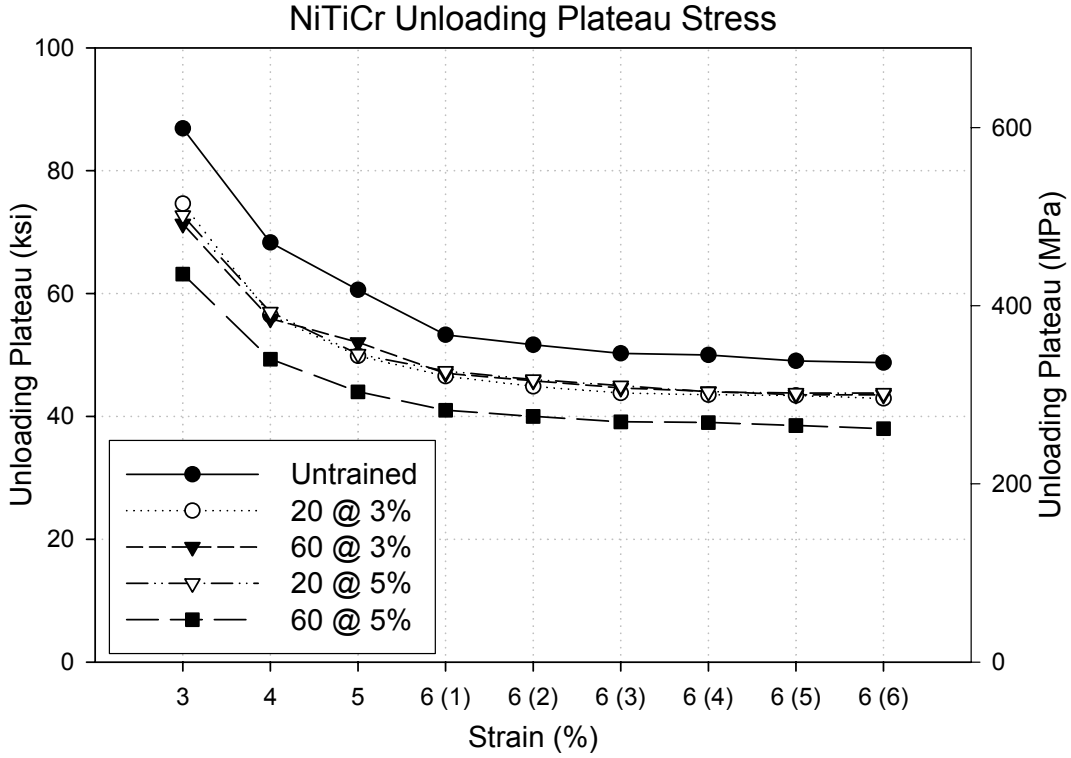

Figure 5.12. NiTiCr unloading plateau stress after training.

NiTiCr Equivalent Viscous Damping

The resulting equivalent viscous damping values after training reveal an increase in equivalent viscous damping with training. Also, training appears to stabilize the decrease in equivalent viscous damping for the six 6% strain cycles. The untrained specimen exhibited a 16% reduction in equivalent viscous damping between the first and sixth 6% strain cycles, while the specimens trained for 20 and 60 cycles at 3% strain, and the specimen trained for 60 cycles at 5% strain exhibit the smallest reduction in

equivalent viscous damping, 5%, between the first 6% strain cycle and the sixth 6% strain cycle. The specimen trained for 20 cycles at 5% exhibits a reduction of approximately 7.5% between the first and sixth 6% strain cycle. Figure 5.13 shows the equivalent viscous damping for the NiTiCr specimens, including the untrained specimens and the four trained specimens.

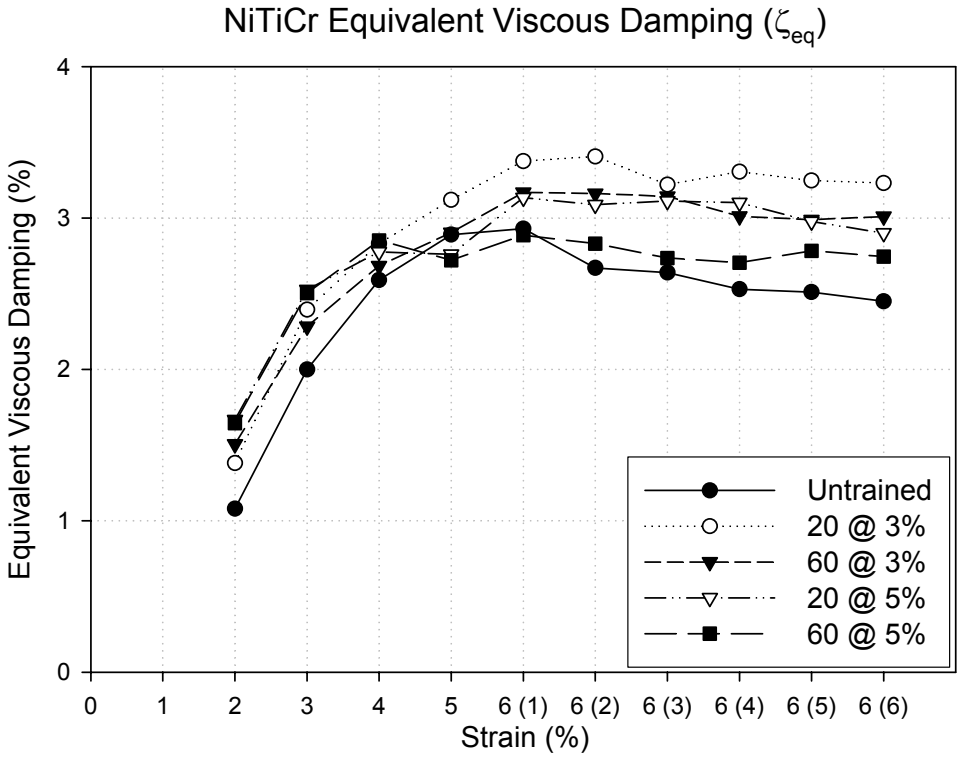

Figure 5.13. NiTiCr equivalent viscous damping after training.

NiTiCr Residual Strain

As expected, the trained specimens exhibit higher residual strains starting with the first 0.5% strain cycle. Also, there does not appear to be any real stabilization of the residual strain for the trained specimens for the six 6% strain cycles. However, for the

specimens trained for 20 and 60 cycles at 5% strain, there appears to be a reduction in the residual strain starting with the 5% strain cycle and the first 6% strain cycle, respectively. Even though these two specimens were subjected to 5% strain, they exhibit lower residual strains than the specimens trained to 3% strain. Figure 5.14 shows the residual strains for the NiTiCr specimens after training and testing, and for the NiTiCr untrained specimens.

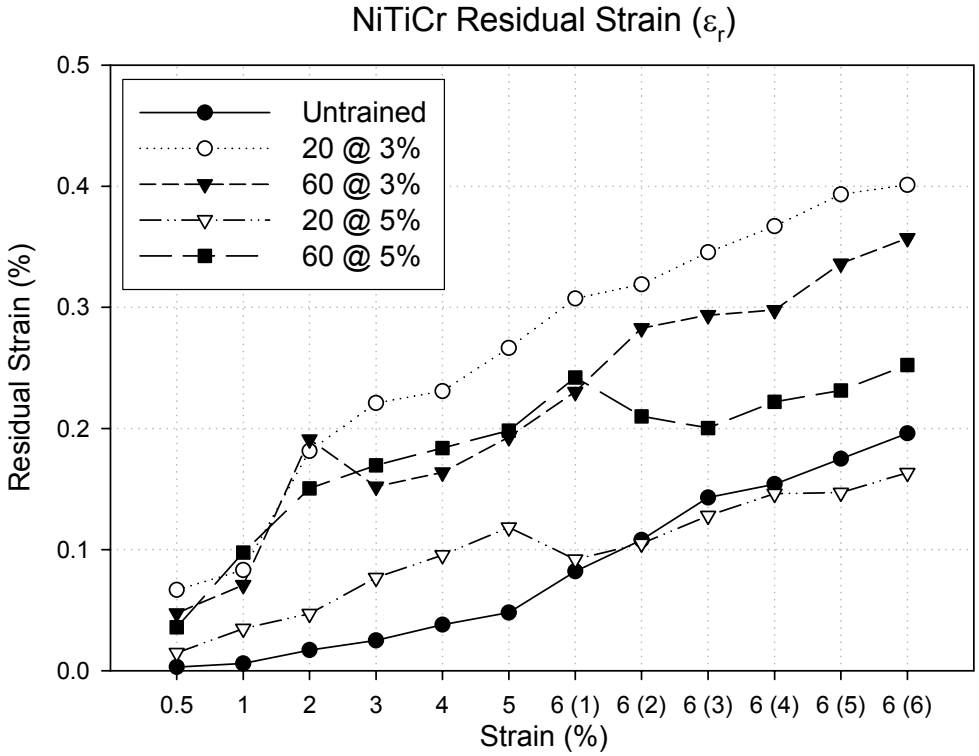

Figure 5.14. NiTiCr residual strain after training.

Effects of Training on SMAs: NiTi vs. NiTiCr

Training appears to have moderate beneficial effects on stabilizing some properties of SMAs, specifically the loading plateau stress, and the equivalent viscous damping. The residual strain does not appear to be affected by training of the specimens.

The loading plateau stress was stabilized efficiently by training both NiTi and NiTiCr specimens. It appears that in both NiTi and NiTiCr specimens, the loading plateau stress decreases in the same proportion with increased training. Also, for both NiTi and NiTiCr specimens, the stabilization of the loading plateau appears to be effected mostly by the higher training strain as opposed to the number of cycles. The specimens trained for 20 and 60 cycles at 5% strain experienced smaller decrease in the loading plateau between the first and sixth 6% strain cycle. For the NiTiCr specimen, training proved to be effective in reducing the decrease in loading plateau between the second and sixth 6% strain cycles from 7% for the untrained specimens to 2.6% for the specimen trained for 60 cycles at 5% strain. Table 5.4 presents the decrease in loading plateau stress for NiTi and NiTiCr specimens between first and sixth 6% strain cycle. Table 5.5 presents the dcrease in loading plateau stress for NiTi and NiTiCr specimens between first and sixth 6% strain cycle.

Table 5.4. Decrease in loading plateau stress for NiTi and NiTiCr specimens between first and sixth 6% strain cycle.

	Decrease in Loading Plateau Stress Between First and Sixth 6% Strain Cycle	
Training Protocol	**NiTi**	**NiTiCr**
Untrained	19%	12%
20 cycles @ 3%	20%	7.3%
60 cycles @ 3%	20%	6.7%
20 cycles @ 5%	16%	6.6%
60 cycles @ 5%	16%	5.7%

Table 5.5. Decrease in loading plateau stress for NiTi and NiTiCr specimens between second and sixth 6% strain cycle.

	Decrease in Loading Plateau Stress Between Second and Sixth 6% Strain Cycle	
Training Protocol	**NiTi**	**NiTiCr**
Untrained	12%	7.0%
20 cycles @ 3%	7.3%	4.5%
60 cycles @ 3%	6.7%	3.7%
20 cycles @ 5%	6.6%	3.5%
60 cycles @ 5%	5.7%	2.6%

The unloading plateau stress does not decrease as much as the loading plateau stress with increased training and appears to be unaffected by training. However, the NiTi specimens trained for 20 and 60 cycles at 3% strain experience a sharper decrease in unloading plateau between the first and sixth 6% strain cycles when compared to the untrained specimens and the specimens trained for 20 and 60 cycles at 5% strain. For NiTiCr, all the trained specimens, as well as the untrained specimens appear to have the same decrease in unloading plateau between the first and the sixth 6% strain cycles.

The equivalent viscous damping for the NiTi specimens does not appear to be significantly effected by training, but it appears to stabilize between the second 6% strain

cycle and the sixth 6% strain cycle for the specimen trained for 60 cycles at 5% strain. For the NiTiCr specimens, training appears to have a positive effect on equivalent viscous damping, increasing the value of ζ_{eq} for all the trained specimens, and stabilizing the decrease in equivalent viscous damping for the six 6% strain cycles. The trained specimens exhibited a decrease of approximately 5% - 7% between the first and the sixth 6% strain cycles, while the untrained specimens exhibited a reduction of approximately 16% between the first and the sixth 6% strain cycles.

Training does not appear to have a stabilizing effect on the residual strains of both NiTi and NiTiCr specimens. As expected, the trained specimens exhibit higher residual strains than the untrained specimens. The NiTiCr specimens trained for 20 and 60 cycles at 5% strain experience a decrease in residual strain between the 5% strain cycle and the first 6% strain cycle, and between the first 6% and the second 6% strain cycle, respectively. After the decrease, the residual strain continues to increase, but the effect is that the overall residual strain is not as high as it would have been without this increase. Even with training, the residual strains are between 0.15% and 0.55%, which is still considered acceptable for civil engineering applications. The NiTiCr specimens experienced smaller residual strains when compared to the NiTi specimens.

CHAPTER 6

CONCLUSION

This study evaluates the cyclical behavior of NiTi and NiTiCr wire for potential seismic mitigation applications. In particular, the effects of annealing temperature and time, strain rate, and training on the cyclical properties are studied. The studies were performed on NiTi and NiTiCr specimens that were 0.085-in. in diameter and 6.5-in. in length, cold drawn and 40% cold worked.

In general, the cyclic characteristics of both NiTi and NiTiCr SMAs are fairly similar. The residual strains for the NiTi specimen are approximately 0.5% and the residual strains for the NiTiCr are approximately 0.23%. The equivalent viscous damping is approximately 3% for NiTi and 2.5% for the NiTiCr. The loading plateau or forward transformation stress is approximately 80 ksi for both NiTi and NiTiCr. The main difference is in the initial elastic modulus, which was calculated at 5532 ksi for NiTi and at 5942 ksi for NiTiCr.

For the annealing temperature study, three NiTi and NiTiCr specimens were subjected to different annealing temperatures and times. The NiTi specimens were annealed at 300°C, 350°C, 400°C, and 450°C for 30 minutes and then water quenched. The NiTiCr specimens were annealed at 300°C, 350°C, 400°C, 450°C, and 500°C for 15 minutes and then water quenched. The specimens were then tested quasi-statically (0.025 Hz) and the optimal annealing temperature was determined such that the minimum residual strain and adequate equivalent viscous damping were obtained. For NiTi specimens, the residual strain and equivalent viscous damping increased with increased

annealing temperatures, and the least amount of residual strain was obtained by annealing the specimens at 350°C for 30 minutes followed by water quenching. For NiTiCr specimens, the residual strains decrease with increased annealing temperature up to 450°C, and then start to increase with increased annealing temperature. The equivalent viscous damping decreases with increased annealing temperature up to 350°C and then increased with increased annealing temperature. The optimal annealing temperature was determined to be 450°C for 15 minutes.

For the strain rate study, two specimens of each type (NiTi and NiTiCr) were tested at the following dynamic strain rates: 6%/s (0.5 Hz), 12%/s (1.0 Hz), and 24%/s (2.0 Hz). These frequencies simulate those that are expected to occur during a typical earthquake. For both NiTi and NiTiCr specimens, the increase in loading rate and loading frequency causes a narrowing of the stress hysteresis. The loading plateau stress increases slowly with increased loading rate and frequency, while the unloading plateau increases rapidly with increased loading rate and frequency. The increase in unloading plateau stress with increased loading rate is more pronounced for the NiTi specimens than for the NiTiCr specimens. The equivalent viscous damping (ζ_{eq}) decreases with increased loading rate for both the NiTi and NiTiCr specimens by approximately 65% - 70%. The residual strain (ε_r) is not affected by changes in loading rate and loading frequency. For the 2.0 Hz loading rate, the maximum residual strain for the NiTi and NiTiCr specimens was approximately 0.2%.

A training study was performed where four NiTi specimens and four NiTiCr specimens were subjected to four different training schemes (one scheme per specimen): 20 cycles strained to 3% strain, 20 cycles strained to 5% strain, 60 cycles strained to 3%

strain, and 60 cycles strained to 5% strain. Then, the specimens were cyclically tested at 0.025 Hz. Based on the results from the training study, it was determined that (1) in order to stabilize the loading plateau stress, it is necessary to train the specimens up to 5% strain, and (2) training causes a decrease of the loading plateau with increased number of cycles and increased cyclic strain. Also, the unloading plateau stress is not significantly affected by training of specimens. For NiTi, training causes a decrease in equivalent viscous damping, and does not appear to affect the stabilization of the equivalent viscous damping. However, for NiTiCr, training causes an increase in equivalent viscous damping, and appears to stabilize the decrease in equivalent viscous damping for the six 6% strain cycles. Training increases the residual strain on both the NiTi and NiTiCr specimens. The residual strains after training range from 0.15% to 0.55%, which is still acceptable for civil engineering applications.

Recommendations for Future Research

Based on the results from this study, the following recommendations for future studies are made:

- It is necessary to study the effects of ambient temperature on SMAs. These alloys are very sensitive to changes in temperature, and all their properties are dependent on temperature. There is a need to understand the effects of varying ambient temperatures on the cyclic performance of NiTi and NiTiCr SMAs.
- More training protocols need to be investigated and studied to find the optimal number of cycles and level of strain that produces a significant improvement in the cyclic properties of NiTi and NiTiCr SMAs.

- The fatigue behavior of NiTi and NiTiCr SMAs needs to be investigated to obtain an accurate estimate of the number of cycles these SMAs can undergo without a significant degradation of the properties that are important to seismic mitigation applications.
- A new annealing temperature study needs to be conducted to obtain the optimum annealing temperature that produces an SMA with the flattest loading plateau stress (forward transformation stress). Then, strain rate and training studies should be conducted to determine if an alloy presenting a flatter transformation plateau is more suited for seismic mitigation applications.

APPENDIX A

MATERIAL INVOICES FROM SPECIAL METALS CORPORATION

SPECIAL METALS CORPORATION

4317 Middle Settlement Road
New Hartford, NY 13413-5392
Tel: (315) 798-2900
Fax: (315) 798-2001

May 27, 2004

Reginald DesRoches, Ph.D.
Assistant Professor, Structural Engineering, Mechanics, and Materials
School of Civil and Environmental Engineering
Georgia Institute of Technology
Atlanta, GA 30332-0355

Dear Prof. DesRoches:

Thank you for your E-mail of couple days ago. I am sending you a 50-ft sample of NiTi redraw wire. Details of the sample are as follows:

0.085" dia. NiTi Redraw Wire, As Cold Drawn, 40% Cold Work, Oxide Free Pickled Surface, As (fully annealed) = - 20°C, Heat # C7-8215-5-6

If you have any questions please contact me.

Thank you for your interest in Special Metals Shape Memory Alloys. I look forward to supply you with Nitinol products.

Best regards,

Subhash Gupta
Product Engineer
Shape Memory Alloys

Cc: Frank Sczerzenie, General Mgr. SMA Division

SPECIAL METALS CORPORATION

4317 Middle Settlement Road
New Hartford, NY 13413-5392
Tel: (315) 798-2900
Fax: (315) 798-2001

March 31, 2004

Reginald DesRoches, Ph.D.
Assistant Professor, Structural Engineering, Mechanics, and Materials
School of Civil and Environmental Engineering
Georgia Institute of Technology
Atlanta, GA 30332-0355

Dear Prof. DesRoches:

I am sending you a 20-ft sample of NiTiCr redraw wire. Details of the sample are as follows:

0.085" dia. NiTiCr Redraw Wire, As Cold Drawn, 40% Cold Work, Oxide Free Pickled Surface, Cr = 0.25 wt %, As (fully annealed) = - 20°C

If you have any questions please contact me.

Thank you for your interest in Special Metals Shape Memory Alloys. I look forward to supply you with Nitinol products.

Best regards,

Subhash Gupta
Product Engineer
Shape Memory Alloys

Cc: Frank Sczerzenie, General Mgr. SMA Division

REFERENCES

Adachi, Y. and Unjoh, S. (1999). "Development of Shape Memory Alloy Damper for Intelligent Bridge Systems." Proceedings of SPIE: International Society of Optical Engineering **3671**: 31-42.

Asai, M. and Suzuki, Y. (2000). "Applications of Shape Memory Alloys in Japan." Materials Science Forum **327-328**: 17-22.

AZoM.com Copper/Aluminium/Nickel Shape Memory Alloys. Web Page. http://www.azom.com/details.asp?ArticleID=1368 2004

AZoM.com Copper/Zinc/Aluminum Shape Memory Alloys. Web Page. http://www.azom.com/details.asp?ArticleID=1367 2004

Barnes, C. (1999). Shape Memory and Superelastic Alloys. Web Page. http://www.copper.org/innovations/1999/07/shape.html 2004

Beauchamp, C.H., Nadolink, R.H., Dickinson, S.C. and Dean, L.M. (1992). Shape Memory Alloy Adjustable Camber (SMAAC) Control Surface. Proceedings of the First European Conference on Smart Structures and Materials.

Bricknell, R. H., Melton, K. N. and Mercier, O. (1979). "The Structure of NiTiCu Shape Memory Alloys." Metallurgical Transactions A **10A**: 693-697.

Castellano, M.G., Indirli, M. and Martelli, A. (2001). "Progress of Application, Research and Development and Design Guidelines for Shape Memory Alloy Devices for Cultural Heritage Structures in Italy." Proceedings of SPIE: International Society of Optical Engineering **4330**: 250-261.

Chandra, R. (2001). "Active Shape Control of Composite Blades Using Shape Memory Actuation." Smart Materials Structures **10**: 1018-1024.

Chopra, A. K. (2001). Dynamics of Structures: Theory and Applications to Earthquake Engineering, Prentice-Hall.

Continuum Dynamics, Inc. (2000). TR Variable Camber. Web Page. http://www.continuum-dynamics.com/research/topics/vttr/index.html 2003

Croci, G. (2001). "Strengthening the Basilica of St Francis of Assisi After the September 1997 Earthquake." Structural Engineering International: 207-210.

DesRoches, R., McCormick, J. and Delemont, M. (2004). "Cyclic Properties of Superelastic Shape Memory Alloy Wires and Bars." Journal of Structural Engineering **130**(1): 38-46.

DesRoches, R. and Smith, B. (2004). "Shape Memory Alloys in Seismic Resistant Design and Retrofit: A Critical Review of their Potential and Limitations." Journal of Earthquake Engineering **8**(3): 415-429.

Dolce, M. and Marnetto, R. (1999). "Seismic Devices Based on Shape Memory Alloy." MANSIDE Project: II105-134.

Dolce, M. and Cardone, D. (2001). "Mechanical Behaviour of Shape Memory Alloys for Seismic Applications 2. Austenite NiTi Wires Subjected to Tension." International Journal of Mechanical Science **43**(11): 2657-2677.

Duerig, T.W., Melton, K. N., Stockel, D. and Wayman, C.M. (1990). Engineering Aspects of Shape Memory Alloys. Essex, Great Britain, Butterworth-Heinmann Ltd, 1990.

eSmart SMA/MEMS Research Group (2001). Aircraft Maneuverability. Web Page. http://www.cs.ualberta.ca/~database/MEMS/sma_mems/flap.html 2003.

Feng, Z., Gao, B., Wang, J., Qian, D. and Liu, Y. (2002). "Influence of Zr Additions on Shape-Memory Effect and Mechanical Properties of Ni-Rich Alloys." Materials Science Forum **394-395**: 365-368.

Gil, F.J. and Planell, J.A. (1999). "Effect of Copper Addition on the Superelastic Behavior of Ni-Ti Shape Memory Alloys for Orthodontic Applications." Journal of Biomedical Material Research **48**(5): 682-688.

Gotthardt, R., Scherrer, P. and Stalmans, R. (2000). "Smart Materials Based on Shape Memory Alloys: Examples from Europe." Materials Science Forum **327**: 83-90.

Graesser, E.J. and Cozzarelli, F.A. (1991). "Shape-Memory Alloys as New Materials for Aseismic Isolation." Journal of Engineering Mechanics **117**(11): 2590-2608.

Hsieh, S.F. and Wu, S.K. (1997). "A Study on the Nickel-Rich Ternary TiNiAl Shape Memory Alloys." Journal of Materials Science **32**(4): 989-996.

Hsu, S.E., Yeh, M.T., Hsu, I.C., Chang, S.K., Dai, Y.C. and Wang, J.Y. (2000). "Pseudo-Elasticity and Shape Memory Effect on the TiNiCoV Alloy." Materials Science Forum **327**: 119-122.

Huang, X. and Liu, Y. (2001). "Effect of Annealing on the Transformation Behavior and Superelasticity of NiTi Shape Memory Alloy." Scripta Materialia **45**(2): 153-160.

Hwang, C.M. and Wayman, C.M. (1983). "Compositional Dependence of Transformation Temperatures in Ternary TiNiAl and TiNiFe Alloys." Scripta Metallurgica **17**(3): 381-384.

Indirli, M., Castellano, M.G., Clemente, P. and Martelli, A. (2001). "Demo-Application of Shape Memory Alloy Devices: The Rehabilitation of the S. Giorgio Church Bell-Tower." Proceedings of SPIE: International Society of Optical Engineering **4330**: 262-272.

Jiang, C. and Xu, H. (2000). "Effect of Pre-Deformation on Hysteresis in TiNiFe Shape Memory Alloys." Materials Science Forum **327**: 111-114.

Kolomytsev, V., Kozlov, A., Seerneels, A., Moorlenghem, W. and Aslanidis, D. (1998). Effect of the Strain Rate and Sample Size on Features of Non-Linear Deformation Behaviour in TiNi-Based Ribbons and Wires. XXYIII Symposium of UIA.

Koval, Y.N. and Monastyrsky, G.E. (1995). "On the Nature of the Variations of Martensitic Transformation Hysteresis and SME Characteristics in Fe-Ni-Base Alloys." Journal de Physique IV **5**(8): 397-402.

Leo, P.H., Shield, T.W. and Bruno, O.P. (1993). "Transient Heat Transfer Effects on the Pseudoelastic Behavior of Shape-Memory Wires." Acta Metallurgica **41**(8): 2477-2485.

Mercier, O., Melton, K. N., Gotthardt, R. and Kulik, A. (1982). "Lattice Instability in the NiTi and NiTiCu Alloys." Metallurgical Society of AIME: 1259-1263.

Miyazaki, S. and Kohl, M. (1998). "Recent Development in TiNi-based Shape Memory Alloys." Proceedings of SPIE: International Society of Optical Engineering **3324**: 2-13.

NDC, Nitinol Devices and Components (2001). Web Page. http://www.nitinol.com. 2002

Ocel, J., Leon, R., DesRoches, R., Krumme, R., Hayes, J. and Sweeney, S. (2002). High Damping Steel Beam-Column Connections Using Shape Memory Alloys. 7th US National Conference in Earthquake Engineering, Boston, Massachussets.

Otsuka, K. and Wayman, C.M., Eds. (1998). Shape Memory Materials. Cambridge, U.K., Cambridge University Press.

Perkins, J. (1981). "Ti-Ni and Ti-Ni-X Shape Memory Alloys." Metals Forum **4**(3): 153-163.

Piedboeuf, M.C., Gauvin, R. and Thomas, M. (1998). "Damping Behaviour of Shape Memory Alloys: Strain Amplitude, Frequency and Temperature." Journal of Sound Vibrations **214**(5): 885-901.

Ranucci, T., Besseghini, S. and Airoldi, G. (2000). "The Pseudoelasticity of a Ni45Ti50Cu5 Alloy." Materials Science Forum **327**: 143-146.

Sadek, F., Mohraz, B., Taylor, A. and Chung, R. (1996). NISTIR 5923: Passive Energy Dissipation Devices for Seismic Applications, National Institute of Standards and Technology.

Scherngell, H. and Kneissl, A.C. (1999). "Influence of the Microstructure on the Stability of the Intrinsic Two-Way Shape Memory Effect." Materials Science and Engineering A **A273-275**: 400-403.

Siegert, W., Neuking, K., Mertmann, M. and Eggeler, G. (2002). "Influence of Nb Content and Processing Conditions on Microstructure and Functional Properties of NiTiNb Shape-Memory Alloys." Materials Science Forum **394-395**: 361-364.

Tadaki, T., Otsuka, K. and Shimizu, K. (1988). "Shape Memory Alloys." Annual Review Material Science **18**: 25-45.

Takaoka, S., Horikawa, H., Kobayashi, J. and Shimizu, K. (2002). "Applications and Development of Shape-Memory and Superelastic Alloys in Japan." Materials Science Forum **394-395**: 61-68.

Tobushi, H., Shimeno, Y., Hachisuka, T. and Tanaka, K. (1998). "Influence of Strain Rate on Superelastic Properties of TiNi Shape Memory Alloy." Mechanics of Materials **30**(2): 141-150.

Van Humbeek, J. and Liu, Y. (2000). "Shape Memory Alloys as Damping Materials." Materials Science Forum **327-328**: 331-338.

Wesolowsky, M. and Wilson, J. (2004). Controlling Seismic Response with Shape Memory Alloy Devices. 13th World Conference on Earthquake Engineering, Vancouver, B.C., Canada.

Wolons, D., Ghandi, F. and Malovrh, B. (1998). "Experimental Investigation of the Pseudoelastic Hysteresis Damping Characteristics of Shape Memory Alloy Wire." Journal of Intelligent Material Systems and Structures **9**(2): 116-126.

Wu, K., Yang, F., Pu, Z. and Shi, J. (1996). "The Effect of Strain Rate on Detwinning and Superelastic Behavior of NiTi Shape Memory Alloys." Journal of Intelligent Material Systems and Structures **7**: 138-144.

Wu, S.K. and Lin, H.C. (2003). "Damping Characteristics of TiNi Binary and Ternary Shape Memory Alloys." Journal of Alloys and Compounds **355**(1-2): 72-78.

Zhao, C. (2001). Shape Memory Stainless Steels. Advanced Materials & Processes. **159:** 33-35.